External Cavity Diode Lasers and Non-Linear Optical Frequency Conversion in Spectroscopic Applications

A thesis to be submitted to the
UNIVERSITY OF ST ANDREWS
for the degree of
DOCTOR OF PHILOSOPHY

by

Anjali Shah BSc (Hons)

School of Physics and Astronomy

University of St Andrews

May 2006

I, Anjali Shah BSc (Hons), hereby certify that this thesis, which is approximately 40000 words in length, has been written by me, that it is the record of work carried out by me, and that it has not been submitted in any previous application for a higher degree.

date _____ *signature of candidate* _____

I was admitted as a research student in October 2002 and as a candidate for the degree of Doctor of Philosophy in October 2003; the higher study for which this is a record was carried out in the University of St Andrews between 2002 and 2006.

date _____ *signature of candidate* _____

I hereby certify that the candidate has fulfilled the conditions of the Resolution and Regulations appropriate for the degree of Doctor of Philosophy in the University of St Andrews and that the candidate is qualified to submit this thesis in application for that degree.

date _____ *signature of supervisor* _____

In submitting this thesis to the University of St. Andrews I understand that I am giving permission for it to be made available for use in accordance with the regulations of the University Library for the time being in force, subject to any copyright vested in the work not being affected thereby. I also understand that the title and abstract will be published, and that a copy of the work may be made and supplied to any *bona fide* library or research worker.

date _____ *signature of candidate* _____

Science knows no country, because knowledge belongs to humanity, and is the torch which illuminates the world.

Louis Pasteur (1822-1895)

Abstract

Semiconductor diode lasers are successful tools in atomic spectroscopy. They are routinely used in frequency conversion applications to develop devices that access regions of the spectrum not directly available. This thesis describes the practical application of novel violet diode laser systems and their possible inclusion in spectroscopic systems.

The design, assembly and successful operation of a doubly resonant optical parametric oscillator is described. There is discussion of the spectral behaviour of the device and the potential for pumping with a violet diode laser. Methods to adapt the output from the solitary diode devices are demonstrated with the use of microlensed diode lasers and extended cavity configurations. Details of the current tuning, linewidth and smooth tuning characteristics of a number of the lasers used are given. A commercial violet diode laser is used within an extended cavity to measure the hyperfine structure of atomic indium from a hollow cathode galvatron source at room temperature. Stabilisation of the diode laser to a line from the indium spectrum is attempted.

The remainder of the thesis is concerned with the development of techniques to deliver clearer and more precise spectral information about trace species. Microlensed red and violet diode lasers are used to generate light at 254nm via sum frequency generation for the direct detection and modulation spectroscopy of mercury vapour, with microlensed lasers with modulation allowing more accurate discrimination between spectral features than direct absorption measurements. In addition Raman tweezers modulation spectroscopy is undertaken to investigate polymer microspheres

and biological cell samples where the use of the modulation technique demonstrated improvements in the acquisition time and clarity of spectra through increased signal to noise and rejection of background fluorescence effects. A comparison between the direct and modulation techniques for all the systems indicates the greater sensitivity of the modulation technique.

Acknowledgement

This PhD thesis would not have been possible without the support and kindness of a great many people. I would like to take this opportunity to thank them.

Dr Majid Ebrahim-Zadeh gave me the chance to pursue PhD studies at the University of St Andrews and introduced me to the CW-OPO group. I am especially indebted to Professor Kishan Dholakia whose enthusiasm and encouragment and willingness to adopt me as his student has allowed me to achieve my PhD and learn a few things along the way! I would like to thank Professor Alan Miller and Professor Steve Lee for their time and useful advice in their role as Heads of School and the School of Physics and Astronomy for generous financial support.

Special thanks must go to Dr Ian Lindsay. From my time as an undergraduate summer student to the first year of my PhD and then at the University of Twente and in the writing of this thesis, he has been a mentor and friend and I am truly grateful for his selflessness and generosity towards me. I must thank my colleagues in the Laser Physics Department at the University of Twente, Professor Dr Klaus Boller for kindly allowing me space to pursue my research in his group, Drs Marvin Klein and Petra Groß, Balaji Adhimoolam and Isabel de la Fuente Valentin.

My colleagues in the physics department have been vital - Dr Michael Spurr and Dr David Bolton and Dr Michael Mazilu provided vital assistance with experimental work and were always willing to answer any of my questions. The Optical Trapping Group has been my home for the majority of my studies and I would like to thank

Tanya, Toni, Daniel and Phil who have influenced and helped with much of the work in this thesis.

More personally my friends have shaped my life here in St Andrews, - staying here for 8 years I was bound to pick up the odd stray! Throughout it all there has always been somebody ready with a smile, bad influences to get me away from work and in most cases have ensured an endless supply of G&T! So to those I've known since my first day , Vari, Sian and Tim (my LaTeXguru!) to those who I have only recently got to know, Tammy, Oli, Donald and Iain, those who slot quite nicely into the middle, Mike, Alex, Laura, Maerkey, Mikey, Lauren, Jeannie, Lynn, Paul, Alison and Mark and not forgetting the home front(!), Katy, Jayne, Ashy, Laura and Sara, who I have known longer than I haven't, a big thankyou!

Finally to my family, Mum, Dad, Sanjay, Tracy, Elsie, Earl, Alka, Mummy Ba and Evelyn - none of this would have been possible without you all and this thesis and the last four years are dedicated to you.

Publications

A.E. Carruthers, T.K. Lake, A. Shah, J.W. Allen, W. Sibbet, and K. Dholakia.
Microlensed red and violet diode lasers in an extended cavity geometry.
Review of Scientific Instruments, 75(10):3360–3362, 2004.

Antonia E. Carruthers, Tanya K. Lake, Anjali Shah, John W. Allen, Wilson Sibbett, and Kishan Dholakia.
Single-scan spectroscopy of mercury at 253.7nm by sum frequency mixing of violet and red microlensed diode lasers.
Optics Communications, 255(4–6):261–266, 2005.

Antonia E. Carruthers, Anjali Shah, Tanya K. Lake, John W. Allen, Wilson Sibbett, and Kishan Dholakia.
Sum frequency mixing of diode lasers for spectroscopy.
In *European Conference on Lasers & Electro-Optics*, Munich, Germany, June 2005.

Contents

List of Figures

List of Tables

Acronyms

Acronym	Definition
AlGaAs	Aluminium Gallium Arsenide
AlGaInN	Aluminium Gallium Indium Nitride
AM	Amplitude Modulation
AR	Anti-Reflection
BBO	Beta-Barium Borate
BPM	Birefringently Phase Matched
C-W	Continuous Wave
DAVLL	Dichroic-Atomic Vapour Laser Lock
DBR	Distributed Bragg Reflector
DFB	Distributed Feedback
DRO	Doubly Resonant Optical Parametric Oscillator
ECDL	External Cavity Diode Laser
FM	Frequency Modulation
FMS	Frequency Modulation Spectroscopy
FSR	Free Spectral Range
GaN	Gallium Nitride
InGaN	Indium Gallium Nitride
IR	InfraRed
LIDAR	Light Detection and Ranging
MDL	Microlensed Diode Laser
MQW	Multiple Quantum Well

NA	Numerical Aperture
OPG	Optical Parametric Generation
OPO	Optical Parametric Oscillator
QPM	Quasi Phase Matched
PCA	Principle Component Analysis
PPKTA	Periodically Poled Potassium Titanyl Arsenate
PPKTP	Periodically Poled Potassium Titanyl Phosphate
PPLN	Periodically Poled Lithium Niobate
PPRTA	Periodically Poled Rubidium Titanyl Arsenate
PZT	Piezoelectric Transducer
SERDS	Shifted Excitation Raman Difference Spectroscopy
SFG	Sum Frequency Generation
SHG	Second Harmonic Generation
SNR	Signal to Noise Ratio
SRO	Singly Resonant Optical Parametric Oscillator
THG	Third Harmonic Generation
TRO	Triply Resonant Oscillator
UV	Ultra Violet
WMS	Wavelength Modulation Spectroscopy
ZnSe	Zinc Selenide

Chapter 1

Introduction and Synopsis

In nature the optical radiation generated from any material is confined to a restricted range of wavelengths (colours) determined by the energy level structure of the material. This is the basic principle of operation of the laser, implying that coherent radiation generated by such sources is over a limited range of wavelengths. When laser light interacts with a medium the behaviour of the light consequently can give rise to many interesting effects, providing users with opportunities to exploit these phenomena within devices. The use of laser devices, particularly those emitting in the violet region of the spectrum, along with the exploitation of non-linear optical phenomena to facilitate generation of a broad, coherent wavelength range for investigation is the major aim of the work described in this thesis.

1.1 Overview

In 1814 Josef Fraunhofer dispersed the solar spectrum into its component colours. For the first time alongside the familiar band of bright colours, narrow dark lines appeared which followed a definite, unaltering pattern. This phenomenon was repeated when the spectra of other sources, most notably in flames, were observed with some sources showing bright lines. This was the birth of spectroscopy and the dark and bright lines were identified as characteristics of chemical elements. The advent of the laser provided spectroscopy with a fundamental tool and the field of laser spectroscopy has grown rapidly, with the laser being used routinely to identify information about trace elements [1, 2]. The applications of laser spectroscopy are wide ranging including pollution monitoring, medical applications and investigations into astronomical phenomena. Their use in the determination of frequency standards and precision time measurements with atomic clocks is crucial and this was attested to with the award of part of the Nobel Prize for Physics in 2005 to Theodor Hänsch for his work on laser based precision spectroscopy for use in the determination of frequency standards. The development of the semiconductor diode laser provided yet another tunable radiation source that allowed spectroscopic investigations to take place.

There is a growing demand in a wide variety of applications such as those mentioned for continuous wave, frequency tunable optical sources. The development of optical devices that are compact and portable yet retain the accuracy and precision of larger lab based devices is vital for the applications of these devices to move from research based to commercial mass produced markets. Such applications require compact portable sources, with a coherent output of high amplitude and frequency stability, narrow linewidth, broad tunability and appropriate output powers for the required application. The semiconductor diode laser has many of these characteristics and its output can be adapted to satisfy any requirements not inherently met.

Many well established tunable laser systems operate in the visible and near to mid infrared regions but until recently there were no available sources emitting in the

violet visible region. The only way to access this region was via frequency conversion methods employing other longer wavelength laser sources. A device emitting in the violet region that exhibited typical diode laser behaviour was the next logical stage [3], satisfying an increasing demand in the optical storage markets. Gallium Nitride (GaN) violet emitting lasers have been very commercially successful soon after their initial demonstrations. Optical storage, reading and writing of memory on compact discs and optomagnetic memories all provide huge markets for blue, blue/green and violet emitting lasers [4]. Storage density within these media is primarily determined by the wavelength of the light. The bit size is determined by the spot size of the laser beam, so for maximum storage, the smallest beam is desirable. The spot size is given by

$$Spotsize(diameter) = \frac{\lambda}{2NA} \tag{1.1}$$

where λ is the wavelength of the light and NA is the numerical aperture of the lens within the focussing system, given by Equation 1.2, determined by the refractive index of the medium and the outer angle of the cone formed by the converging light, given by

$$NA = nsin\theta_{max} \tag{1.2}$$

Therefore a violet emitting laser is likely to increase the storage density by a factor of four compared to the red and infrared lasers commonly used. The violet laser also proves to be of great benefit in biological and medical applications where the shorter wavelength light can be favourable because of the reduction in scattering. The GaN diode laser is now being developed in similar fashion to its longer wavelength counterparts and they are starting to be used in applications where traditionally a frequency conversion system was used to generate the violet light. Violet diodes have been successfully incorporated within optical feedback configurations such as external cavity diode lasers [5]. ECDLs retain in large measure the compactness

and simplicity of solitary cavity diode lasers and in addition provide a number of performance enhancements such as operation on a single longitudinal mode and a narrower linewidth.

This thesis studies diode lasers emitting in the violet region of the spectrum and investigates their use with frequency conversion techniques to generate tunable laser output suitable for spectroscopic investigations. Both home built and commercial single frequency violet diode lasers are used to access spectral lines both directly in the violet and UV regions via frequency conversion techniques.

Central to the applications described here is the the phenomena of non-linear optics and the use of materials possessing a non-linear susceptibility. The first observation of frequency conversion using a non-linear material was by Franken *et al* [6] in 1961 and since then a wide range of practical devices harnessing the non-linear process have been demonstrated. Non-linear optical processes can be used to access regions of the spectrum that are difficult to access through direct laser emission. The advancement of violet diode laser devices has provided laser output at a new range of wavelengths, introducing exciting new possibilities for less complicated methods to allow access to the UV region. Both optical parametric generation (OPG) and sum frequency generation (SFG) offer this through the subtraction and addition of fundamental laser frequencies. In Chapters 4 and 5 the applications described exploit the second order non-linear effect where both OPG and SFG are realised experimentally. Both effects are used to adapt the output from diode lasers to achieve tunable radiation sources by using the non-linear response of certain media.

The optical parametric oscillator (OPO) is a device based upon the OPG non-linear interaction. Since its first demonstration, many different types of OPO have been developed as wavelength tunable sources of both pulsed and continuous wave coherent light [7]. OPOs are now available in a wide spectral range from the UV to IR providing average output powers in the range of a few mW to several watts. The wavelength tuning capabilities and high power efficiency make OPOs ideal devices for applications

such as high resolution spectroscopy and trace gas detection, precision frequency metrology, environmental monitoring and light detection and ranging LIDAR.

The initial aim of this PhD project was to develop an optical parametric oscillator pumped by a violet diode laser. The OPO is an optical converter that converts monochromatic laser emission (pump) into tunable output via a three-wave mixing process and delivers high peak or average powers, high conversion efficiency and broad continuous tunability. The heart of an OPO is a non-linear optical crystal. In the crystal the pump photon is converted, via the parametric generation process, into two photons of lower energy (i.e longer wavelengths), termed the signal and idler, that retain the coherent and spectral properties of the laser pump source. The energy of the generated signal and idler photons is equal to that of the pump. The typical characteristics of OPOs make them highly suitable devices for use in spectroscopy.

There are many powerful laser based systems for trace gas detection. Wieman and MacAdam [8, 9] give excellent accounts of the use of saturated absorption spectroscopy techniques using diode lasers. Absorption spectroscopy simply looks for depletion in power between a reference beam and a beam that interacts with the trace species. The sensitivity of these techniques can be refined by introducing modulation of the laser without any major changes to the experimental setup. This has the effect of improving the signal to noise ratio and can bring more clarity to an absorption spectrum, identifying less abundant features. A review of these techniques is given in [10].

All of the work described in this thesis is united by the central themes of semiconductor diode lasers, non-linear optics and spectroscopy.

1.2 Synopsis

Throughout this thesis the laser devices used are all semiconductor diode lasers. In Chapter 2, I present a review of diode lasers, detailing their development since

their first demonstration over forty years ago. Their spatial, spectral and tuning characteristics of diode lasers along with techniques that enhance these properties are described. The recent violet emitting diode laser is introduced with a discussion of the structure of the laser and and the difficulty that there was in manufacturing a structure that allows a laser to emit light in the violet region of the spectrum.

Chapter 3 introduces the basic theory behind non-linear optical processes that are used throughout this thesis. The theory of non-linear optics, the origin of the non-linear susceptibility and second order processes is given followed by detailed theory of optical parametric generation. The optical parametric oscillator and its common configurations are introduced. Finally sum frequency generation is introduced.

Chapters 4, 5 and 6 detail the experimental work that was carried out. These chapters bring together the ideas introduced in Chapters 2 and 3, to develop devices based upon diode lasers used in non-linear optical interactions suitable for spectroscopic applications.

Chapter 4 details the design and operation of a doubly resonant optical parametric oscillator (DRO) device pumped by a diode laser. The spectral characteristics of the DRO output are discussed and then mechanisms and solutions that improve the output from the DRO to make it more suitable for spectroscopic trace gas detection applications are given. The cluster hopping phenomena described is a crucial factor that must be overcome to obtain smoothly tuning output from the device. Pumping an OPO with a violet diode laser would hope to address some of these tuning effects and also provide a new range of the spectrum that is accessible with this type of device. This would be the first time that mechanisms to improve the spectral output from the DRO will have been implemented and the first opportunity to experimentally verify the theoretically predicted results. Due to factors outwith the laboratory the work described was unable to be brought to a satisfactory conclusion. The extensive discussion and review of modelling work carried out on tuning behaviour is presented as a guide to the direction in which the experimental work would have gone towards.

Chapter 5 describes the characterisation of the lasers used within the experimental applications within this thesis. The current and temperature tuning properties and spectral output are investigated for a Nichia violet diode both free running and in external cavity for use as a pump source for an OPO, red and violet microlensed diode lasers for generation of UV light for spectroscopy and a commercial violet ECDL for use in spectroscopy. This laser was then used to measure the hyperfine structure of indium using a hollow cathode discharge source. Preliminary results on the stabilisation of the violet laser to an indium line are also presented.

Chapter 6 describes the generation of UV radiation using sum frequency generation of two microlensed diode lasers. This UV output is then used to identify the fine structure of mercury through direct absorption spectroscopy. Modulation spectroscopy techniques are then used to refine the technique and allow resolution of individual isotopes within the mercury vapour. A comparison between this method and the direct detection method is drawn. For both cases an accurate frequency calibration of the fine structure features of mercury is given. In addition the technique of Raman spectroscopy using diode lasers is used in combination with modulation spectroscopy techniques to provide refinement and improvement in the clarity of recorded spectra.

In the final chapter, Chapter 7, the results and observations described within the thesis are brought together and suggestions for improvements and further research are also proposed.

Bibliography

[1] Wolfgang Demetroder. *Laser Spectroscopy : Basic Concepts and Instrumentation*. Springer, 2nd edition, 1996.

[2] Alan Corney. *Atomic and Laser Spectroscopy*. Oxford Science Publications, 2 edition, 1979.

[3] Shuji Nakamura and Gerhard Fasol. *The Blue Laser Diode*. Springer Verlag, 1st edition, 1997.

[4] Henk van Houten and Jean Schleipen. Optical data storage. *Physics World*, 11(10):33–37, 1998.

[5] R.S. Conroy, J.J. Hewett, G.P.T. Lancaster, W. Sibbett, J.W. Allen, and K. Dholakia. Characterisation of an extended cavity violet diode laser. *Optics Communications*, 175(1–3):185–188, 2000.

[6] P.A. Franken, A.E. Hill, C.W. Peters, and G. Wienreich. Generation of optical harmonics. *Physical Review Letters*, 7:118, 1961.

[7] Malcolm H. Dunn and Majid Ebrahimzadeh. Parametric generation of tunable light from continuous wave to femtosecond pulses. *Science*, 286(5444):1513–1517, 1999.

[8] Carl E. Wieman and Leo Hollberg. Using diode lasers for atomic physics. *Review of Scientific Instruments*, 62(1):1–20, 1991.

[9] K.B. MacAdam, A. Steinbach, and Carl Wieman. A narrow-band tunable diode laser system with drating feedback and a saturated absorption spectrometer for Cs and Rb. *American Journal of Physics*, 60(12):1098–1111, 1992.

[10] Kyuseok Song and Euo Chang Jung. Recent developments in modulation spectroscopy for trace gas detection using tunable diode lasers. *Applied Spectroscopy Reviews*, 38(4):395–432, 2003.

Chapter 7

Conclusion

This thesis has brought together the theory of non-linear optical frequency conversion with the use of semiconductor laser based devices to provide practical tools for applications in spectroscopy. The results obtained demonstrate the versatility of the blue diode laser and show that its characteristics and uses are as valuable as those of the more well established diode lasers at longer wavelengths. The major aim of the practical work was to demonstrate the use of diode lasers for atomic spectroscopy and investigate techniques that improve the detection to yield clearer spectra and provide a more detailed insight into the properties of the samples under investigation.

7.1 Summary of Thesis

Following a brief introduction, Chapter 2 described the main characteristics of diode lasers and the mechanisms used to improved the quality and behaviour of the output that were then successfully applied practically in the experiments described in this thesis. After identifying the spectral and spatial characteristics, and some of their limitations of diode lasers, mechanisms to improve the operating characteristics and tailor their output, loosely termed 'coherence enhancement' were introduced. The sensitivity of the diode laser to optical feedback and the use of this phenomenon to obtain narrow linewidth operating lasers was described along with some devices that exploit this sensitivity such as microlensed diode lasers (MDLs) and external/extended cavity diode lasers (ECDLs).

Chapter 3 gave a discussion of the regime of non-linear optics which underpinned the frequency conversion techniques described in Chapters 4 and 6. The background to non-linear optics was discussed extensively with particular emphasis on the processes of optical parametric generation and sum frequency generation. The basic characteristics of an optical parametric oscillator including details of cavity configurations and threshold requirements was given and the concepts examined in Chapter 4 were introduced. Laser systems that are based on non-linear optical conversion techniques such as optical parametric oscillators and sum frequency generation were successfully demonstrated.

In Chapter 4, the design, construction and operation of a doubly resonant optical parametric oscillator (DRO) was described along with a discussion into how this tool was to have been used in future work. The DRO was successfully operated using an IR emitting diode laser in both single and double pass configurations with threshold powers of 42mW and 21mW respectively. The OPO was operated through three grating periods of the PPLN crystal and tuning ranges for the 21.6 grating period was 5THz and the total signal and idler tuning ranges were $1.2\mu m$ to $1.23\mu m$ for the signal and $2.3\mu m$ to $2.6\mu m$ for the idler wavelengths. An estimate of the conversion

efficiency of the DRO was obtained as 65% and 82% for the single and double pass configurations respectively. The low threshold power of the device obtained showed promise for the use of this type of device with violet diode laser pumping. The opportunities for development of this work and the methods that could be employed to investigate the spectral and tuning characteristics of the OPO were discussed.

In Chapter 5 the characteristics of a variety of diode lasers used in the experimental applications were given. An elementary characterisation of a GaN diode laser was presented showing that the behaviour of this devices followed typical diode laser behaviour. The violet laser has a threshold of 33mA in free running mode and 27mA when operated within an external cavity. In external cavity the single mode oscillation was demonstrated by observation of the spectral output and a mechanism of phase continuous tuning by varying the length of the solitary and extended cavity in phase allowed 16.5GHz of smooth mode-hop-free tuning. It is noted in this conclusion that since this work was carried out the speed of development of violet diode lasers coupled with the huge research interest in these relatively novel devices has meant that operating characteristics of the lasers are continually improving. The properties of the red and violet microlensed diode lasers were given as well as the properties of a commercially built T-Optica violet external cavity diode laser. The T-Optica laser was then used, within an absorption spectroscopy application, to identify the hyperfine structure of indium. The wavelength of the violet laser was set at 410.293nm and all four absorption features were resolved within a single scan of the laser (37GHz) and the features matched those given in the literature. Side-of-fringe stabilisation of the violet laser to an indium absoprtion feature was attempted and although inconclusive provided promising elementary results, indicating that with more time and stronger indium features the stabilisation would be more successful.

The combination of microlensed diode lasers with non-linear frequency conversion and trace gas detection techniques was used to great success in Chapter 6. The use of red and violet MDLs to generate 253.7nm using SFG allowed generation of over 50nW of UV power, over an order of magnitude greater than previous work. The

conversion efficiency of the SFG process was $2.45.10^{-4}\%$, again much greater than any previously reported. The UV light was used to resolve the hyperfine structure of mercury via direct detection absorption spectroscopy in a single scan. Furthermore, modulation spectroscopy techniques were used within the system to refine the spectra obtained and enable individual isotopes within the natural mix to be resolved, providing a degree of precision not seen previously with this type of spectroscopy measurement. This precision was due in a large part to the greater UV power and non-linear conversion efficiency as a result of using MDLs. The parameters for modulation spectroscopy of mercury were refined systematically to find results that would yield the clearest spectra. Detection at different harmonics was performed to identify the optimum operating parameters for the system and show that for this system there was no benefit in shifting the detection to higher harmonics as had been the case in previous studies on similar modulation spectroscopy systems. Accurate calibration of the fine structure of mercury with separations between the features of the spectrum was given and the results obtained with the direct detection system and the wavelength modulated system were in agreement. In addition spectroscopy on a single isotope source indicated the presence of features that were only resolved when the modulation system was used, due to the improved signal to noise ratio.

Finally, elementary results for the use of modulation techniques for Raman spectroscopy on trapped particles were given. Comparisons between direct and modulated Raman spectra were recorded for polymer microspheres and for cervical cancer cells. In each case the modulation system allowed resolution of features within a much shorter acquisition time than for the direct technique and methods to improve the signal to noise of the spectral data and the effective rejection of the effects of background fluorescence were shown to be successful.

7.2 Future Work

The main results obtained within the experimental chapters of this thesis point to a wide variety of future work that would be possible.

Section 4.7 in Chapter 4 alluded to the work that could continue on from the demonstration of the DRO. To the best of my knowledge the problems caused by the cluster hopping phenomena have not yet been resolved and in addition an OPO pumped directly by a violet diode laser has not yet been reported. Alterations could be made to the device such as the introduction of passive and active stabilisation measures. These could include the manufacture of new OPO cavity mounts that are more vibration sensitive and the stabilisation of the pump laser to an external stable reference to minimise the effect of the laser instability on the OPO operation. The spectral output could be observed for the single and double passing case and a comparison made. In addition, the spectral output at different grating periods and temperatures could be recorded to gain insight into the tuning behaviour. Modelling indicated that the use of a shorter pump wavelength would improve the tuning output of the device and if an OPO pumped by a violet diode could be designed and operated a great opportunity would arise to not only observe the effect upon the spectral characteristics of the OPO but also explore applications with this device, not only within spectroscopy but in other spheres most notably medical and biological applications.

The improved stabilisation of the blue diode laser using the indium line provides an additional study to add to the already highly successful area of stabilisation to atomic resonances. Subsequently, a more in-depth investigation could examine the effect of stabilisation to different lines within the indium spectrum and a comparison between different methods, for example top-of-fringe or current/PZT locking.

The mercury spectroscopy system demonstrated the advantages of the use of MDLs in maximising non-linear conversion and the potential for these types of SFG systems as UV sources. There are a number of factors that could potentially improve the

SFG system in its current configuration. The UV power output from our system was still below the theoretically predicted value and there would be great benefit in investigation of methods that may improve the non-linear conversion. These could include the use of periodically poled non-linear materials that have already been shown to yield greater output powers when used within parametric generation devices or the use of different coatings on a crystal more suited for the wavelengths that are being generated. The use of an enhancement cavity system would provide a mechanism to enhance the intensity of the sum frequency generation process. An enhancement cavity would be built around the non-linear crystal, although a simple linear cavity configuration such as that used in the OPO application is not suitable. A more appropriate geometry would be a 'bow tie' cavity using two plane mirrors and two concave mirrors. Stabilisation of the violet diode laser to a stable cavity would allow the frequency of the violet diode to be fixed, which is a crucial factor in accessing the mercury line, and make the system more suitable for use as a mobile pollution detector system. In addition, locking techniques could be used to lock the violet or red MDLs to either the direct detected mercury absorption feature or the derivative signals obtained through modulation spectroscopy.

A simple search on a database such as that operated by NIST [11] shows a large number of spectral absorption lines that are close to the UV wavelength of 254nm used in this system. These include cobalt (253.596nm), iridium (254.397nm) and tungsten (255.135nm). The success of the mercury spectroscopy suggests that this system could be easily adapted to allow investigations into these spectral lines. The wavelengths generated by the SFG system are variable by tuning of the two lasers and only a very minor adjustment of the grating of the violet ECDL would be required to access these spectral lines.

There is a great deal of investigation that can still be carried out into the wavelength modulation system parameters. Firstly, modelling of the Gaussian, Lorentzian and Voigt profiles to fit the lineshapes of the mercury features that were obtained would provide greater insight into the broadening effects occurring within the sample

and allow further refinement of the system parameters. In addition increasing the modulation frequency could take the system into the regime of frequency modulation spectroscopy, where the FM spectra have only a single sideband, providing higher sensitivities.

Wavelength modulation Raman spectroscopy is a very promising area of research. The results presented in Chapter 5 were elementary but identified the potential of this technique and how it could be developed to deliver clear spectra in short acquisition times. The improved signal to noise and rejection of background shows that it will be possible to identify weaker features and information on the composition of cell lines will be easier to deduce. The combination of short acquisition time and clearer spectra mean that there is the possibility of *in vivo* cell tissue studies. The parameters of this wavelength modulation system would benefit greatly from detailed investigation to determine the nature of the features and the optimum modulation parameters. The effects of detection at higher harmonics may yield more clarity if the detector noise from the CCD can be eliminated. Again, the variation of modulation index may have a significant effect upon the clarity of the spectra and with many of the features from biological samples as yet unidentified the use of this system to provide new information as to the nature of biological tissue would be very promising.

Chapter 2

Semiconductor Diode Lasers Review

Since their invention in 1961, semiconductor lasers have revolutionised the commercial laser market, dominating it as a result of their favourable physical and operational characteristics and ease of mass production. They now play a principal role in consumer electronics but retain a major importance in the research laboratory, providing a degree of flexibility, adaptability and economy that had been previously unavailable to users. Researchers now have a wider choice than ever of diode laser devices, encompassing a wide range of operating wavelengths and with rapidly improving spectral, spatial and tuning characteristics. The success of applications employing diode lasers continues to motivate the futher development of devices.

2.1 Introduction

Semiconductor lasers have successfully moved from specialised research applications to the mass consumer market with the manufacture of high power GaAlAs and InGaAsP laser diodes. In recent years, the highly successful development of Gallium Nitride (GaN) light emitting diodes (LEDs) and laser diodes region by the Nichia corporation have further developed the market and provided users with a new device for research applications. Although still in their infancy, both the research and commercial possibilities of violet diode lasers are being realised with considerable success. Much of the work in this thesis concerns the employment of violet diode lasers.

The wavelength of the diode laser output depends upon the band gap of the material used to construct the laser structure. Commercial diode lasers can be classed according to laser materials as shown in Table 2.1.

As the technology surrounding diode lasers has evolved, there have been dramatic improvements in the efficiency, spectral characteristics and functional lifetime of devices. The evolution of laser diode configurations has delivered devices that retain the positive attributes of diode lasers, yet address some of their limitations, providing tools that are readily compliant with the requirements of highly specialised research or high volume consumer electronics markets. The structure of diode lasers that we have today is efficient, compact and gives inherently tunable laser output, suitable for wide ranging applications.

Some of the output beam properties of diode lasers are not appropriate for specific applications, and must be corrected by the addition of optical elements or by other mechanisms. In this chapter a brief review of the development of diode lasers is given followed by a description of their characteristics. The methods employed to enhance the output from diode lasers are discussed and the recent development of short wavelength diode lasers emitting in the blue region, a major concern in this thesis, is reviewed. Finally, some examples of research applications using diode lasers

Compound	Wavelengths(nm)
GaN	< 400
ZnSe	$460 - 530$
AlGaInP	$630 - 680$
GaInP	670
$Ga_{1-x}Al_xAs$	$620 - 895$
GaAs	904
InGaAs	980
InGaAsP	$1100 - 1650$
InGaAsSb	$1700 - 4400$
PbEuSeTe	$3300 - 5800$
PbSSe	$4200 - 8000$
PbSnTe	$6300 - 29000$
PbSnSe	$8000 - 29000$

Table 2.1: **Important Semiconductor Laser Materials**

are presented.

2.2 Semiconductor Laser Review

The light emitted by a semiconductor diode arises from the recombination of electrons and holes at a p-n junction as current flows through it in the forward direction. An electron from the n-layer conduction band recombines with a hole from the p-layer emitting a photon. If the current is sufficiently large and the recombination layer (active layer) is narrow enough, this radiative process dominates over the losses. This mechanism was first proposed by Wantanabe and Nishizawa in 1957 [1] and eventually realised in 1962 with the first homojunction diode laser [2, 3]. These original laser

diodes were made from a single material (GaAs), selectively doped to form a p-n junction. However, they suffered from large losses and thus required very high threshold currents as there was no device to confine carriers to the junction region. In addition, there was considerable absorption across the junction region into the n and p type material layers which caused overheating and then premature breakdown of the device, as well as increasing the threshold current. This resulted in early semiconductor lasers operating at cryogenic temperatures and with pulsed output, severely limiting their practical use. Thus, a primary objective in the future design of these laser devices was the prevention of internal losses by developing methods of confinement to maximise the efficiency and output power of the laser and also improve spatial and spectral beam characteristics.

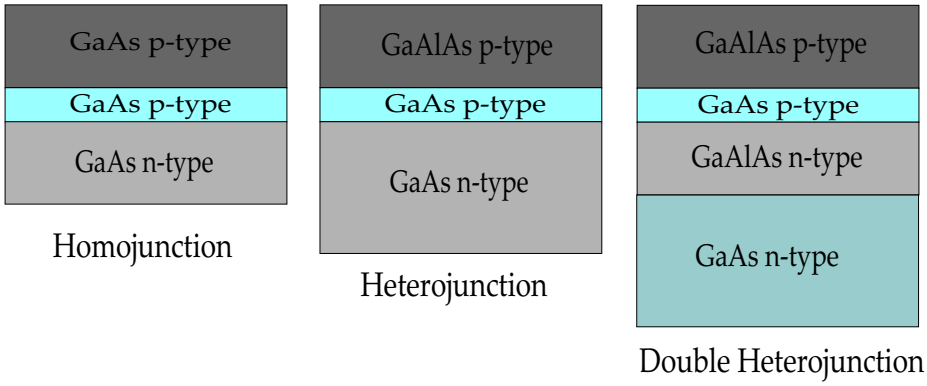

Figure 2.1: **Evolution of the Diode Laser**
The evolution of the diode laser from homojunction to heterojunction to double heterojunction.

To overcome these issues, the heterojunction and later the double-heterojunction lasers were developed, shown in Figure 2.1. The heterojunction appeared to solve the threshold issue, however room temperature continuous wave (C-W) operation was not achieved until the development of the double heterojunction. A double-heterostructure junction laser consists of a thin active layer sandwiched between two cladding layers. The active layer has a lower band gap and a higher refractive index than those of the cladding layers. Because of the lower band gap of the active layer, the electrons and holes are confined to this region where they recombine to yield optical

gain. Furthermore, the optical mode is also confined to the active layer because of its higher refractive index. The confinement of both charge carriers and photons in the active layer results in a reduction in the threshold current density for the C-W operation of diode lasers at room temperature. Confinement can be refined with the introduction of stripe geometries in the structure of the laser material normally involving narrow active layers.

Two of the most basic methods of altering the material geometry to improve confinement are index guiding and gain guiding. In the index guided structure, the electric field confinement in the transverse direction perpendicular to the junction plane occurs through dielectric wave guiding. This design relies upon a waveguide groove that is formed in the wafer during the deposition process. The groove, adjacent to the active junction, creates a geometry that confines laser radiation by surrounding the narrow active region on four sides by a low refractive index, wide band gap material which serves to contain both the charge carriers and the photons. In the gain guided structure, the variation of the optical gain in the lateral direction parallel to the junction direction is controlled by changing the current flow through the active layer. However the performance of gain guided lasers may be degraded due to their undesirable characteristics which are described next.

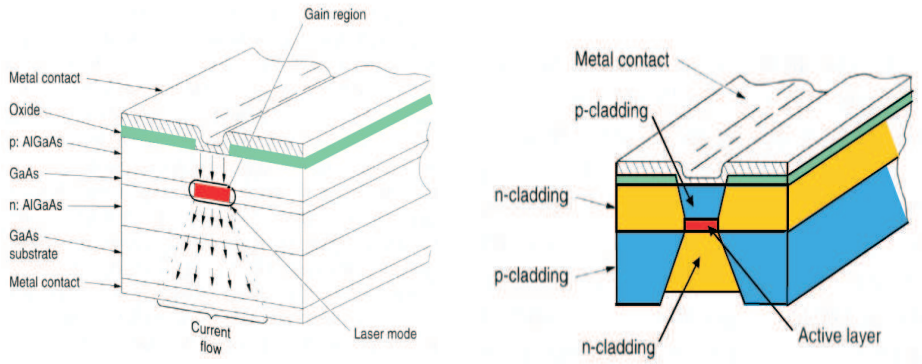

Figure 2.2: **Index guided and gain guided semiconductor laser**

The degree of ellipticity of the output beam from the diode laser is determined by its guiding mechanism. In an index-guided laser, the guiding mechanism is the same

in both the parallel and perpendicular junction planes. In contrast, a gain-guided diode laser has a gain-guiding mechanism parallel to the junction plane and an index-guiding mechanism perpendicular to the junction plane. The narrow active region of an index-guided laser can generate a tight, coherent beam. Gain-guided lasers generate a broader, less coherent beam which allows them to reach higher optical powers than index-guided lasers but with poorer beam quality.

The development of the double-heterostructure laser (GaAs/AlGaAs) operating at room temperature with continuous-wave output, provided a platform and trigger for many subsequent developments in laser structure through different stripe geometries such as those described above and the multiple quantum well (MQW) structure.

2.3 Theory of the Semiconductor Laser

The detailed theory of the semiconductor laser has been discussed extensively [4, 5, 6]. However, it is useful here to focus on certain features of these devices to understand their applications and their role in the work herein.

2.4 Diode Laser Characteristics

The output of a diode laser is highly susceptible to changes in the temperature and the input current. Figure 2.2 shows the output power of a typical laser as a function of injection current. The abrupt change in slope occurs at the threshold current. At and above this current input, the device is showing laser operation.

The common method of wavelength tuning for the diode laser is to change the temperature of the material. Changes in temperature result in a change of the refractive index of the active medium followed by a change of the optical path length of the cavity which governs the longitudinal cavity modes through interference. In addition,

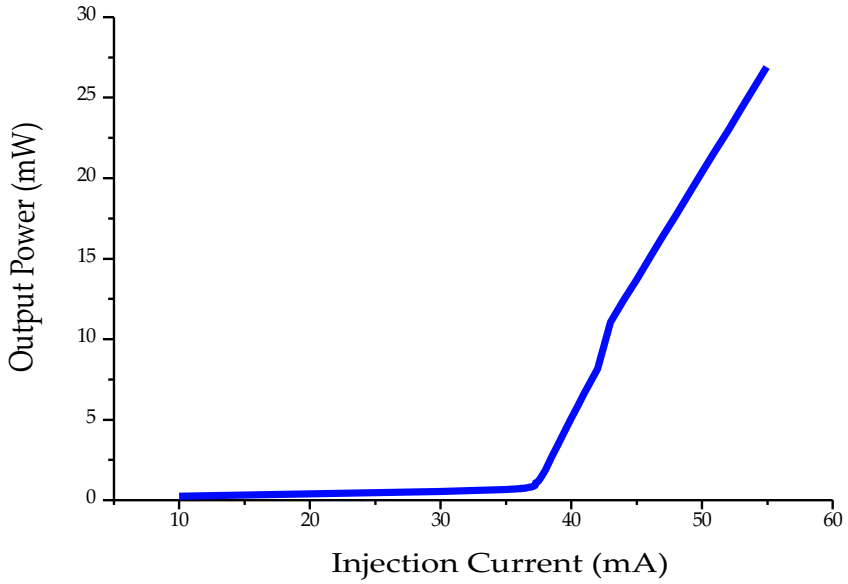

Figure 2.3: **Output Power versus input current for a diode laser**
The sharp change in the slope indicates the threshold injection current and marks the beginning of laser operation.

changes in the gain curves result from the change in temperature. Usually quite different behaviours between the optical path length and shifts in gain curve are the main reason for mode-hops, the major drawback in using diode lasers for measuring the whole absorption spectrum. Changes in the current affect the junction temperature because of Joule heating. Figure 2.3 shows the wavelength variation with tuning of the temperature for a typical diode laser.

The short continuous segments or 'steps' indicate tuning of a single longitudinal mode caused by variation of the optical path length. The steps are caused when the peak of the gain is shifted too far and the laser jumps to oscillate on another mode.

The most valuable advantage of diode lasers is that the wavelength (or frequency) can be tuned very easily and rapidly by coarse variation of the temperature and injection current.

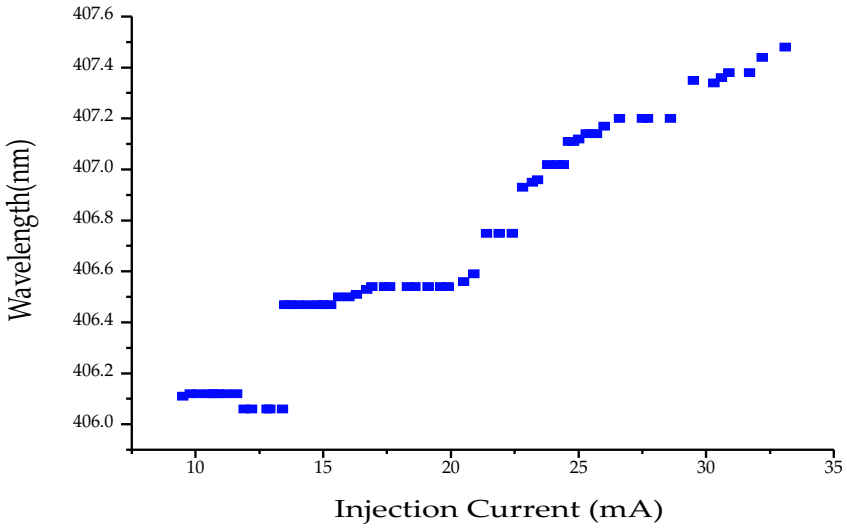

Figure 2.4: **Wavelength versus temperature for a diode laser**
Short continuous segments of similar wavelength values show the tuning of a single longitudinal mode as a result of varying the optical path length.

Spatial Characteristics

The output beam from a diode laser is emitted from a rectangular aperture whose dimensions are of the same order as the wavelength of the emitted light. This results in diffraction of the beam through the aperture and thus a large divergence. A typical output beam has a divergence angle of 30^o in the parallel and 10^o in the perpendicular direction. This beam is then collimated using a lens with a short focal length to give an elliptical profile shown in Figure 2.5.

If a circular beam profile is required, beam shaping optics can be included in the optical system using prisms, cylindrical lenses or fibre coupling. Recently, microlensed diode lasers that provide inherently circular beams have been developed and are described in Section 2.7. A circular output beam is required for many of the applications described throughout this thesis.

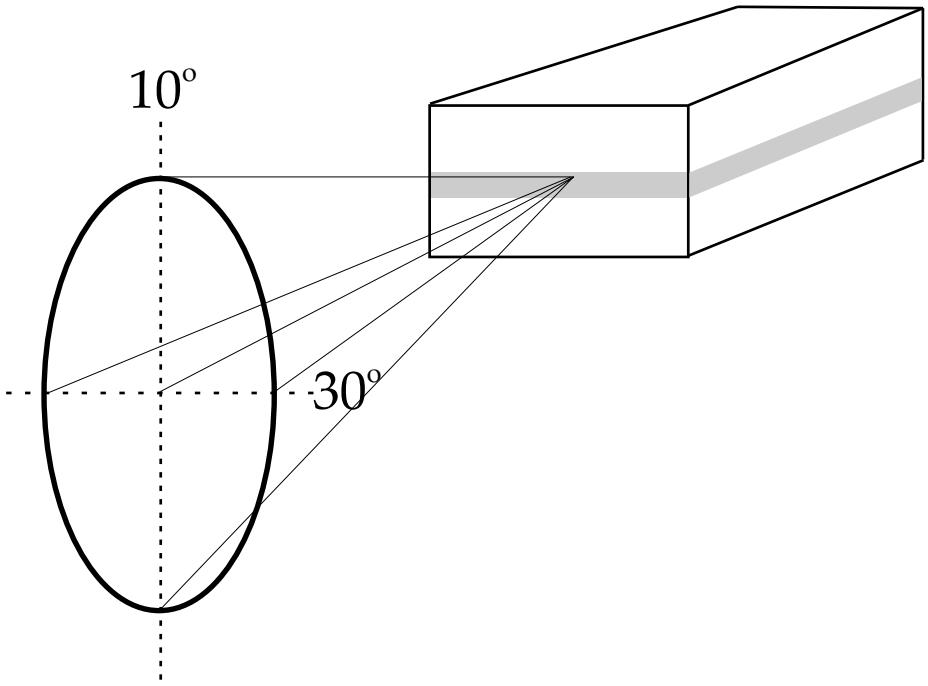

Figure 2.5: **Elliptical Beam Output from Diode Laser**

Linewidth Characteristics

The resonating cavity, formed by the cleaved facets of the diode laser supports longitudinal modes defined by the free spectral range (FSR) of the cavity with the laser outputting one or more modes. At low powers, just above threshold, it is common for the laser to run multimode. As the injection current increases the effect of competition between supported modes increases, with one or two modes dominating.

Linewidth broadening is caused by two mechanisms - 'technical' noise caused by external noise such as mechanical vibrations of the laser cavity and the 'fundamental' broadening, caused by quantum fluctuations.

Tuning Characteristics

The wavelength of a diode laser is primarily determined by the bandgap energy of the semiconductor material used. However, smaller changes in the wavelength can

be obtained by varying the temperature and operating current of the diode laser. This coarse tuning capability is one of the diode laser's most powerful features and is exploited widely in the applications discussed in this thesis. This tuning capability offers considerable control over the device, allowing tailored systems to be developed within the limits of the structure and material composition.

The variation in wavelength with temperature and injection current has a 'staircase' type pattern with a period of continuous change followed by a mode hop. The slope of each step represents the tuning of that particular cavity mode whilst the jump represents hopping from one mode to another. In the continuous tuning region the wavelength is precisely tunable via fine control of the temperature and current. A linear relationship is especially desirable for spectroscopic applications. Mode hopping forces wavelength jumps along several modes and prevents continuous tuning. Mode hops are caused because the change in the laser gain spectrum is greater than the wavelength of the cavity mode.

2.5 Limitations of Semiconductor Diode Lasers

Solitary diode lasers are characterised by multimode operation and have large linewidths due to a short photon cavity lifetime and strong coupling between the phase and amplitude of the intracavity optical field. Temperature and current tuning have limited ranges and cannot access all spectral regions. This means that it is not possible to fully exploit the broad semiconductor gain bandwidth with temperature and current tuning. The continuous tuning range of a commercial diode laser is limited by mode hops which occur because the cavity length cannot be tuned synchronously with the gain profile. Other disadvantages include limited output power, sensitivity to current and temperature changes, sensitivity to randomly phased feedback radiation and acoustic vibrations. The frequency instability and susceptibility of diode lasers to mode hopping limit their long term stabilisation.

2.6 The Blue Diode

Diode lasers emitting in the IR, mid IR and red visible region have been in mass production for the last two decades. Their characteristics are well known and they are in widespread use within research, industrial and commerical applications. There are circumstances where the longer wavelength light is not always appropriate for use and the desire to have diode lasers emitting at shorter visible wavelengths motivated much research into development of these devices.

In 1996 Nakamura and colleagues reported room temperature operation of an Indium gallium nitride (InGaN)-based multiple quantum well (MQW) providing at that time the shortest wavelength from a semiconductor at 417nm [7]. Further research yielded C-W operation and commercialisation of this diode.

Nakamura's achievement in successfully manufacturing a laser emitting in the blue region of the spectrum was particularly notable as the development of diode lasers that emit in the shorter wavelength visible region had lagged behind the longer wavelength diode lasers due to problems with the semiconductor structure. Additionally the experience with longer wavelength diode laser devices had already guaranteed market and commercial success with these new devices.

Several materials were investigated in the process of developing a blue laser diode. It had been impossible to achieve room temperature operation from a C-W diode laser at this wavelength. The major reason for this was due to problems in the characteristics of the materials used. Zinc Selenide (ZnSe) had a very high number of crystal defects which resulted in excessive non-radiative recombination of electrons and holes. These defects cause overheating and eventual breakdown of the device. III-V nitrides such as GaN exhibited low carrier concentrations which meant that sufficient population inversion to achieve laser operation was unobtainable. The development of these devices followed great effort in amending the growth processes to prevent defects and increase carrier concentrations [8].

A tunable diode laser emitting in the violet/blue region offers many new opportunities for applications. Previously, researchers wanting to perform experiments had limited options in obtaining a tunable C-W source of blue light. There were three possibilities; optical parametric oscillators (OPOs) [15], a Ti:Sapphire laser [10] and frequency doubled semiconductor lasers [11].

The structure of the Nichia Indium Gallium Nitride (InGaN) multiple quantum well (MQW) laser is shown in Figure 2.6.

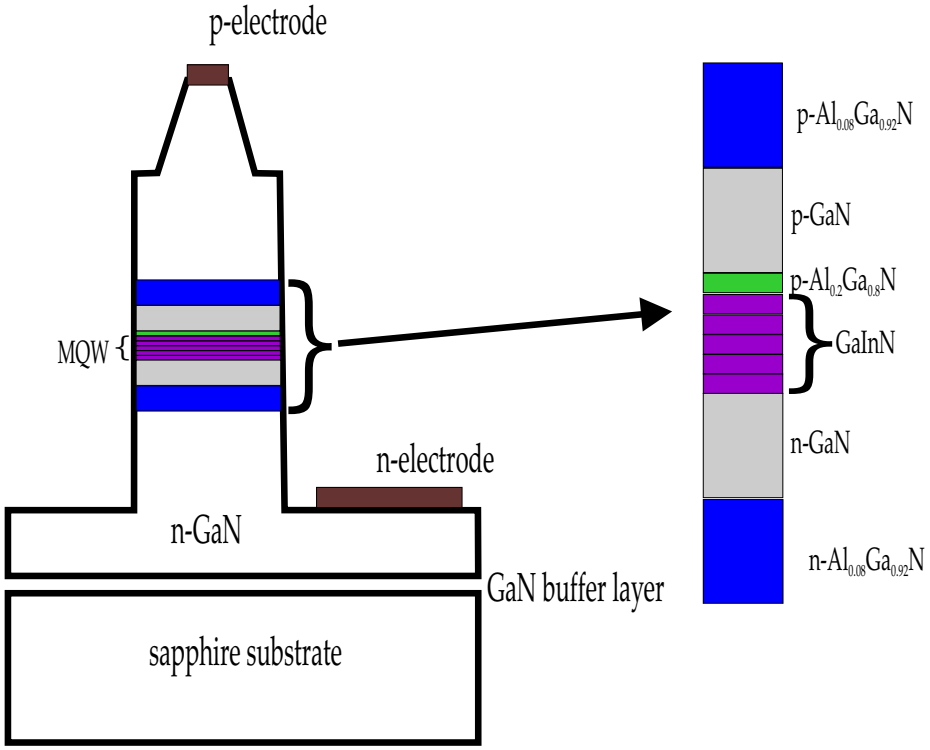

Figure 2.6: **Structure of Blue Diode Laser**
Diagram showing the GaN layer arrangement in a Nichia diode laser with an MQW structure (reproduced from [12])

The layers surrounding the MQW structure exist to minimise the defects in the crystal and aid carrier confinement and stimulated photon emission. This overcomes the two major problems in achieving a device emitting at these wavelengths. The n and p-type GaN layers that surround the MQW are used for guiding whilst confinement is achieved by the n and p-type AlGaN layers. This structure forms the basis of the first Nichia diode laser with the lowest wavelength generated from an electrically pumped

diode laser [7].

Since their first demonstration the blue lasers have developed rapidly, with operating characteristics and lifetimes improving considerably (typical output powers now are 40mW compared with 15 mW from the first demonstration) and their properties are being further developed for a wide variety of applications.

2.6.1 Applications using blue diode lasers

The main market for violet laser diodes is optical data storage, however the combination of their short wavelength and coherence enhancement schemes for generic diode lasers have meant that they have been successful in applications in atomic physics and chemistry for trace gas detection, offering an alternative to complicated frequency conversion techniques that have been traditionally used to access the short wavelength region.

Although the characteristics of blue diode lasers for atomic and molecular spectroscopy are similar to those of the red and near-IR diode lasers, their relative infancy has meant that to date there are far fewer spectroscopic applications. This has provided a new and potentially fruitful area of investigation adding to the already significant body of work in tunable diode laser spectroscopy.

Blue diodes operating below 420nm have been used to access a number of different trace gases and elements, and more recently lasers emitting in the 420-450nm range have been applied to similar studies. The first instance of the use of violet diode lasers for spectroscopy was in the study of pottassium [13]. More recently blue diodes have been used in spectroscopy of gallium atoms within a hollow cathode discharge lamp (HCL) [14]. A stabilised blue diode has been used for spectroscopy of rubidium atoms within a cell [15] and blue diode lasers have been used for absorption spectroscopy of aluminium atoms in a hollow cathode discharge [16]. Violet diode lasers have been used in atom and ion cooling experiments [17].

Violet diodes operating above 420nm have been less prevalent in spectroscopic studies. For those applications requiring wavelengths around 450nm frequency conversion systems have been used. Diode lasers are an attractive alternative to these systems. Recently spectroscopy of indium at 450nm has been carried out and subsequently laser induced fluorescence of indium within a flame has been sucessfully done [18].

2.7 Feedback in Diode Lasers

One of the unique features of diode lasers relative to other lasers is their high sensitivity to optical feedback arising from a number of factors. Firstly, the gain curve is a very flat function of wavelength; secondly, the cavity finesse is quite low; thirdly, the cavity is very short. As a result, the overall gain of the system has an extremely weak dependence on wavelength and there are relatively few photons in the cavity causing the lasing frequency to be easily perturbed.

Optical feedback affects the output from a diode laser. Feedback is achieved by creating a cavity external to the diode's own front and back facets by using an extra optical element to return a fraction of the output light back to the diode. The laser adopts those characteristics defined by the extended cavity whilst the diode provides optical gain. Optical feedback can have both detrimental and beneficial effects on the performance of a diode laser. In most cases unwanted reflections returning to the laser cavity can be eliminated by an optical isolator. Feedback into diode lasers can sometimes contribute to further instability in the system.

The major benefits of frequency selective optical feedback include single mode operation, increased tunability, narrow linewidth and increased frequency stability. Several stabilisation methods have been implemented, which couple the laser to an external, high Q cavity or to a diffraction grating. In the first case, a proportion of the output beam is coupled back to the diode laser. This geometry provides linewidths typically below 10kHz but the method is technically complex. In contrast the use of a diffrac-

tion grating in the geometry achieves linewidths of order 100KHz which is sufficent for the experimental applications and far simpler to realise. The level of feedback tolerance is dependent on the application of the laser. Lasers that have an AR coated output facet are more sensitive to optical feedback than uncoated lasers. Conversely, lasers using strong optical feedback to control the wavelength are correspondingly less sensitive to unwanted feedback.

2.8 Diode lasers with a circular output beam

Some of the issues regarding the spectral and spatial beam quality of the elliptical output beam from a laser diode have recently been addressed by the development of laser diodes which have a circular beam output [19]. Microlensed diode lasers (MDLs) have an incorporated cylindrical glass microlens which is used to improve the spatial profile of the diode laser. A schematic of the MDL is shown in Figure 2.7. A microlens acts as a simple reflecting element which returns light back to the laser diode at an angle similar to that incident upon it. This does not affect the spectral profile of the device. The resulting improvement in the beamshape and quality means there are fewer beam shaping optics required in an optical system, thus minimising power loss through the system and allowing the opportunity to maximise non-linear frequency conversion. In addition, the introduction of the microlens encourages single longitudinal mode behaviour by incorporating a small amount of feedback into the laser from the reflection off the back facet of the microlens [20]. The MDL configuration results in the creation of an effective external cavity, the effect of which is described in Section 2.11, which encourages narrow linewidth and single longitudinal mode operation. Although the microlens provided optical feedback similar to a diffraction grating, the crucial difference between the methods is the lack of a mechanism of wavelength selectivity with the microlens.

The microlens is a cylindrical glass lens ($\sim$ 250microns thick) which is located approximately 50 microns from the diode laser facet. The lens has a high numerical

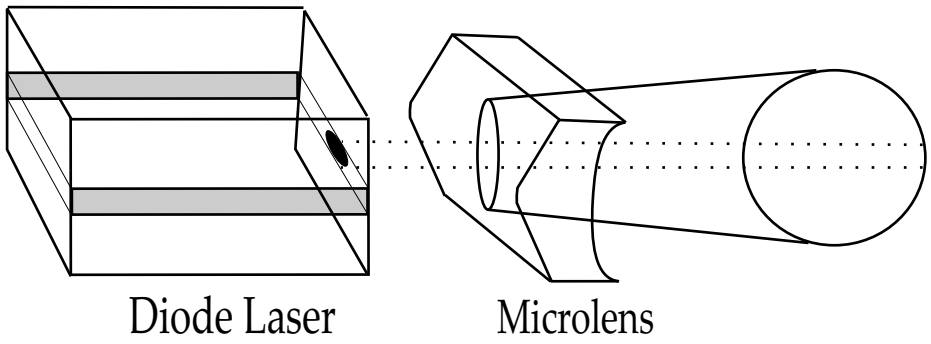

Figure 2.7: **Microlensed Diode Laser**
The microlens acts to beam shape the output from the diode and results in a circular beam. In addition a small amount of feedback from the lens into the diode encourages oscillation on a single longitudinal mode.

aperture (NA) (~ 0.7) which maximises the capture of the entire output beam thus ensuring maximum efficiency when the power is converted when the beam is shaped. The microlens improves the astigmatism of the beam, because the output facet of the diode laser is the same size in both axes. In a standard diode laser assembly the output facet is greater in one axis than the other causing two foci for the x and y planes of the beam. This effect is diminished with the use of a microlens.

The extended cavity effect observed with an MDL means that the issue of competition between modes within the cavities is a consideration. We expect that the tuning range will not be as large as for a standard diode laser due to this external cavity effect [19]. However it has been proven that competition at near IR wavelengths is not detrimental to the laser operation [20] and now we have shown that this is also the case for more challenging diodes emitting in the red and violet region of the spectrum [19, 21].

The use of microlensed lasers has the potential to improve on spectroscopic work that has already been performed using their predecessors. In Chapter 5, the spectroscopy of mercury using microlensed diode lasers is described, and the significant improvements upon previous work are a direct result of the use of microlensed diode lasers. Notably, we have demonstrated in previous work that such microlensed diodes may be operated in extended cavity mode with a grating offering exceptionally low linewidths

suitable for laser cooling and spectroscopy [19]. This study shows that there is limited influence in extended cavity mode from any competition between the grating and the microlens. A violet microlensed diode laser is characterised and compared to a red microlensed diode laser in [21] and their use in spectroscopic applications is described in [22] and in Chapter 5 of this thesis.

2.9 Single Frequency Lasers

Different methods have been investigated to reduce the linewidth of diode lasers and achieve single frequency operation. The most significant of these include the distributed-feedback arrangement (DFB) Figure 2.7(a), distributed Bragg-reflector (DBR) Figure 2.7(b), cleaved coupled cavity(C3) Figure 2.7(d) and the external wavelength selective feedback method (ECDL) Figure 2.7(c).

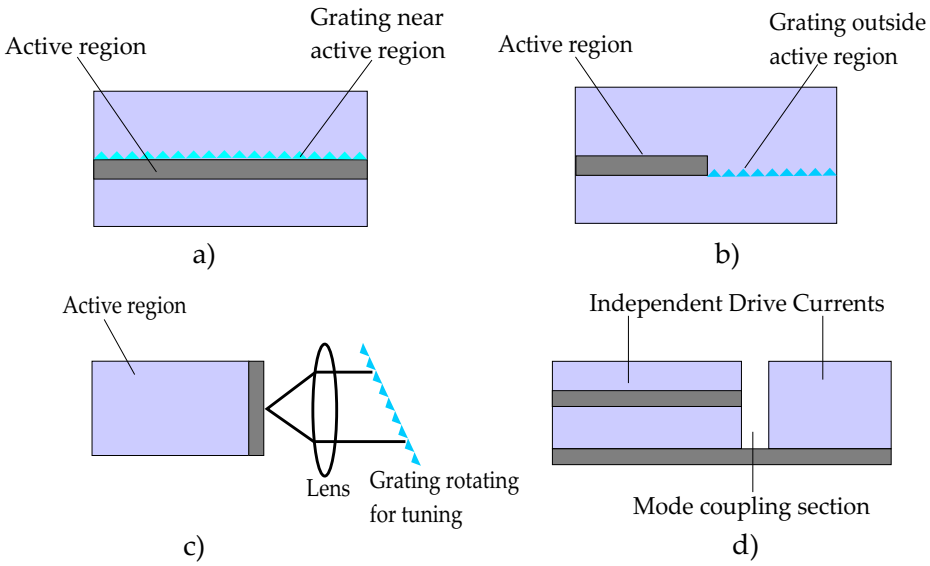

Figure 2.8: **Principle Designs of Single Frequency Diode Lasers**
a) DFB laser; b) DBR laser; c) ECDL; d) Coupled Cavity Laser;

Distributed Feedback (DFB) Laser

To improve the longitudinal mode selection DFB lasers were developed. The feedback necessary for the lasing action is distributed along the cavity length using a grating etched so that the thickness of the active layer varies periodically along the cavity length. The grating reflects a little light over each period of the grating until there is no more light at the back of the grating. Since the light is being reflected by the grating the reflected light is always in the correct phase no matter from which portion of the grating it was reflected. DFB lasers have a periodic, spatially-modulated gain, with strong selectivity for the wavelength that matches the period of the gain modulation and lase in the same single longitudinal mode from threshold up to the maximum operating power. DFB lasers typically have linewidths of 1-10MHz. Tuning of a DFB laser can be achieved through either thermal or electrical tuning. This adjusts the effective grating period.

By far the largest application of distributed-feedback lasers is in fiber optic transmission systems. Most DFB lasers sold commercially have typical output powers range from 1 to 35 mW in the fiber. A small number are used for various interferometric or spectroscopic applications. Distributed-feedback lasers have been demonstrated for such applications at wavelengths from 633 to 2000 nm and beyond [23, 24].

Distributed Bragg Reflector (DBR) Laser

The distributed Bragg reflector (DBR) laser adopts the same concept of DFB lasers but the grating is etched outside of the active layer. The Bragg reflector is a volume grating providing wavelength selective feedback at one end of the cavity. These lasers lase on a single longitudinal mode but the lasing hops between longitudinal modes to stay near the peak of the reflectivity of the Bragg reflector as temperature and current are changed.

The grating encourages the distributed-feedback laser to operate single frequency.

More complicated laser structures combine gratings with grating-free waveguide regions and two or more contacts to give monolithic tunable lasers. The distributed Bragg reflector (DBR) laser replaces one of the facets of a Fabry-Perot laser with a grating similar to that of the DFB. It provides higher CW powers than an equivalent DFB laser, at the cost of introducing mode hops with drive current. Addition of a second contact to the grating region gives wideband tunability. DBR lasers are used for various spectroscopic and instrumentation applications [25].

Cleaved Coupled Cavity Laser

The coupled cavity laser structure consists of two independent cavities that are fabricated in close proximity to one another. The cavity lengths are similar so there is no mode competition and as such the C3 laser is very stable and resistant to mode hops.

The C3 laser is manufactured from a single piece which is then cleaved to create the two cavities. The base electrode remains in tact and as such the two cavities are in perfect alignment. The current to each portion can be applied separately and in practice one portion is kept above threshold, acting as the laser whereas the other portion is operated below threshold but sufficiently strong to alter the carrier density and thus the refractive index of the cavity. This allows tuning of the frequency over a wide range.

2.10 External Cavity Diode Lasers (ECDLs)

The design that is used throughout the work described here is the external cavity diode laser which is a method used to improve the spectral purity and tuning range of a diode laser. By using the diode as the gain medium within a longer external cavity, the cavity length formed by the cleaved facets is extended to the length of the

external cavity. A free running diode laser is a high gain device with a very low cavity finesse producing a relatively large fundamental linewidth as the linewidth is inversely proportional to the photon lifetime in the cavity. High reflectivity mirrors will increase the photon lifetime thus also reducing the linewidth of the laser. Typically, free running laser diode sources emit over a band perhaps 10-15MHz wide, but with this ECDL configuration a linewidth as small as 1MHz or less may be achieved, more than sufficient to resolve the natural linewidth of an atomic transition.

A tunable external cavity laser comprises an optical gain medium (e.g a diode laser), optics to couple the output of the gain medium to the free space mode of the external cavity, wavelength selective filters and one or more mirrors that define an external feedback path, with the use of a piezoelectric transducer (PZT) for fine tuning. The crucial determinant for desired operation of the ECDL is the separation between the optical elements.

2.10.1 Diffraction Gratings

Diffraction gratings are mechanically tuned filters used in spectrographic equipment as the principal optical element to separate light into its component wavelengths by diffracting them at various angles. Dispersion of light from a grating can have the effect of narrowing the linewidth of the laser and allows a degree of wavelength selectivity across the gain bandwidth of the laser material. A small portion of light is returned to the diode from the diffraction grating, the wavelength being dependent on the angle of the diffraction grating. There is often a difference between the grating stabilised wavelength and that of the free running diode.

The behaviour of the diffraction grating is governed by the grating equation:

$$\alpha(sin\theta_i + sin\varphi_m) = m\lambda \tag{2.1}$$

where α is the grating spacing, θ_i is the incident angle, φ_m is the diffracted angle of the m^{th} order and m is the order of diffraction. When light of wavelength λ is incident on a grating at a certain angle, there is a unique set of diffraction angles at which light leaves the grating with reinforced intensity. At other angles the intensity of the light is reduced. The diffracted light is dispersed, with different wavelengths appearing at different angles. By differentiating the grating equation we obtain an expression for the angular dispersion D which describes the variation in the diffraction angle with the wavelength.

$$D = \frac{d\varphi_m}{d\lambda} = \frac{m}{\alpha cos\varphi_m} = \frac{(sin\theta_i + sin\varphi_m)}{\lambda cos\varphi_m} \tag{2.2}$$

When a beam of light is incident on a grating, each groove generates a diffracted wavelet. For each wavelength in the incident beam the constructive interference of the diffracted components from each groove occurs at a unique set of discrete directions called the orders of the grating. In ECDLs, diffraction gratings are normally operated in the first order, i.e *m=1*. The *m=0* order is sometimes used for output coupling. An ECDL will operate on a single external cavity longitudinal mode without the need for active stabilisation. The degree of available modes is determined by the ratio of the external to the solitary cavity lengths.

There are two major external cavity configurations, the Littman-Metcalf and the Littrow. In both designs a diffraction grating is used to control both the emission wavelength and the selection of a single longitudinal mode of oscillation of the laser diode. This ensures single frequency operation, vital for high-resolution spectroscopy. The Littman-Metcalf external cavity geometry, shown in Figure 2.9 consists of a laser diode, diffraction grating and a tuning mirror.

The first order diffraction beam is directed towards the tuning mirror where it is reflected back and returned to the laser diode via a second pass of the grating. The zeroth order diffraction beam is coupled out of the laser. The benefits of this configuration is that the beam angle and position remain constant as wavelength tuning is

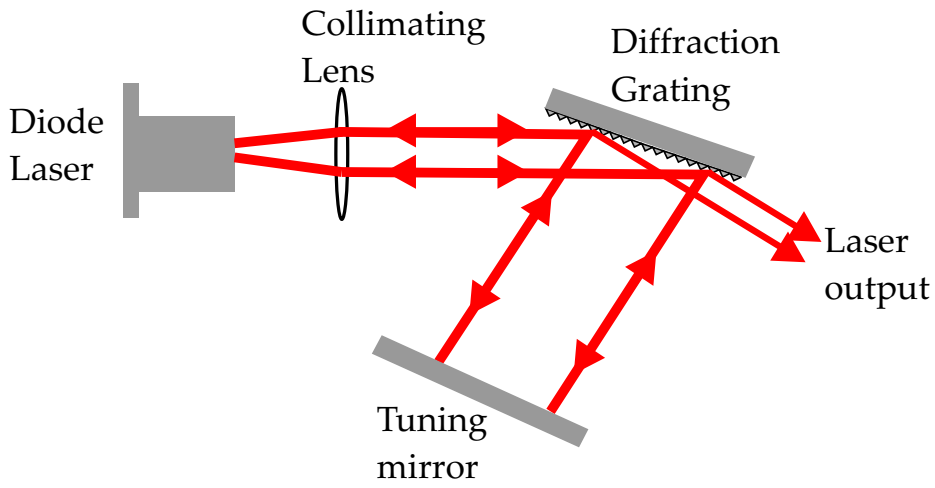

Figure 2.9: **External Cavity Diode Laser in Littman-Metcalf Configuration**

achieved via rotation of the tuning mirror.

The Littrow configuration, described next, is used throughout the work here both in commercial and home built systems.

2.10.2 Littrow ECDL Geometry

The Littrow extended cavity geometry was first incorporated within a diode laser system by Fleming *et al* [26]. This followed on from the successful demonstration of the grating tuning by Hänsch in 1972 [27] using a pulsed dye laser. The schematic of the geometry when used with diode lasers is shown in Figure 2.10.

In this design, the first order diffraction beam of the grating is directed back into the laser diode. The zeroth order diffraction beam is coupled out of the laser. One of the advantages of the Littrow ECDL is that it is possible to achieve much higher output power with more straightforward alignment than the Littman-Metcalf ECDL. A major disadvantage, however, is a shift in the position of the beam whilst attempting to tune the wavelength by adjusting the grating angle.

A standard diode laser in Littrow configuration can be coarsely tuned over its gain

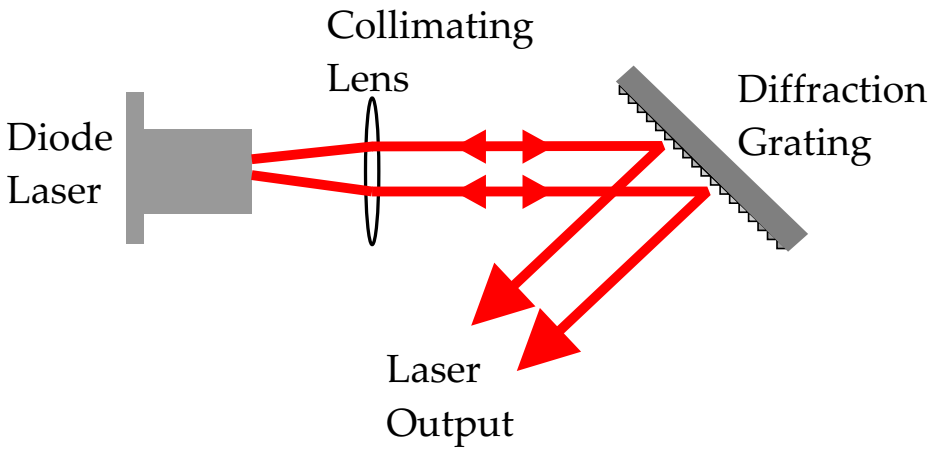

Figure 2.10: **External Cavity Diode Laser in Littrow Configuration**

bandwidth through rotation of the grating. It will generally emit at a single narrow linewidth longitudinal mode, and exhibits a much better spectral stability than the free running laser.

Coarse tuning is achieved by rotating the mirror mount about the pivot point. Fine tuning is possible by the use of a piezoelectric transducer (PZT) beneath the adjustment screw which then influences the motion of the grating and thus the length of the extended cavity. A voltage is applied to the PZT and by varying the cavity lengths in the same ratio, which assists with achieving large tuning ranges. To obtain large, continuous tuning, the cavity length and the gain dispersion should be varied synchronously, supporting the same mode over all wavelengths. Single mode oscillation is achieved by having one extended cavity mode coincide with one peak of the diode laser transmission.

To avoid mode-hops during tuning, the length of the external cavity must be changed in synchronicity with the grating angle to preserve the number of cavity modes. Furthermore, the position of the active diode laser mode must be tuned at the same rate as the extended cavity mode, to preserve the mode overlap. Normally the synchronized cavity length variation and grating angle tuning is achieved by fixing the grating element to a mechanical arm, which is allowed to rotate around a pivot point, located at the intersection of the grating plane and the diode laser back facet plane.

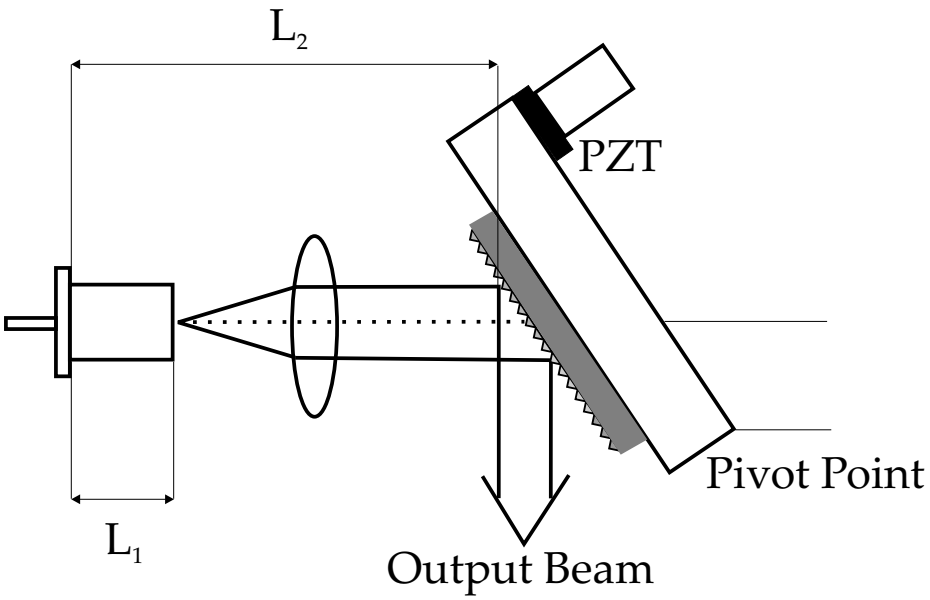

Figure 2.11: **Cavities in the Littrow ECDL**
There are two cavities present in the Littrow geometry; L_1 is the solitary diode cavity and L_2 is the extended cavity.

A schematic of this is shown in Figure 2.11. To achieve long, mode-hop free tuning ranges, the output facet of the diode is normally AR coated, to suppress the diode mode structure. There are two problems with this design, the first being that a custom made mount is needed, allowing for precise adjustments of the pivot point position of the ECDL grating. Second, the application of a custom made anti-reflection coating is an expensive process which furthermore risks damaging the diode laser unit.

To fully understand the combination of the solitary and extended cavities, it is useful to look at the relationship between the grating dispersion, the solitary diode mode structure and the extended cavity mode structure. There is inherent competition between the modes within the two cavities. Figure 2.12 shows how the competing factors come together to determine the operating wavelength of the laser.

It is clear that there are numerous possible external cavity modes under the broad gain curve of the solitary laser, but the grating selectivity allows the selection of one of these modes. For a given incident angle the maximum spectral gain and grating selectivity aligns with one of the external cavity modes.

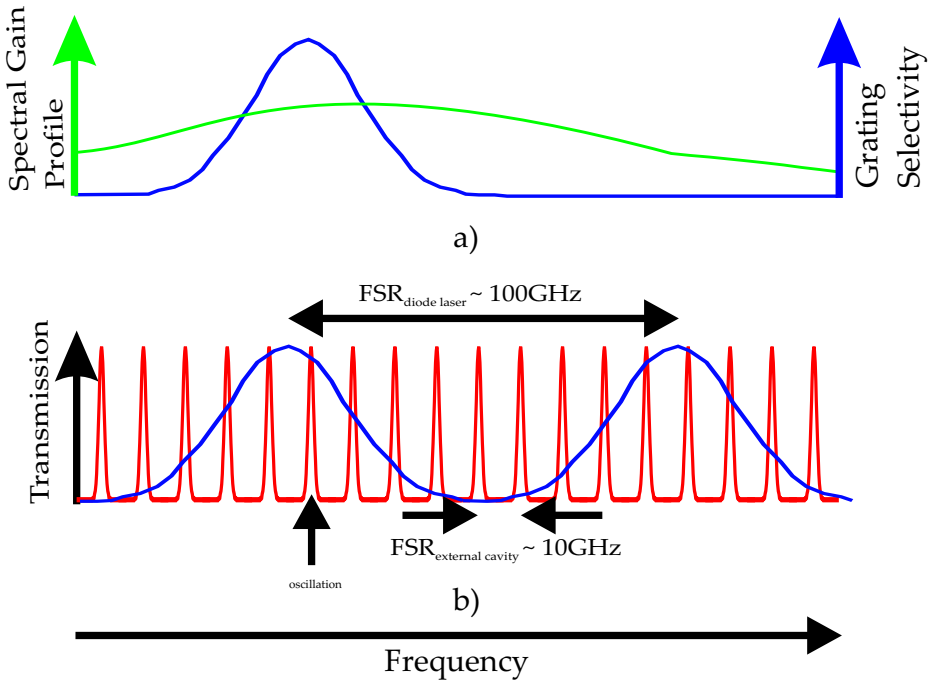

Figure 2.12: **Competition between cavities within the Littrow configuration** A representation of the competing processes that occur when there is the external cavity and feedback from a diffraction grating. The spectral gain profile of the laser (green line) and the grating selectivity (blue line) are shown in (a) whilst the modes that can be sustained within the diode laser and the extended cavity are represented by the blue and red lines respectively in (b). Figure reproduced from [12]

It is now possible to build successful ECDL systems without the need for anti-reflection (AR) coating of the back facet of the laser diode. This in turn removes the need for custom precision mounting apparatus thus making ECDLs within a home built system practical and more affordable.

Ricci *et al* [28] outlined the reasoning behind a shorter external cavity in their work. The choice is a tradeoff between a narrow linewidth and wide bandwidth. The use of a short external cavity allows single mode operation to be obtained without any additional AR coatings on the laser. The design used by Ricci is now adopted in many of the reported uses of ECDLs [15, 29, 19, 30].

2.10.3 Phase Continuous tuning

For continuous mode-hop-free tuning of the ECDL, the number of half wavelengths between the laser cavity mirrors must remain constant whilst the wavelength is varied. There exists both long and short range continuous phase tuning. Short range (few GHz) can be accomplished by adjustment of the cavity length whilst tuning the temperature/injection current of the diode.

The ECDL has two cavities, the first defined by the grating and the back facet of the diode and the second defined by the front and back facets of the diode. To facilitate wavelength continuous tuning, the optical fields in both of these cavities must remain in phase with each other, otherwise the continuous mode-hop-free tuning range is severely limited. Where the phase shift between the two fields is greater than 2π, a mode hop will occur. As the length of the external cavity decreases, the continuous tuning range increases. A variation ΔL of the optical path length L of the external cavity yields a relative frequency detuning given by $\frac{\Delta\nu}{\nu} \cong -\frac{\Delta L}{L}$. The detuning $\Delta\nu$ is inversely proportional to L and therefore a short external cavity will yield large frequency scans and quick scanning rates which can be important in atomic physics experiments.

A simpler and cheap solution to the mode hop problem is to vary the injection current and the angle of the grating simultaneously in a prescribed numerical ratio using an electronic circuit. The ratio is dependent upon the properties of the PZT, the scanning characteristics of the diode laser and the ECDL design [31].

2.11 Stability

The frequency and intensity stabilities of the extended cavity laser are often poor. The frequency is susceptible to fluctuations in environmental conditions that cause thermal expansion of the cavity medium with pressure and temperature. In addi-

tion, mechanical and acoustic disturbances and electrical noise may broaden the laser linewidth typically to a few hundred KHz or even to several MHz, the order of a free-running diode. These effects also influence the output intensity with variations in the losses from the laser cavity. In most ECDL designs there is a trade-off between the rigidity of the device and its adjustability. There are two major stages in stabilisation of lasers, passive stability and active stability.

Passive stability involves adjusting the mechanical design and construction of the device to make the cavity insensitive to external effects. Laser frequency is dependent upon the optical length of the cavity which in turn is affected by any change in the refractive index of the cavity medium (the diode, lens, air) and any changes in physical cavity length. This passive stabilisation is achieved through temperature stabilisation of diode laser mountings, use of materials in mountings that have minimal thermal expansion effects (although this is then balanced by the cost and availability of materials), vibration sensitive mounts and floated optical tables.

2.11.1 Active Stabilisation

For many applications in atomic physics such as trace gas detection and laser cooling and trapping it is desirable to keep the laser frequency stabilised at or near the atomic resonance for long periods of time. There are several techniques that have been proposed to help stabilise or 'lock' the output of the ECDL to a particular wavelength. These techniques include side-of-fringe locking, top of fringe known as Pound-Drever locking [32, 33] and dichroic atomic vapour laser locking (DAVLL) [34, 35]. For an ECDL stabilisation system to be effective it must involve a fine tuning mechanism by which the laser frequency may be adjusted and a frequency reference by which any drift in the frequency can be assessed and corrected. Fine tuning can be achieved by current modulation or cavity length variation. Transmission peaks from stable cavities such as Fabry-Perot etalons [36, 37], and molecular and atomic absorption lines are commonly used as frequency references [38]. Frequency locking is typically

implemented by applying a small frequency modulation or 'dither' to the laser to generate the first derivative of the transmission or absorption peak. By applying negative feedback the laser can then be locked to the zero error of the derivative signal. The laser frequency can be locked to either the peak, (peak locking) or a side of one of these transitions, (side-of-fringe locking). Side-of-fringe locking delivers a simple lock using elementary electronics whilst allowing a variation in the locking frequency over the width of the locking slope. Peak locking provides a more robust solution at the expense of more complicated electronics and being unable to vary the locking frequency without additional optics.

Servo-locking Loop

A servo locking system allows negative feedback to be applied to stabilise a laser to a particular frequency. A basic servo-loop is shown in Figure 2.13. The system requires a signal and a reference to compare it to. The reference can take the form of a stable optical cavity or, as in this case, an atomic transition. There is a perturbation in the laser in the form of noise which causes the frequency to vary over time. The comparison between the two signals is used to create an error signal indicating how far the signal frequency is from the reference, which is fed through compensation electronics to create a negative feedback loop. The feedback signal is used to cancel the effect of perturbations in the laser operation and return the laser to operation at the reference point.

In an ECDL, the method of feedback is the piezo-electric transducer (PZT) which is attached to the cavity grating. In some laser locking scenarios it is possible to employ two servo systems simultaneously, one with a fast response and one with a slow response to correct for noise across an increased frequency range. In ECDLs, the PZT corrects for slow drift and the current compensates for high frequency noise. This is known as current/PZT locking. This is a similar theory to the use of current/PZT variation in achieving mode-hop-free tuning ranges.

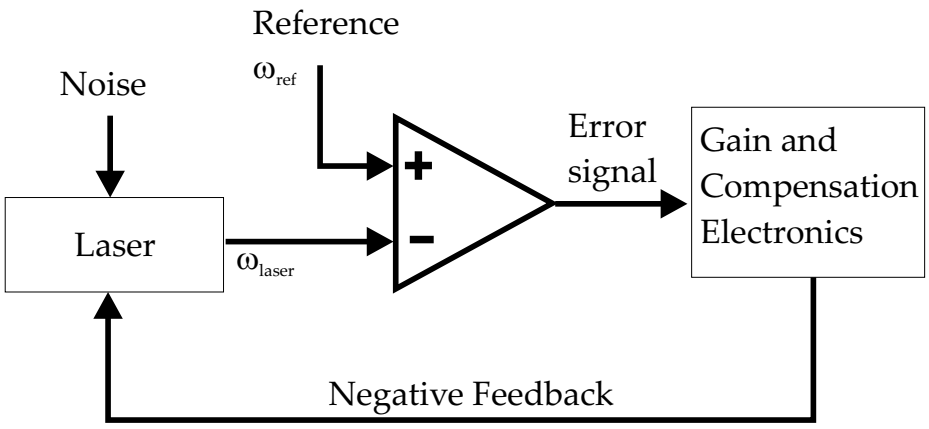

Figure 2.13: **Schematic of basic servo loop**

PID Locking

A laser can be stabilised using a control that incorporates locking electronics into the control box of the laser. This proportional, integral, differential stabilisation circuit (PID) automatically feeds back to the laser scan and current control circuits [39]. The PID lock is referenced to a DC value that is set by finding an appropriate point where it crosses the absorption signal.

To achieve stabilisation the scan rate of the laser is reduced to minimum value and the PID circuit is then used. The regulator scans the PZT across a range and it will stabilise when the lockpoint and the reference level coincide. If this reference level is not found then the process begins again and the PID continues to scan the PZT until the appropriate signal level is obtained.

The parameters of the PID are adjusted to fine tune the circuit to focus in on the reference lock point. This is a trick used to find an appropriate operating point when the servo locking range is limited. The PID levels are set by adjustment of potentiometers. Once the coarse scan range was set the integrator (I) contribution is first adjusted, increased from zero to the point at which oscillation in the error signal is achieved, then reduced to just below the point at which oscillation occurs. A similar scheme is then adopted for the proportional (P) and derivative (D) controls.

The levels of these contributions are reduced to the point just below where feedback starts to have an effect. This is a measure taken to avoid the laser jumping across the scan to other points where the reference and signal may coincide that may not be across a frequency reference feature.

2.12 Applications

Single-mode continuous-wave (C-W) laser sources with wide wavelength tuning ranges are very useful for high resolution spectroscopy. Applications range from laser cooling to trace gas analysis, industrial process monitoring and combustion diagnostics. For such applications it is essential that tuning is continuous and free from mode-hops. When an enhancement scheme such as the extended cavity is implemented the output from diode lasers satisfies the requirements for these varied applications.

Optical data storage, consumer electronics, telecommunications have all found uses for diode lasers within their systems, bolstering the commercial market for these lasers and in turn further influencing the direction of research in both industry and academia.

2.12.1 Optical Communications

Coherent optical communications systems require single frequency narrow linewidth sources. Commercially, ECDLs play an important role in the test and measurement of components for optical communications systems, such as filters, couplers and isolators in wavelength division multiplexing (WDM) systems [40], measuring the wavelength dependence characteristics and isolation of these devices. Dispersion and polarisation measurements in optical components have also been made using ECDLs [41, 42].

2.12.2 Biological Applications

The use of lasers within biological applications has flourished in recent years, forming its own area of study known as biophotonics. Diode lasers have found many uses in this area both within diagnostic equipment and in studies of behaviour of biological samples [43, 44]. Laser spectroscopy is used widely in biology to identify characteristics of samples, an application of which, involving Raman tweezers spectroscopy, is described in Chapter 5.

Diode lasers have now replaced traditional Argon-ion and dye lasers as the source used in confocal microscopy assemblies. To be able to excite many of the common fluorospheres, blue or UV light was required which had been obtained from Argon-ion lasers. These sources were unsuitable for a number reasons but the introduction of violet diodes has allowed their use in a variety of confocal microscopes [45], overcoming many of the limitations seen as a result of the original laser sources.

2.12.3 Atomic and Molecular Applications

Diode lasers in extended-cavity configurations have been extensively for detailed atomic and molecular spectroscopy [46, 47, 29, 48, 49] They have also been used successfully in laser cooling of rubidium, caesium and lithium [50, 51]. This has underpinned studies of Bose-Einstein condensation and Fermi gases in these elements [52].

For most absorption spectroscopy measurements the spectral characteristics of the laser beam such as linewidth and tuning capability are more important than the spatial characteristics. Tunable diode laser spectroscopy is a wide ranging and highly successful technique, that is now used routinely for trace gas detection, frequency standards and atomic clock measurements [53, 54, 55] to pollution monitoring and environmental detection [9].

Rapid wavelength modulation capability is at the heart of diode laser based modulation spectroscopy for trace element analysis. The ease with which a diode laser can be tuned makes it ideally suited for modulation techniques. Chapter 5 describes this approach applied to the spectroscopy of mercury using diode lasers.

2.13 Summary

This chapter has described how semiconductor diode lasers have been developed to become ideal devices for a wide variety of applications. The benefits of a diode laser within an external cavity that emits a high quality circular beam can be easily seen. The narrow linewidth and broad tuning range creates a tool that fulfills the stringent requirements of laser spectroscopy. The work described in this thesis is wholly based upon applications of ECDLs where the benefits of an external cavity configuration are key to the success of the application. The successful demonstration of the violet emitting diode laser has opened several new applications, some of which are described herein. Schemes for the stabilisation and coherence enhancement of the output from diode lasers were presented and an overview of the applications that currently employ diode lasers. Overall the chapter shows the versatility of diode lasers and the success and relative ease with which they can be manipulated to suit individual applications.

Bibliography

[1] Y. Watanabe and W. Nishizawa. Semiconductor MASER. Japanese Patent no.273217, 1957.

[2] R.N. Hall, G.E. Fenner, J.D. Kingsley, T.J. Soltys, and R.O. Carlson. Coherent light emission from GaAs p-n junctions. *Physical Review Letters*, 9:366–368, 1962.

[3] M.I. Nathan, W.P. Dumke, G. Burns, J.F.H. Dill, and G. Lasher. Stimulated emission of radiation from GaAs p-n junctions. *Applied Physics Letters*, 1:62–64, 1962.

[4] O. Svelto. *Principles of Lasers*. Plenum Press, 227 West 17th Street, New York, N.Y. 10011, fourth edition, 1998.

[5] A.E. Siegman. *Lasers*. University Science Books, 20 Edgehill Road, Mill Valley, CA, 94941, 1986.

[6] D.A. Neamen. *Semiconductor Physics and Devices*. Richard D. Irwin Inc., second edition, 1992.

[7] S. Nakamura, M. Senoh, S. Nagahama, N. Iwasa, T. Yamada, T. Matsushita, H. Kikoyu, and Y. Sugimoto. InGaN-based multi-quantum-well-structure laser diodes. *Japanese Journal of Applied Physics*, 35(1B):L74–L76, 1996.

[8] Daniel Steigerwald, Serge Rudaz, Heng Liu, R. Scott Kern, Werner Gotz, and Robert Fletcher. III-V nitride seminconductors for high performance blue-green light emitting devices. *Journal of the Minerals, Metals and Materials Society (JOM)*, 49(9):18–23, 1997.

[9] B. Ruffing, A. Nebel, and R. Wallenstein. High-power picosecond LiB_3O_5 optical parametric oscillators tunable in the blue spectral range. *Applied Physics B : Lasers and Optics*, 72(2):137–149, 2000.

[10] Y.-W. Liu and P.E.G. Baird. Measurement of the caesium $6s_{1/2} \rightarrow 8p_{1/2}$ transition frequency. *Applied Physics B: Lasers and Optics*, 71(–):567–572, 2000.

[11] E.U. Rafailov, W. Sibbett, A. Mooradian, J.G. McInerney, H. Karlsson, S. Wang, and F. Laurell. Efficient frequency doubling of a vertical-extended-cavity-surface-emitting laser diode by use of a periodically poled KTP crystal. *Optics Letters*, 28(21):2091–2093, 2003.

[12] Gavin P.T. Lancaster. *Experimental Studies of Diode Lasers and Cold Atom Guiding*. PhD thesis, School of Physics and Astronomy, University of St Andrews, 2001.

[13] U. Gustafsson, J. Alnis, and S. Svanberg. Atomic spectroscopy with violet laser diodes. *American Journal of Physics*, 68(7):660–664, 2000.

[14] O.M. Marago, B. Fazio, P.G. Gucciardi, and E. Arimondo. Atomic gallium laser spectroscopy with violet/blue diode lasers. *Applied Phyiscs B Lasers and Optics*, 77(8):809–815, 2003.

[15] Kazuhiro Hayasaka. Frequency stablisation of an extended-cavity violet diode laser by resonant optical feedback. *Optics Communications*, 206(4–6):401–409, 2002.

[16] H. Scheibner, S. Franke, Samir Solyman, J.F. Behnke, C. Wilke, and A. Dinklage. Laser absorption spectroscopy with a blue diode laser in an aluminium hollow cathode discharge. *Review of Scientific Instruments*, 7(2):378–382, 2002.

[17] G.P.T. Lancaster, H. Haffner, M.A. Wilson, C. Bechner, J. Eschener, F. Schmidt-Kaler, and R. Blatt. Doppler cooling a single Ca ion with a violet extended-cavity diode laser. *Applied Physics B*, 76(8):805–808, 2003.

[18] Iain Stewart Burns, Johan Hult, and Clemens Friedrich Kaminski. Spectroscopic use of a novel blue diode laser in a wavelength region around 450nm. *Applied Physics B - Lasers and Optics*, 79(4):491–495, 2004.

[19] G.P.T. Lancaster, W. Sibbett, and K. Dholakia. An extended-cavity diode laser with a circular output beam. *Review of Scientific Instruments*, 71(10):3646–3647, 2000.

[20] H. Talvitie, M. Merimaa, and E. Ikonen. Frequency stabilisation of a diode laser to doppler-free spectrum of molecular iodine at 633nm. *Optics Communications*, 152(3):182–188, 1998.

[21] A.E. Carruthers, T.K. Lake, A. Shah, J.W. Allen, W. Sibbet, and K. Dholakia. Microlensed red and violet diode lasers in an extended cavity geometry. *Review of Scientific Instruments*, 75(10):3360–3362, 2004.

[22] Antonia E. Carruthers, Tanya K. Lake, Anjali Shah, John W. Allen, Wilson Sibbett, and Kishan Dholakia. Single-scan spectroscopy of mercury at 253.7nm by sum frequency mixing of violet and red microlensed diode lasers. *Optics Communications*, 255(4–6):261–266, 2005.

[23] C.S. Edwards, G.P. Barwood, S.A. Bell, P. Gill, and M. Stevens. A tunable diode laser absorption spectrometer for moisture measurments in the low parts 10^9 range. *Measurement Science and Technology*, 12(8):1214–1218, 2001.

[24] K. Namjou, S. Cai, E.A. Whittaker, J. Faist, C. Gmachl, F. Capasso, D.L. Sivco, and A.Y. Cho. Sensitive absorption spectroscopy with a room-temperature disributed-feedback quantum-cascade laser. *Optics Letters*, 23(3):219–221, 1998.

[25] I.D. Lindsay, B. Adhimoolam, P. Groß, M.E. Klein, and K-J. Boller. 110ghz rapid, continuous tuning from an optical parametric oscillator pumped by a fiber-amplified dbr diode laser. *Optics Express*, 13(4):1234–1239, 2005.

[26] M.W. Fleming and A. Mooradian. Spectral characteristics of external cavity controlled semiconductor lasers. *IEEE Journal of Quantum Electronics*, QE-17(1):44–59, 1981.

[27] T. W. Hänsch. Repetitively pulsed tunable dye laser for high resolution spectroscopy. *Applied Optics*, 11(4):895–899, 1972.

[28] L. Ricci, M. Weidemüller, T. Esslinger, A. Hemmerich, C. Zimmerman, V. Vuletic, W.K önig, and T.W. Hänsch. A compact grating-stabilised diode laser system for atomic physics. *Optics Communications*, 117(5–6):541–549, 1995.

[29] T. Hof, D. Fick, and H.J. Jansch. Application of diode lasers as a spectroscopic tool at 670nm. *Optics Communications*, 124(3–4):283–286, 1996.

[30] R.S. Conroy, J.J. Hewett, G.P.T. Lancaster, W. Sibbett, J.W. Allen, and K. Dholakia. Characterisation of an extended cavity violet diode laser. *Optics Communications*, 175(1–3):185–188, 2000.

[31] C.Petridis, I.D.Lindsay, D.J.M Stothard, and M. Ebrahimzadeh. Mode-hop-free tuning over 80GHz of an extended cavity diode laser without antireflection coating. *Review of Scientific Instruments*, 72(10):3811–3815, 2001.

[32] Eric D. Black. An introduction to Pound-Drever-Hall laser frequency stabilisation. *American Journal of Physics*, 69(1):79–87, 2001.

[33] R.W.P. Drever, J.L. Hall, F.V. Kowalski, J. Hough, G.M. Ford, A.J. Munley, and H. Ward. Laser phase and frequency stabilisation using an optical resonator. *Applied Physics B : Lasers and Optics*, 31(2):97–105, 1983.

[34] M.A. Clifford, G.P.T. Lancaster, R.S. Conroy, and K. Dholakia. Stabilisation of an 852nm extended cavity diode laser using the zeeman effect. *Journal of Modern Optics*, 47(11):1933–1940, 2000.

[35] M.G. Boshier, D. Berkeland, E.A. Hinds, and V. Sandoghdar. External cavity frequency stabilisation of visible and infrared semiconductor lasers for high resolution spectroscopy. *Optics Communications*, 85(4):355–359, 1991.

[36] B. Dahmani, L. Hollberg, and R. Drullinger. Frequency stabilisation of semiconductor lasers by resonant optical feedback. *Optics Letters*, 12(11):876–878, 1987.

[37] A. Hemmerich, D.H. McIntyre, D. Schropp Jr, D. Meschede, and T.W. Hänsch. Optically stabilised narrow linewidth semiconductor laser for high resolution spectroscopy. *Optics Communicatins*, 75(2):118–122, 1990.

[38] Steve Lecomte, Emmanuel Fretel, Gaetano Mileti, and Pierre Thomann. Self-aligned extended-cavity diode laser stabilised by the zeeman effect on the cesium D2 line. *Applied Optics*, 39(9):1426–1429, 2000.

[39] David W. St Clair. Controller tuning and control loop performance (PID without the math: A Primer). Straight Line Control Company Inc., Newark, Delaware. 2nd Edition.

[40] I.H. White, K.O. Nyairo, P.A. Kirkby, and C.J. Armistead. Demonstration of a 1x2 mulitchannel grating cavity laser for wavelength division multiplexing (WDM) applications. *Electronics Letters*, 26(13):832–834, 1990.

[41] Y. Horiuchi, Y. Namihira, and H. Wakabayashi. Chromatic dispersion measurement in 1.55 microns narrow band region using a tunable exernal cavity laser. *IEEE Photonics Technology Letters*, 1:458–460, 1989.

[42] B. Heffner. Automated measurement of polarisation diespersion using jones matrix eigenanalysis. *IEEE Photonics Technology Letters*, 4:1066–1069, 1992.

[43] T.K. Lake, A.E. Carruthers, L. Paterson, M. Taylor, F. Gunn-Moore, J.W. Allen, W. Sibbett, and K. Dholakia. Optical trapping and flourescence excitation with violet diode lasers and extended cavity surface emitting lasers. *Optics Express*, 12(4):670–678, 2004.

[44] L. Paterson, B. Agate, M. Comrie, R. Ferguson, T.K. Lake, J.E. Morris, A.E. Carruthers, C.T.A. Brown, W. Sibbett, P.E. Bryant, F. Gunn-Moore, A.C. Riches, and K. Dholakia. Photoporation and cell transfection using a violet diode laser. *Optics Express*, 13(2):595–600, 2005.

[45] J.M. Girkin, A.I. Ferguson, D.L. Wokosin, and A.M. Gurney. Confocal microscopy using an InGaN violet laser diode at 406nm. *Optics Express*, 7(10):336–342, 2000.

[46] K.B. MacAdam, A. Steinbach, and Carl Wieman. A narrow-band tunable diode laser system with drating feedback and a saturated absorption spectrometer for Cs and Rb. *American Journal of Physics*, 60(12):1098–1111, 1992.

[47] A. Hemmerich, D.H. McIntyre, D. Schropp Jr., D. Meschede, and T.W. Hänsch. Optically stabilised narrow linewidth semiconductor laser for high resolution spectroscopy. *Optics Communications*, 75(2):118–122, 1990.

[48] P. Werle. Tunable diode laser absorption spectroscopy:recent findings and novel approaches. *Infrared Physics and Technology*, 37(–):59–66, 1996.

[49] P. Werle. A review of recent advances in semiconductor laser based gas monitors. *Spectroschimica Acta Part A - Molecular and Biomolecular Spectroscopy*, 54(2):197–236, 1998.

[50] G.P.T. Lancaster, R.S. Conroy, M.A. Clifford, J. Arlt, and K. Dholakia. A polarisation spectrometer locked diode laser for trapping cold atoms. *Optics Communications*, 170(1–3):79–84, 1999.

[51] A.G. Truscott, N.R. Heckenberg, and H. Rubinsztein Dunlop. Frequency stabilised grating feedback laser diode for atom cooling applications. *Optical and Quantum Electronics*, 31(5–7):417–430, 1999.

[52] Carl E. Wieman and Leo Hollberg. Using diode lasers for atomic physics. *Review of Scientific Instruments*, 62(1):1–20, 1991.

[53] G. Santarelli and A. Clairon. Heterodyne optical phase locking of extended cavity semiconductor lasers at 9GHz. *Optics Communications*, 104(4–6):339–344, 1994.

[54] P.B. Coates. External cavity stabilisation of gain guided laser diodes for metrological applications. *Journal of Physics E - Scientific Instruments*, 21(8):812–816, 1988.

[55] Y. Millerioux, D. Touahri, L. Hilico, A. Clairon, R. Felder, F. Biraben, and B. Beauvoir. Towards an accurate frequency standard at 778nm using a laser diode stabilised on a hyperfine component of the doppler-free two-photon transitions in rubidium. *Optics Communications*, 108(1–3):91–96, 1994.

[56] Hans Edner, Gregory W. Faris, Anders Sunesson, and Sune Svanberg. Atmospheric atomic mercury monitoring using differential absorption lidar techniques. *Applied Optics*, 28(5):921–930, 1989.

Chapter 3

Non-Linear Optics

The invention and subsequent widespread commercial availability of the laser provided users with a light source that had sufficient intensity for optical frequency mixing within dielectric media to be observed. Non-linear optical frequency conversion is an attractive option to users in order to extend the coverage of the spectrum currently available with conventional laser sources. This has motivated experimental demonstrations of non-linear processes including second harmonic generation (SHG), optical parametric generation (OPG) and sum frequency generation (SFG). This is also the principal motivation for much of the work described in this thesis.

3.1 Introduction

Non-linear optics is a branch of optics where the polarisation of a medium responds non-linearly with the application of an electric field. The phenomena is widely used to adapt the outputs from existing light sources such as lasers to gain light of different wavelengths through mechanisms of frequency conversion, namely up and down conversion and frequency doubling and tripling.

The recent introduction of blue laser diodes emitting in the blue region of the visible spectrum has opened up the field to work within a spectral region previously only available via complicated frequency conversion methods. Now, the short wavelength visible spectrum is accessible and these lasers can be used in frequency conversion schemes to obtain access to the UV region of the spectrum. The work in Chapters 4 and 6 has used non-linear optical effects to access those regions of the spectrum unattainable with single devices.

Non-linear optical processes such as those referred to in the chapter abstract have only been possible since the development of techniques that enhance the efficiency of the frequency conversion process. The efficiency of these processes can be vastly improved by ensuring that the interacting waves travelling through the medium have matching phase velocities and ensuring that the energy flow within a non-linear process, characterised by the non-linear susceptibility, χ^2, is maintained. This process, called phasematching, exploits the natural birefringence of the optical anisotropic materials used as non-linear media and now in conjunction with periodically-poled phase matching underpin the success of devices based upon non-linear optical phenomena today.

In this chapter the basic theory of non-linear optics is introduced and the concept of a three wave mixing process is described. Ways of maximising the non-linear optical interaction through the technique of phasematching and a description of techniques used for this are introduced. The phenomenon of optical parametric generation (OPG) and

its practical incarnation, the optical parametric oscillator (OPO) are described and then its inverse process, sum frequency generation (SFG) is introduced.

3.2 Linear and Non-linear Optical Processes

Linear and non-linear optics concern the interaction of dielectric materials with electromagnetic radiation. When such a medium is subjected to electromagnetic radiation the electrons within that medium are polarised with respect to its nuclei. Where the electric field associated with the radiation is small (i.e we have low optical powers), the induced polarisation of the medium is linearly proportional to the applied field according to

$$P(t) = \varepsilon_0 \chi E(t) \tag{3.1}$$

where $P(t)$ and $E(t)$ are the polarisation and electric field vectors respectively and ε_0 is the permittivity of free space. The interaction between the electric field and polarisation takes place via the susceptibility, χ. At these low field strengths this relationship is linear and as such is the starting point for the regime of linear optics which governs effects such as dispersion and absorption. This relationship is analogous to Hooke's Law.

The linear dependence of the induced polarisation is, in fact, an approximation and is valid only for small electric fields. The Hooke's Law analogy can be used to good effect here to describe the change from linear to non-linear optics. When a spring is subject to a force the dependency of the force on its extension is linear, provided the force is small. When a large force is applied to the spring Hooke's Law breaks down - the relationship between the force and extension ceases to be linear. Similarly when the optical electric field strength is comparable in size to the inter-atomic electric field within the material, as can be the case with laser radiation, the linear polarisation

response is no longer sufficient and a power series expansion must be used to yield

$$P(t) = \varepsilon_0(\chi^{(1)}E(t) + \chi^{(2)}E^2(t) + \chi^{(3)}E^3(t) + ...) \tag{3.2}$$

The first term represents the linear polarisation. This is identified by the first order susceptibility $\chi^{(1)}$ and the linear electric field $E(t)$. The subsequent terms represent the second, third and higher order polarisations, each governed by a separate susceptibility. These terms can be referred to as non-linear terms. In most materials the effect of susceptibilities higher than the third order is small and can only be observed at very high intensities. Third order effects include the optical Kerr effect [1], two photon absorption [2] and Brillouin and Raman scattering [3, 4, 5]. Therefore we are most interested in the effect of the second order susceptibility $\chi^{(2)}$. By considering the second order susceptibility alone the expression above can be written as

$$P(t) = \varepsilon_0(\chi^{(2)}E^2t) \tag{3.3}$$

3.2.1 Second Order Nonlinear Optical Processes

For the second order susceptibility to have an influence, the dielectric material must be non-centrosymmetric, as $\chi^{(2)}$ vanishes in materials that are centrosymmetric i.e materials that have a centre of symmetry within the unit cell of their lattice structure. If the field incident on the dielectric consists of a single frequency ω_1 then it is simple to show, from Equation 3.3, that the resulting polarisation term will oscillate at $2\omega_1$. However there are a number of possiblities if the electric field consists of two oscillating components, ω_1 and ω_2. The electric field is now:

$$E(t) = E_{(1)}\cos(\omega_1 t) + E_{(2)}\cos(\omega_2 t) \tag{3.4}$$

Substituting this equation into Equation 3.3 gives an expression for the polarisation

$$P(t) = \varepsilon_0 \chi^{(2)} \left(\frac{E_1}{2}[\cos(2\omega_1 t)] + \frac{E_2}{2}[\cos(2\omega_2 t)] + \frac{E_1}{2} + \frac{E_2}{2} + E_1 E_2[\cos(\omega_1+\omega_2)t + \cos(\omega_1-\omega_2)t] \right) \tag{3.5}$$

This expression contains terms that describe fundamental second order non-linear processes. Examination of these terms show that the $\chi^{(2)}$ interaction gives rise to frequencies at twice that of the interacting fields, $2\omega_1$ and $2\omega_2$, Second Harmonic Generation (SHG); the sum and difference of the two frequencies, $\omega_1 + \omega_2$ and $\omega_1 - \omega_2$, Sum Frequency Generation (SFG) and Difference Frequency Generation (DFG) and a final, frequency independent term at DC. The two types of non-linear interaction described in the work in this thesis involve difference frequency generation through the mechanism of optical parametric generation and the process of sum frequency generation. SFG is simply the inverse process of DFG and thus a theoretical treatment of this will be the inverse of the theory of DFG. Maxwell's wave equation for a non-absorbing, non-conducting dielectric medium containing no free charge is

$$\nabla^2 E = \mu\varepsilon_0 \frac{\delta^2 E}{\delta t^2} + \mu \frac{\delta^2 P}{\delta t^2} \tag{3.6}$$

where μ is the permeability of the medium and ε_0 is the permittivity of free space . Equation 3.3 is substituted into Maxwells equation to account for non-linear polarisation. If the interacting fields are along the z-axis, the wave equation that describes the propagation of electromagnetic fields in non-linear media is given by:

$$\frac{\delta^2 E}{\delta z^2} = \mu\varepsilon \frac{\delta^2 E}{\delta t^2} + \mu \frac{\delta^2}{\delta t^2}(\varepsilon_0 \chi^{(2)} E^2) \tag{3.7}$$

where ε is the permittivity of the medium.

A second order non-linear process can be viewed as a three wave mixing process and thus the frequencies of the optical fields must satisfy energy conservation and the relationship

$$\omega_3 = \omega_1 + \omega_2 \tag{3.8}$$

where ω_3 is the highest frequency component within the interaction and ω_1 the lowest. The electric fields of each of the waves involved in the interaction can be defined as

$$E_1(z,t) = \frac{1}{2}\left[E_1(z)e^{i(k_1 z-\omega_1 t)} + E_1^*(z)e^{-i(k_1 z-\omega_1 t)}\right] \tag{3.9}$$

$$E_2(z,t) = \frac{1}{2}\left[E_2(z)e^{i(k_2 z-\omega_2 t)} + E_2^*(z)e^{-i(k_2 z-\omega_2 t)}\right] \tag{3.10}$$

$$E_3(z,t) = \frac{1}{2}\left[E_3(z)e^{i(k_3 z-\omega_3 t)} + E_3^*(z)e^{-i(k_3 z-\omega_3 t)}\right] \tag{3.11}$$

By substituting into the Maxwell nonlinear wave equation and with some manipulation it can be shown that

$$\frac{\delta E_1 z}{\delta z} = -i(2\omega_1\varepsilon_0)\left[\frac{\mu_0}{\varepsilon_1}\right]^{1/2} d_{eff}E_3(z)E_2^*(z)e^{i\Delta kz} \tag{3.12}$$

$$\frac{\delta E_2(z)}{\delta z} = -i(2\omega_2\varepsilon_0)\left[\frac{\mu_0}{\varepsilon_2}\right]^{1/2} d_{eff}E_3(z)E_1^*(z)e^{i\Delta kz} \tag{3.13}$$

$$\frac{\delta E_3(z)}{\delta z} = -i(2\omega_3\varepsilon_0)\left[\frac{\mu_0}{\varepsilon_3}\right]^{1/2} d_{eff}E_1(z)E_2(z)e^{i\Delta kz} \tag{3.14}$$

Equations 3.12 to 3.14 are known as the coupled wave equations. d_{eff} is the effective non-linear coefficient. d_{eff} is the fundamental mechanism of non-linear optics by which the three interacting fields are coupled, enabling energy flow between fields. These equations are the starting point for the analysis of many non-linear optical effects and they can be applied universally to any three wave mixing process that involves $\chi^{(2)}$. Physically this coupling is responsible for the exchange of energy amongst

the interacting fields as they propagate through the medium. The coupled wave equations can be used to describe the precise gain and depletion within the interacting fields in a non-linear optical process.

Before considering the method of solving the coupled wave equations, we first consider a useful set of relations that can be derived from the. Recalling equations 3.12 to 3.14 and multiplying them by E_1^*,E_2^* and E_3^* gives

$$\frac{\delta|E_1 z|^2}{\delta z} = i(2\omega_1\varepsilon_0)\left[\frac{\mu_0}{\varepsilon_1}\right]^{1/2} d_{eff}E_3(z)E_2^*(z)E_1^*(z)e^{i\Delta kz} \tag{3.15}$$

$$\frac{\delta|E_2 z|^2}{\delta z} = i(2\omega_2\varepsilon_0)\left[\frac{\mu_0}{\varepsilon_2}\right]^{1/2} d_{eff}E_3(z)E_2^*(z)E_1^*(z)e^{i\Delta kz} \tag{3.16}$$

$$\frac{\delta|E_3 z|^2}{\delta z} = -i(2\omega_3\varepsilon_0)\left[\frac{\mu_0}{\varepsilon_3}\right]^{1/2} d_{eff}E_3(z)E_2^*(z)E_1^*(z)e^{i\Delta kz} \tag{3.17}$$

From these equations it can be seen that

$$\frac{n_1}{\omega_1}\frac{\delta|E_1(z)|^2}{\delta z} = \frac{n_2}{\omega_2}\frac{\delta|E_2(z)|^2}{\delta z} = -\frac{n_3}{\omega_3}\frac{\delta|E_3(z)|^2}{\delta z} \tag{3.18}$$

The intensity of an electromagnetic field wave of amplitude $E(z)$ is

$$I = \frac{1}{2}\varepsilon_0 nc|E(z)|^2 \tag{3.19}$$

where n is the refractive index and c is the speed of light. By substituting for the intensity in Equations 3.15 to 3.19 and simplifying we obtain

$$\frac{\delta}{\delta z}\left(\frac{I_1}{\omega_1}\right) = \frac{\delta}{\delta z}\left(\frac{I_2}{\omega_2}\right) = -\frac{\delta}{\delta z}\left(\frac{I_3}{\omega_3}\right) \tag{3.20}$$

Equation 3.20 is the most common form of the Manley-Rowe relations which can be used to describe the flow of power between monochromatic fields which are coupled through one specific order of non-linearity. The Manley-Rowe relations show that the destruction of any single pump photon results in the creation of exactly one photon at each of the downconverted frequencies. This is based upon the assumption that the phase relationship between the waves is correct to allow energy to be transferred from the incident to the downconverted waves. If the total intensity I_T is defined as the sum of I_1,I_2 and I_3 and recalling Equation 3.8 then

$$\frac{\delta I_T}{\delta z} = \frac{\delta I_1}{\delta z} + \frac{\delta I_2}{\delta z} + \frac{\delta I_3}{\delta z} = 0 \tag{3.21}$$

showing that there is conservation of energy within a second order non-linear optical process.

3.2.2 Phasematching

The solutions to the coupled wave equations describe the evolution of the three interacting fields as they propagate through non-linear medium during the process of OPG. The use of these equations to analyse non-linear optical effects requires some assumptions to be made. Firstly the waves should be Gaussian rather than plane waves as this is a more accurate depiction of the physical reality of the field. Secondly we assume that the amplitude of the optical fields remains constant over the length of the crystal. The detailed method for the solution of these equations has been given in reviews of Boyd and Ashkin [6] and Byer [7] and in [8]. Here I will draw on and summarise the most relevant details.

Recalling the coupled wave equations we can choose a new variable α such that $|\alpha|^2$ is the normalised photon flow. By expressing the coupled wave equations in terms of this new parameter we obtain simple first order differential equations which are further manipulated via integration to give

$$\alpha_1(L) = \alpha_1(0) + 2\tau\alpha_3(0)\alpha_2^*(0) \tag{3.22}$$

$$\alpha_1(L) = \alpha_1(0) + 2\tau\alpha_3(0)\alpha_1^*(0) \tag{3.23}$$

$$\alpha_3(L) = \alpha_3(0) + 2\tau\alpha_1(0)\alpha_2(0) \tag{3.24}$$

It appears that there is gain at the weak fields α_1 and α_2 and depletion at the strong pump α_3. However the factor τ in these expressions defined below

$$\tau = \kappa L sinc(\frac{\Delta kL}{2}) \exp^{i(\frac{\Delta kL}{2})} \tag{3.25}$$

is crucial. κ is a constant factor that is determined by the non-linear coefficient d_{eff}, the coupling between the three Gaussian beams and the frequency and refractive index of each beam. L is the propagation distance or the crystal length. However, the crucial determinant as to whether a field will experience gain or loss is the sinc function $sinc(\frac{\Delta kL}{2})$. The Δk term is the wavevector mismatch and it represents the difference in the momentum of the three waves. It is given by

$$\Delta k = k_3 - k_2 - k_1 \tag{3.26}$$

where

$$\Delta k = \frac{n_3\omega_3}{c} - \frac{n_2\omega_2}{c} - \frac{n_1\omega_1}{c} = 0 \tag{3.27}$$

Equation 3.27 is the phasematching equation. Figure 3.1 is the plot of the sinc function which can be thought of as a gain curve describing the parametric generation process.

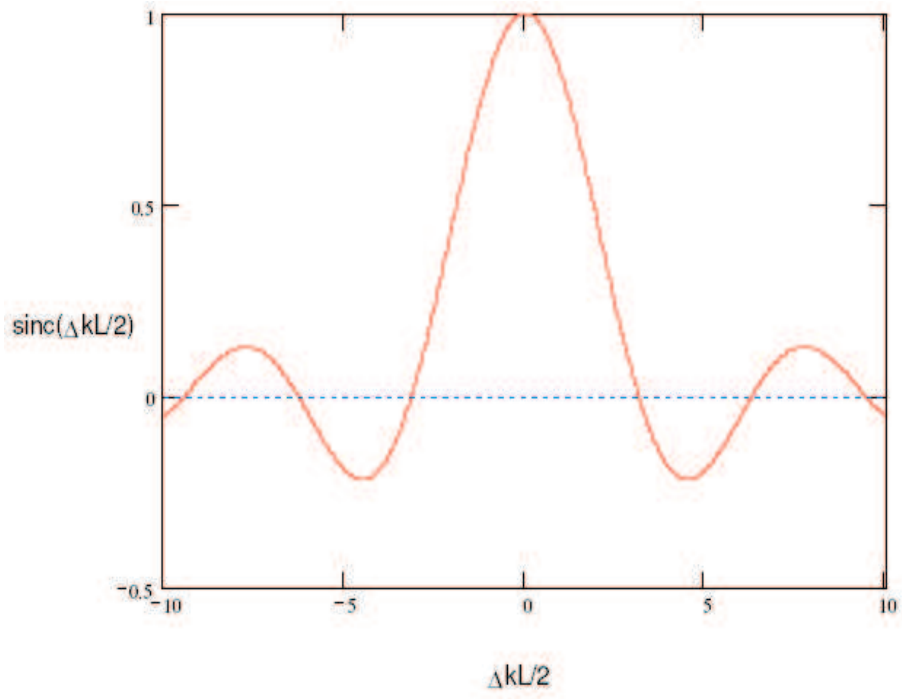

Figure 3.1: **Sinc Function**
The sinc function is at maximum value where the wavevector mismatch is zero - perfect phasematching. However, phasematched behaviour is still possible as the function decreases away from the peak.

For maximum gain Δk , the difference in momentum between the three waves, and thus the wavevector mismatch must be zero. This maximises the strength of the non-linear interaction and is known as perfect phasematching. For any non-zero value of Δk the gain rapidly decreases, and the efficiency of the non-linear interaction is reduced. If Δk is non-zero, as the beam propagates through the crystal (i.e as L increases) eventually the sinc function becomes negative. This results in energy being transferred back to the strong field from the weaker downconverted fields. The power in these downconverted waves reaches a maximum when $L = \frac{\pi}{\Delta k}$. This length is the coherence length which determines the length of the non-linear crystal over which non-linear conversion is possible. In practice the coherence length is usually of the order of a few tens of microns. From this we can introduce the concept of the phasematch bandwidth which is defined as the interval over which

$$| \Delta k | \leq \frac{\pi}{L}.$$

To satisfy the phasematching condition the refractive indices of each wave must be the same. In reality the refractive index of a material is a function of frequency and therefore the refractive indices of the three waves will always be different. Two well established solutions to this problem are birefringent phasematching and quasi-phasematching.

3.2.3 Birefringent Phasematching

Birefringent phasematching attempts to overcome the problem that material dispersion introduces in the attempt to phasematch and thus maximise the efficiency of the non-linear process. This technique exploits the tendency of materials used in non-linear optics to have anisotropic refractive indices. In such cases the refractive index of a material at a given wavelength is dependent upon the propagation direction of light and its polarisation. Waves polarised parallel to a plane containing the so-called optic axis experience a refractive index that is dependent upon the angle of propagation. For waves polarised normal to the plane the refractive index is the same and independent of the angle of propagation. Therefore if one chooses the correct angle of propagation and polarisation for each of the three waves it is possible to have all three refractive indices the same and thus satisfy Equation 3.27 and phasematch the parametric process. A detailed discussion on the phase-matched tuning mechanisms in birefringent non-linear materials is given in [9].

3.2.4 Quasi Phasematching

For a non-phasematched interaction the maximum power generated in the signal and idler waves occurs after one coherence length l_c. Beyond this length the propagating fields and the fields created by the driven polarisation interfere destructively and

there is a decrease in power. However if a phaseshift were applied periodically to the oscillating polarisation every coherence length there is continuous constructive interference. As a result that the power in the signal and idler fields would increase throughout the length of the crystal. This is the concept of quasi-phasematching. This technique was first demonstrated in 1966 [10] and is usually achieved via a technique known as periodic poling first demonstrated by Yamada *et al* [11]. This involves 'flipping' the direction of ferro-electric domains within the non-linear material in order to always ensure a phaseshift of π. A schematic of a periodically poled material is shown in Figure 3.2.

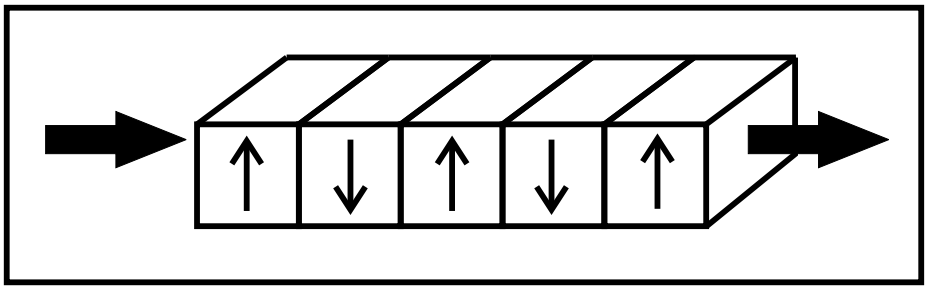

Figure 3.2: **Quasi-Phase Matched Non-Linear Material**
A periodically poled material has the sign of the non-linear coefficient modulated every period to correct for phase mismatch

While this does not affect the linear refractive indices of the waves (and thus their k-vectors), the phase of the local polarisation oscillations induced by the pump wave via the $\chi^{(2)}$ susceptibility is different by π in adjacent crystal sections. A suitable spatial poling period (often referred to as the grating period), which represents the length between each domain inversion, is chosen using:

$$\Delta k = k_3 - k_2 - k_1 - K = 2\pi\left(\frac{n_3}{\lambda_3} - \frac{n_2}{\lambda_2} - \frac{n_1}{\lambda_1} - \frac{1}{\Lambda}\right) \tag{3.28}$$

in which $\Delta k \neq 0$ is the remaining mismatch due to the dispersion of the crystal and Λ is the grating period. This ensures that the waves generated by the local polarisation are on average in phase with the waves generated at other locations along the beam path. Thus there is constructive interference of the generated waves along the entire

crystal.

QPM has several important advantages over BPM. Firstly QPM can be achieved for any pair of downconverted waves and is not limited by the natural birefringence of suitable non-linear crystals. Secondly, QPM gives access to the highest non-linear coefficient (usually found with parallel polarisations of all three waves) which results in highest output powers and conversion efficiencies and in the lowest threshold for parametric processes. Furthermore, QPM allows one to design crystals that provide simultaneous phase matching of several different frequency conversion devices based upon a single crystal. Finally using QPM, the shape of the phasematching curve i.e the parametric gain of the phase mismatch can be designed.

The work in this thesis uses both QPM and BPM materials. The OPO described in Chapter 4 uses periodically poled lithium niobate (PPLN) and the sum frequency generation described in Chapter five uses beta-barium borate (BBO), a birefringently phasematched non-linear crystal. Although the benefits of QPM materials have been highlighted here, this is in particular reference to the benefits seen in OPOs and the benefits of BPM materials are still acknowledged not least in the successful work described in this thesis.

3.3 Optical Parametric Generation and Oscillation

Optical Parametric Generation (OPG) is a non-linear optical effect that is a result of the interaction between a strong optical field, called the pump, at a frequency ω_3 with the electrons in a non-centrosymmetric crystalline material. This interaction yields a pair of optical fields at frequencies ω_2 and ω_1 such that

$$\omega_3 = \omega_2 + \omega_1 \tag{3.29}$$

The two downconverted fields are the signal and idler, terms that traditionally refer

to the higher and lower frequency waves respectively.

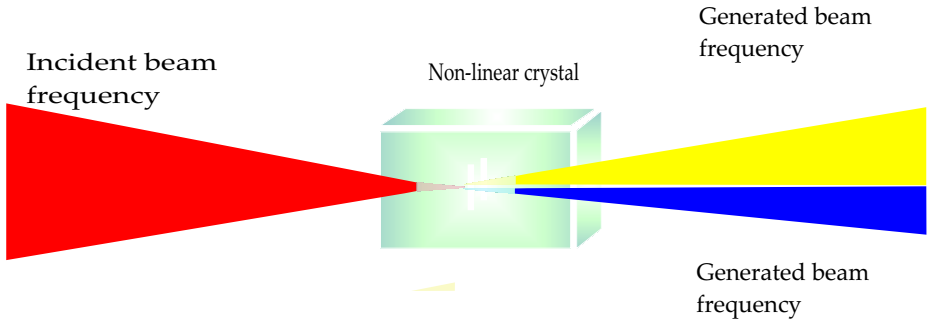

Figure 3.3: **Optical Parametric Generation**
The pump wave is incident upon the non-linear crystal. Via the second order susceptibility $\chi^{(2)}$ the signal and idler waves are generated.

OPG can be described as a photon splitting process - the pump photon of energy E splits into two lower frequency photons the energies of which sum to the energy of the pump photon. When coupled with phasematching techniques described earlier, the OPG process forms the basis of an optical parametric amplifier (OPA). A single round trip wave does not provide any useful or significant output power. To produce significant continuous wave output powers it is necessary for at least one of the three waves to be resonant in an optical cavity surrounding the non-linear crystal. To understand this process in more detail we need to consider the propagation of the pump, signal and idler through the non-linear material, in terms of a three-wave mixing process. The majority of parametric devices are operated within an oscillator configuration, as in a conventional laser, by enclosing the non-linear gain medium within an optical cavity to provide feedback at generated waves. This type of configuration is known as an optical parametric oscillator (OPO). The amplification of the parametric waves to macroscopic levels is achieved by successive passes through the non-linear crystal and coherent output can be extracted from the oscillator. For a qualitative description of the working principle of the OPO we must consider the most basic setup of an OPO as shown schematically in Figure 3.4.

A laser beam at the pump source at an optical frequency ω_p is sent through the non-linear crystal placed in an optical resonator formed by the mirror M1 and M2.

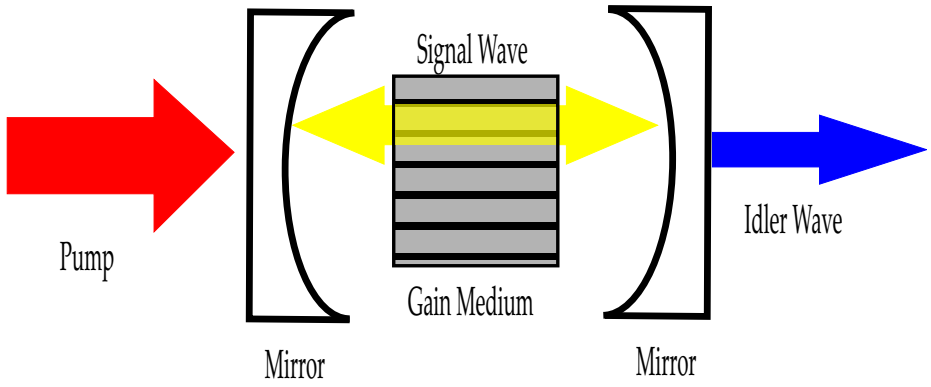

Figure 3.4: **Generic Optical Parametric Oscillator**
OPG is initiated within a cavity whereby there is feedback at the generated waves and the parametric waves are amplified with output obtained at the output mirror of the cavity.

The non-linear crystal is selected for providing significant second order dielectric susceptibility $\chi^{(2)}$ which enables a three wave mixing process. As a result the pump wave travelling through the crystal provides gain for the signal and idler waves. The output waves satisfy the energy conservation law

$$\omega_p = \omega_s + \omega_i \tag{3.30}$$

The gain provided by the pump wave for the signal and idler waves means that weak signal and idler waves travelling through the crystal are amplified whilst the pump power depletes. An initial signal and idler intensity is present due to vacuum fluctuations within the nonlinear crystal. As a result it is only necessary to provide the pump laser beam from an external source. By placing the non-linear crystal inside a resonator for the signal wave the signal is fed back into the crystal where it is further amplified through power transfer from the pump wave.

The Manley-Rowe relations in Equation 3.20 show that power is transferred between the propagating waves as they travel through the non-linear medium. The gain increases with the intensity of the pump wave, and as a consequence, there is a minimum pump intensity at which the amplification of the signal wave in the crystal compensates for the round trip losses in the resonator (due to mirror transmission,

absorption and scattering). At this threshold pump intensity, optical parametric oscillation sets in i.e a periodically oscillating signal wave is generated from an initially random field fluctuation. At the same time a significant portion of the pump power is converted into signal and idler power. This transfer of power from the pump wave to the generated waves reduces the pump intensity inside the non-linear crystal and thus the signal gain. In close analogy to the case of laser oscillation this effect is called 'gain saturation'. This leads to to steady state operation of the OPO where the signal power generated in the crystal exactly balances the resonator losses for the signal wave. The frequencies of the two generated waves are not fixed but can be tuned over wide wavelength ranges. This frequency tunable down-conversion of the pump laser in the OPO is caused by the non-linear interaction of the three waves via the $\chi^{(2)}$ susceptibility. This process can be highly efficient, with the vast majority of the pump laser radiation converted to the two lower frequency beams.

While Equation 3.30 states that the sum-frequency of a signal and idler wave pair is equal to the pump frequency, it does not determine which of all possible signal-idler frequency pairs will actually be generated. In steady-state operation, the signal and idler frequency pair that is generated has a minimum threshold pump intensity (in analogy to a laser with spectrally broadened gain). Thus, the generated frequencies, and with them the ratio of the signal and idler frequencies are determined by the frequency dependence of the parametric gain in the crystal and by the frequency dependence of the resonator losses. In general, the parametric gain in the crystal provides only a coarse selection of the frequency ranges of the signal and idler wave, whereas the exact frequencies are given by the frequency selectivity of the OPO resonator. Therefore an OPO tends to operate at signal idler frequencies for which the wavevector mismatch, Δk, is minimum. By changing the refractive indices for the three waves, for example by changing the crystal temperature or the direction of the beams through the crystal, this condition can be fulfilled for different frequency combinations, allowing, within certain limits, the output frequencies of an OPO to be coarsely tuned.

3.4 Optical Parametric Oscillators

In 1965, Giordmaine and Miller demonstrated the first optical parametric oscillator (OPO) a device that exploits the non-linear optical frequency conversion phenomenon of optical parametric generation (OPG) and converts laser radiation into two coherent waves with lower frequencies [12]. Following this there was slow progress in the development of devices due to a lack of suitable non-linear materials and pump laser sources. However recently, with the development of better pump laser sources, particularly those based on diode pumped solid state gain media and QPM materials such as PPLN there has been much progress in this area. These improved apparatus allow a variety of cavity geometries to be investigated for CW-OPOs. These include the singly resonant oscillator (SRO), double pass (DP), doubly resonant oscillator (DRO), triply resonant oscillator (TRO), pump enhanced (PE), split cavity and intra cavity. The main consideration in this review will be the SRO and the DRO. The operating principles of the OPO are well documented [13, 1, 15]. OPOs have been demonstrated in all temporal regimes from femtosecond to continuous wave (C-W). In most pulsed applications OPOs are configured as singly-resonant oscillators (SROs) but in the C-W regime, DROs are more common.

The optical parametric process can be initiated in the presence of at least one resonant field (signal or idler). The specific resonated field depends upon the desired wavelength to be used as an output from the device and on the power capabilities of the pump source. The OPO can be categorised according to the number of the resonating fields within the cavity. If only one of the optical parametric fields is resonant within the cavity then the configuration is called singly resonant OPO (SRO). If both parametric waves are resonant within the cavity the device is known as a doubly resonant OPO (DRO). When the pump as well as the signal and idler is resonant within the cavity the system is called triply resonant OPO (TRO). This latter type of OPO is rarely implemented due to complication with maintaining three resonant waves within a single optical cavity.

The number of waves brought to resonance within the OPO cavity drastically affects the operating characteristics of the device. The important differences between the various resonant cavities include the pump power threshold, the conversion efficiencies and the pump frequency stability requirements.

Singly Resonant Oscillators

The most practically robust and simple configuration is the SRO. The main advantage is that with only one wave resonant within the cavity any frequency perturbations in the pump field are taken up in the non-resonant field, obviating the need to keep the cavity actively locked.

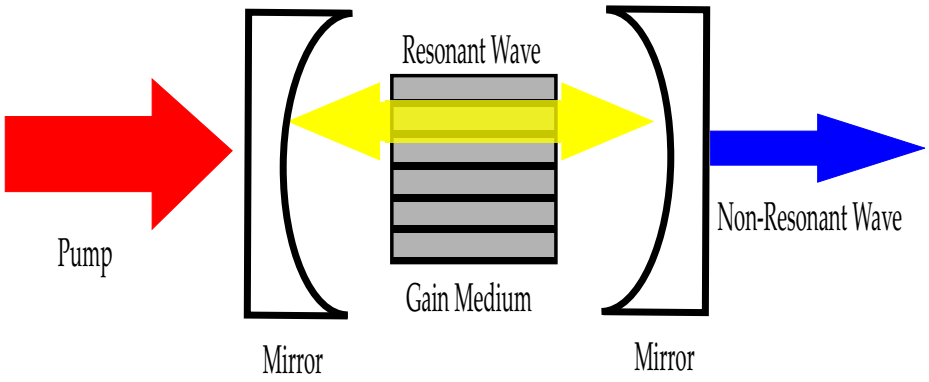

Figure 3.5: **Singly Resonant OPO (SRO)**
Only one of the downconverted waves (either the signal or idler) is resonant within the cavity

Either the signal or the idler wave is resonant whilst the non-resonant generated wave and the pump exit the cavity after a single pass through the crystal. With only one resonant wave the SRO is simple to realise and is a stable device which exhibits smooth tuning characteristics. The disadvantage of this device is the high operational threshold typically displayed by these devices, in the multi-watt region described in Section 3.4.2.

3.4.1 Doubly Resonant Oscillators

Doubly resonant oscillators have both the signal and idler resonant in the cavity.

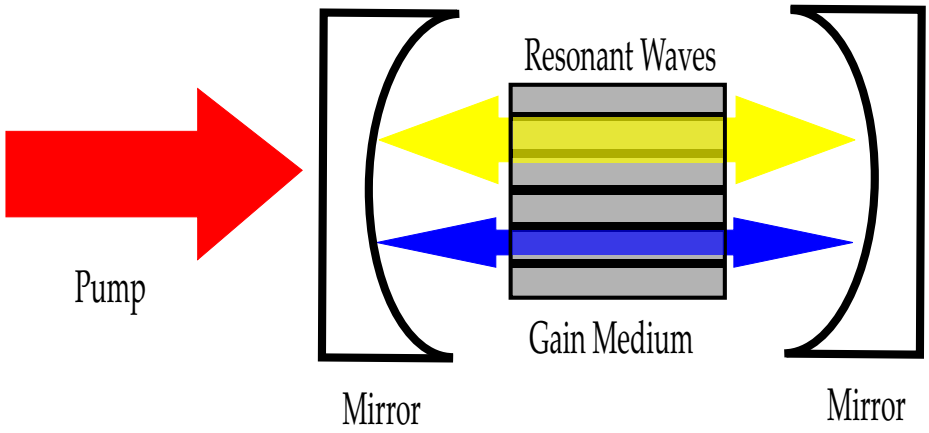

Figure 3.6: **Doubly Resonant OPO (DRO)**
Both the signal and idler waves are resonant within the cavity

A detailed description of the design and operation of a DRO device is given in Chapter 4. The characteristics of this device are described in more detail examining the methods used to adapt the output from a DRO to make it smooth, mode-hop-free and stable, suitable for use in applications such as trace gas detection.

Significant reductions in threshold of the OPO can be achieved by using the DRO configuration. In order to maintain resonance of both the parametrically generated waves the DRO has very strict cavity requirements to keep the waves on resonance within the cavity. The strict cavity stability requirements along with the complications in smoothly tuning the DRO whilst keeping both the signal and idler on resonance had hindered the development of the DRO into practical devices for spectroscopic applications. Recent developments in pump sources and cavity refinements have brought about the realisation of the potential of the DRO particularly in the field of high resolution spectroscopy.

3.4.2 Threshold in OPOs

The threshold of an OPO is the amount of pump power required to achieve optical oscillation [15], corresponding to the point where the gain just equals the losses in the resonator. The threshold power in a CW-OPO is affected by the level of focusing of the pump into the non-linear crystal and the length of the cavity. An expression for the threshold of an OPO can be derived by equating the gain with loss for each wave for a single round trip of the cavity. The exact procedure is dependent upon the OPO configuration, the particular cavity and the pump focussing conditions. For any OPO, the minimum threshold occurs when the confocal parameter of the pump beam is made equal to the length of the non-linear crystal to minimise the pump volume and hence maximise the intensity inside the crystal.

Threshold expressions can be derived by equating the gain and loss for each wave on a single round trip of the cavity. The exact procedure depends upon the particular cavity and pump focussing conditions. For any OPO the minimum threshold occurs for the case of confocal pump focussing. In such a configuration the confocal parameter of the pump beam is made equal to the length of the non-linear crystal to minimise the pump volume and hence maximise the intensity inside the crystal.

The SRO has only one resonant wave and it is assumed that the idler wave leaves the non-linear crystal after a single pass. The pump propagates through the medium in the forward direction only so parametric gain occurs for the propagation of the signal in this direction only. We also assume that the losses from the signal wave from the cavity are small so to a first approximation we can assume that the signal wave is constant throughout the non-linear medium. The threshold power for a confocally pumped SRO is [1, 9]:

$$P^{in}_{p,th,min} = \frac{n_p \varepsilon_0 c^4}{\pi L d^2_{eff} (1-\delta^2)^2 \nu_p^3 \Im_s} \tag{3.31}$$

In Equation 3.31, $\Im_s$ is the finesse of the cavity for the resonant signal wave, L is the

crystal length, n_p is the refractive index at the pump, δ is $\frac{2\nu_s-\nu}{\nu_p}$ and is a parameter that defines the degree away from degeneracy at which the OPO operates.

In a DRO the crystal experiences two intense waves (the resonant signal and idler waves). Consequently the pump power required to reach oscillation threshold is much lower for the DRO than for the SRO. Both resonant waves experience small fractional power losses on each round trip and so we assume that both are constant throughout the length of the crystal. Close to threshold we also assume that both the signal and idler fields are much smaller than the pump. The expression for the threshold of a DRO is similar to that of the SRO but it is necessary to adapt Equation 3.31 by dividing by a factor to account for the additional cavity finesse associated with the double resonance requirement to yield:

$$P^{in}_{p,th,min} = \frac{n_p^2 \varepsilon_0 c^4}{2Ld^2_{eff}(1-\delta^2)^2\nu_p^3 \Im_s \Im_i} \tag{3.32}$$

Equation 3.32 shows that the threshold is halved for each resonant wave. This is to be expected as the wave makes two passes through the crystal, which effectively doubles the crystal length. Similarly, double passing the pump further reduces the threshold as the pump interacts with both downconverted waves over twice the crystal length :

$$P^{in}_{p,th,min} = \frac{n_p^2 \varepsilon_0 c^4}{8Ld^2_{eff}(1-\delta^2)^2\nu_p^3 \Im_s \Im_i} \tag{3.33}$$

Equation 3.33 shows that there is a factor of four reduction in the threshold for the double passing of the pump compared to the single pass case. There is a significant reduction in the threshold for a DRO compared to that required for a SRO, often from watts [16] to the order of tens of milliwatts i.e a factor of 100 difference, as shown in [17] and in the results given in Chapter 4. For a full derivation and consideration of threshold see [15, 9, 19]. The high threshold requirements for a SRO place strict power requirements upon the pump laser source for these devices and negates the use of diode lasers within these devices.

Generally the threshold of OPOs is reduced if their pump waves is within the visible spectrum. The threshold power that is required scales with the cube of the pump wavelength. Pumping an OPO in the visible has not been possible given problems with absorption in non-linear media at short wavelengths limiting output power from OPO devices. Chapter 4 details the construction of an OPO device using an IR laser with suitably low threshold requirements such that it could be adapted for pumping by a violet laser diode.

3.5 Sum Frequency Generation (SFG)

Sum Frequency Generation (SFG) is an inverse process of OPG. In SFG, two fundamental beams are brought together in a non-linear crystal and the resulting output beam is of higher frequency than the fundamental beams, shown in Figure 3.7. The mathematical treatment of SFG can be described as an inverse of OPG theory. The origin of SFG is in the $\omega_1 + \omega_2$ term described in Equation 3.5. The detailed derivations of SFG can be found in a number of excellent accounts [20], the most relevant details are indicated here. The energy conservation condition for SFG is the same as in the OPG case, except that with frequency up-conversion, the generated beam is of much higher energy than the fundamental beams. Recalling Equation 3.8, the energy conservation condition can be applied here with the higher frequency component, ω_3 attributed to the generated wave and the lower frequency components, ω_2 and ω_1 are the fundamental waves. The phasematching conditions are applied in a similar way.

Sum Frequency Generation SFG where the two input waves are of the same wavelength is a special case knows as frequency doubling or second harmonic generation. Frequency tripling or third harmonic generation is another special case that can yield extremely high energy, short wavelength output.

In Chapter 6, SFG is used to generate ultra-violet (UV) light from the mixing of a red and violet diode laser, to obtain a source of UV light appropriate for spectroscopic

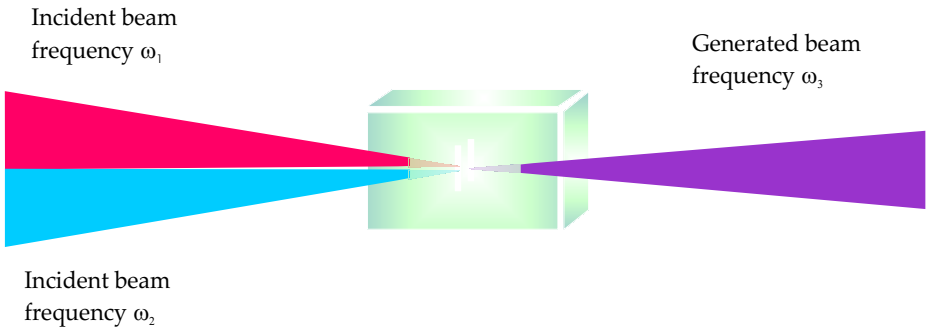

Figure 3.7: **Sum Frequency Generation (SFG)**
Two waves propagate through a non-linear crystal and the output is a wave of higher energy and frequency than the input waves

investigations. The theoretical power generated from the SFG interaction is directly proportional to the product of the fundamental beam powers, shown in Equation 3.34 [10, 9]:

$$P_3 = \frac{16 d_{eff}^2 m^2 l^2 \omega_1 \omega_2 P_1 P_2}{\pi \varepsilon_0 c^3 n_1 n_2 n_3} \tag{3.34}$$

Here P_i is the power, where i=1,2 are the fundamental beam powers and i=3 is the sum frequency power. The respective beams have a frequency ω_i, modified by a refractive index n_i inside a crystal of length l. d_{eff} is the effective nonlinear coefficient, c is the speed of light and ε_0 is the permittivity of free space. The factor m is included to take into account the difference of the beam focussing within the crystal to waists of w_i for each respective beam described as

$$m = \frac{w_1 w_2 w_3}{w_1^2 w_2^2 + w_1^2 w_3^2 + w_2^2 w_3^2} \tag{3.35}$$

Equation 3.34 is a generalised expression that can be used for combination of any two beams within a crystal. The generated power can be maximised by careful consideration of the parameters of two focussed beams. This alternative approach is described in greater detail in Section 6.3.1.

The technique of SFG has been widely used in frequency conversion applications. Dye

and argon ion lasers have been used in conjunction with frequency doubling and sum frequency generation techniques [22, 23]. Additionally, these lasers have been used alongside diode lasers to generate light in the UV. To increase the output power from these systems an enhancement cavity can be used to multipass the non-linear crystal. This type of configuration has been used to access the UV region at 194nm, 213nm and 369nm [24, 25, 26]. The non-linear conversion efficiency with these techniques is on the whole quite poor, as such the suitability of the output radiation from the conversion is only applicable for those applications where low power is required. In the case of diode lasers for this application, microlensed diode lasers were used for SFG, where the maximisation of the non-linear process was a key consideration in gaining sufficient output for a spectroscopic application. We were successful in gaining output an order of magnitude greater than that previously reported which went on to allow improved spectroscopic investigations as described in Chapter 6. The SFG technique has been especially successful in the application of vibrational spectroscopy at interfaces [27, 28]

3.6 Summary

The ability of single frequency lasers to be incorporated into frequency conversion systems is a tool widely used to obtain wavelengths that are difficult to obtain through direct methods. This chapter described the use of non-linear optics that allows this to take place. The origins of the non-linear susceptibility χ was shown along with the different orders of polarisation that arise to describe the behaviour of light when it interacts with media. The work herein is concerned with second order effects and these were described in detail, particularly the specific situations of parametric generation in both frequency up-conversion (SFG) and down-conversion (OPG). Both these techniques have been experimentally realised in Chapters 4 and 6.

Bibliography

[1] R.W. Minck, R.W. Terhune, and C.C. Wang. Nonlinear optics. *Applied Optics*, 5(10):1595–1612, 1966.

[2] W. Kaiser and G.C.B. Garrett. Two-photon excitation in CaF2Eu2+. *Physics Review Letters*, 7:229–231, 1961.

[3] R.Y. Chiao and B.P. Stoicheff. Brillouin scattering in liquids excited by a HeNe laser. *Journal of the Optical Society of America*, 54(–):1286–1287, 1964.

[4] G. Eckhardt, R.W. Hellwarth, F.J. McClung, S.E. Schwarz, D. Weiner, and E.J. Woodbury. Stimulated raman scattering from organic liquids. *Physics Review Letters*, 9:455–457, 1962.

[5] Y.R. Shen and N. Bloembergen. Theory of stimulated brillouin and raman scattering. *Physical Review*, 137(6A):A1787–A1805, 1965.

[6] G.D. Boyd and A. Ashkin. Theory of parametric oscillator threshold with single mode optical masers and observation of amplification in $LiNbO_3$. *Physical Review*, 146(1):187–198, 1966.

[7] R.L. Byer. *Quantum Electronics : a Treatise*, chapter Optical Parametric Oscillators. Academic Press: New York, 1975.

[8] I.D. Lindsay. *High Spatial and Spectral Quality Diode-Laser-Based Pump Sources for Solid-State Lasers and Optical Parametric Oscillators*. PhD thesis, University of St Andrews, 1999.

[9] I.D. Lindsay. *High Spatial and Spectral Quality Diode-Laser-Based Pump Sources for Solid-State Lasers and Optical Parametric Oscillators*. PhD thesis, University of St Andrews, 1999.

[10] G.D. Boyd and N.K. Patel. Enhancement of optical second harmonic generation (SHG) by reflection phase matching in ZnS and GaAs. *Applied Physics Letters*, 8(12):313–315, 1966.

[11] M. Yamada, N. Nada, M. Saitoh, and K. Watanabe. First-order quasi-phasematched $LiNbO_3$ waveguide periodically poled by applying an external field for efficient blue second harmonic generation. *Applied Physics Letters*, 62(5):435, 1993.

[12] J.A Giordmaine and R.C Miller. Tunable coherent parametric oscillation in $LiNbO_3$ at optical frequencies. *Physics Review Letters*, 14(24):973–976, 1965.

[13] A. Yariv and W.H. Louisell. Theory of the optical parametric oscillator. *IEEE Journal of Quantum Electronics*, 2(4):418–424, 1966.

[14] Malcolm H. Dunn and Majid Ebrahimzadeh. Parametric generation of tunable light from continuous wave to femtosecond pulses. *Science*, 286(5444):1513–1517, 1999.

[15] Optical Society of America. *Handbook of Optics Volume IV: Fibre Optics and Non-linear Optics*, chapter 22. McGraw Hill, New York, second edition, 2000.

[16] W.R. Bosenberg, A. Drobshoff, J.I. Alexander, L.E. Myers, and R.L. Byer. Continuous-wave singly resonant optical parametric oscillator based on periodically poled $LiNbO_3$. *Optics Letters*, 21(10):713–715, 1996.

[17] I.D. Lindsay, G.A. Turnbull, M.H. Dunn, and M. Ebrahimzadeh. Doubly resonant continuous wave optical parametric oscillators pumped by a single mode diode laser. *Optics Letters*, 23(24):1889–1891, 1998.

[18] I.D. Lindsay. *High Spatial and Spectral Quality Diode-Laser-Based Pump Sources for Solid-State Lasers and Optical Parametric Oscillators*. PhD thesis, University of St Andrews, 1999.

[19] F.G. Colville. *An analysis of the performance characteristics of Continuous Wave Optical Parametric Oscillators*. PhD thesis, University of St Andrews, 1994.

[20] P.N. Butcher and D. Cotter. *The elements of non-linear optics*. Cambridge University Press, Cambridge, 1990.

[21] G.D. Boyd and D.A. Kleinman. Parametric interaction of focussed gaussian light beams. *Journal of Applied Physics*, 39(8):3597, 1969.

[22] Sandra Johansson, Stefan Spiekermann, Sunhua Wang, Valdas Pasiskevicius, Fredrik Laurell, and Katrin Ekvall. Generation of turquoise light by sum frequency mixing of diode-pumped solid-state laser and a laser diode in periodically poled ktp. *Optics Express*, 12(20):4935–4940, 2004.

[23] Dana J. Berkeland, Flavio C. Cruz, and James C. Bergquist. Sum-frequency generation of continuous-wave light at 194nm. *Applied Optics*, 36(18):4159–4162, 1997.

[24] H. Hemmati, J.C. Bergquist, and W.M. Itano. Generation of continuous-wave 194nm radiation by sum frequency mixing in an external ring cavity. *Optics Letters*, 8(2):73–75, 1983.

[25] J. Sakuma, Y. Asakawa, T. Imahoko, and M. Obara. Generation of all-solid-state, high power continuous wave 213nm light based on sum-frequency mixing in $CsLiB_6O_{10}$. *Optics Letters*, 29(10):1096–1098, 2004.

[26] K. Sugiyama, J. Yoda, and K. Sakurai. Genration of continuous wave ultraviolet light by sum-frequency mixing of diode laser and argon ion laser radiation in β-BaB_2O_4. *Optics Letters*, 16(7):449–451, 1991.

[27] Franck Vidal and Abderrahmane Tadjeddine. Sum-frequency generation spectroscopy of interfaces. *Reports on Progress in Physics*, 68(5):1095–1127, 2005.

[28] Philippe Guyot-Sionnest. The mature years of sum-frequency generation are ahead. *Surface Science*, 585(5):1–2, 2005.

Chapter 4

Design and Operation of Doubly Resonant Optical Parametric Oscillator Pumped by an External Cavity Diode Laser

---

An Optical Parametric Oscillator (OPO) is an ideal device for trace gas detection as it gives a wide tunable wavelength output. By incorporating the new violet diode lasers to pump an OPO, the blue/green region of the spectrum will be accessible , allowing investigations into atomic species with transitions in this region. Applications of OPOs in spectroscopy have been wide ranging and very successful. Here I report the design and operation of an OPO device suitable for pumping with a violet diode laser.

4.1 Introduction

Since the first realisation of the OPO, many different types have been developed as sources of both pulsed and continuous wave (CW) coherent light. OPOs are now available in a wide spectral range from the ultra-violet to the infra-red, providing average output powers in the range of a few mW to several watts. The wavelength tuning capabilities and high power efficiency make OPOs ideal for many applications [1].

Following the first demonstration of the OPO both pulsed and continuous wave (C-W) devices were demonstrated [2, 3]. Whilst other frequency mixing techniques were limited in their tuning range by the tuning characteristics of the laser sources used, OPOs allowed broad tunability from a single fixed-wavelength pump source. These devices use cavities that resonated both of the parametrically generated waves (signal and idler), known as the doubly resonant OPO (DRO), in order to reduce the threshold pump power. However this double resonance requirement results in a high degree of instability in output power and wavelength.

This chapter details the design, modelling and operation of a doubly resonant OPO pumped directly by an external-cavity diode laser (ECDL). This device was to be used to investigate the tuning characteristics of a doubly resonant optical parametric oscillator (DRO) and attempt to address some theoretically predicted solutions to the stability challenges posed by the double resonance condition. In addition the design of the DRO was to be later adapted for pumping with a violet emitting diode laser. The implications and potential advantages of an OPO device that is pumped in the blue are discussed and future work based upon this device design is proposed.

4.2 OPO Tuning Behaviour

The basic theory and configuration of an OPO was given in Chapter 3. OPOs can be tuned in a variety of methods. Temperature tuning involves varying the temperature of the non-linear crystal. Angle tuning involves changing the propagation angle of the crystal. Varying the wavelength of the pump source is known as pump tuning. Grating tuning involves changing the grating period of the quasi-phasematched (QPM) crystal. These are all coarse tuning methods.

The spectral characteristics of an OPO are determined by a number of factors including the phasematching conditions, cavity resonance restrictions and energy conservation requirements. The major factors in wavelength selection criteria for an OPO are the energy conservation and phasematching requirements introduced in Chapter 3. For the phasematching condition to be met, the wavelengths must satisfy Equation 2.10. From this we can define the phasematching bandwidth. This is the range of signal and idler wavelengths for which we obtain parametric gain. Coarse tuning defines a broad spectral region over which the signal and idler frequencies are phase matched, the fine tuning properties are the critical requirement in providing narrow-linewidth, amplitude-stable, continuously tunable OPOs. These frequency selection processes are closely linked to the output power stability.

In the case of a singly resonant oscillator, the resonant wave adopts the frequency of the cavity mode closest to the maximum gain of the phasematching bandwidth. The non-resonant wave is free to adopt any frequency that satisfies the phasematching condition so the frequency stability of the resonant wave is determined by the stability of the OPO cavity. Any fluctuations in the frequency of the pump wave result in shifts in the frequency of the non-resonant wave which will adjust to maintain the phasematching condition. Singly-resonant optical parametric oscillators (SROs) have an obvious advantage over doubly-resonant optical parametric oscillators (DROs) with respect to tuning capability. The signal can be tuned continuously with the idler (which is non-resonating) within one free spectral range (FSR) of the OPO

cavity. As there is only one resonant field the SRO is more stable and more tolerant of any large noise perturbations. It is important to note here that SROs are not completely without sensitivity to perturbation. Any small perturbation for example in the cavity length will always be transferred to the signal wave and consequently the idler. In this instance, a DRO is fairly robust to small perturbations and any changes will only affect the output power and not the frequencies whereas they will have more impact on the output from an SRO. However large perturbations result in far more predictable and long range frequency changes in a DRO than in an SRO [4].

4.2.1 Tuning Behaviour of Doubly Resonant Optical Parametric Oscillators

In a DRO, 4 conditions must be satisfied simultaneously: energy conservation, phasematching, and cavity resonances for both the signal and idler. Whilst the DRO offers threshold powers compatible with common narrow linewidth CW lasers it is widely recognised to be overconstrained. This introduces stability and tuning restrictions which were first observed in 1968 ([3] and which have since been well documented since in literature [5, 6, 7]).

Signal and idler frequencies that satisfy the energy conservation condition are called mode-pairs, shown in Figure 4.1. Normally there are several mode-pairs within the phasematching bandwidth whose signal and idler frequencies are close to the cavity modes. The cavity modes of the signal and idler are plotted on two scales which have a common point at the degeneracy frequency. The signal scale increases in frequency from left to right while the idler scale decreases in frequency at the same rate. Any pair of points on the two scales which are vertically aligned represent a pair of frequencies that conserve energy for the given pump frequency. Any pair of cavity modes in vertical alignment represents satisfaction of both the double resonance and energy conservation requirements. Dispersion causes different cavity modes for the signal and idler to have different FSRs. Modes that are in vertical alignment show

the ideal operating point for the cavity as this represents conservation of energy.

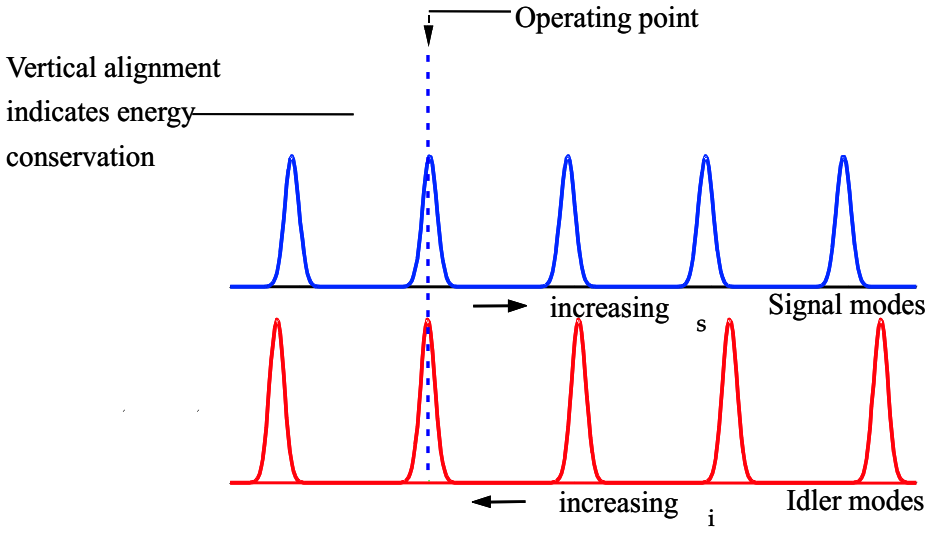

Figure 4.1: **Alignment of Mode Pairs in a DRO**
The signal and idler modes on different scales increasing in opposite directions. The modes that are in perfect alignment are shown as the operating point of the DRO.

Comparatively small changes in either cavity length or pump frequency can cause the OPO output to switch from one mode pair to another. Depending upon the degree of mismatch in the free spectral ranges (FSRs) of the signal and idler waves, the new mode pair is either adjacent to the original pair or many mode pairs removed. These two possibilities are, respectively, a mode hop and a cluster hop. The degree of mismatch dictates the level of detuning of either the cavity length or pump frequency required to cause a mode hop. In addition, it is useful to know the amount of detuning required to move from the centre of one cluster to the centre of the next cluster.

The critical parameter affecting mode selection in a DRO is the mismatch between the intermode spacing of the signal and idler modes compared to the cavity finesse. If the mismatch is large compared to the width of the cavity resonances, then the DRO is prone to cluster hop. If the mismatch is small, a mode hop within the central cluster is more likely. Figures 4.2 and 4.3 describe mode and cluster hops. The simultaneous

resonance condition is only satisfied at intervals a number of FSRs apart. The interval over which this occurs is referred to as the cluster spacing. Changes in cavity length or pump frequency results in two combs of modes moving across each other in opposite directions, causing new mode pairs to come into alignment. This indicates a change in the signal and idler frequencies. The three potential outcomes, mode-hopping, cluster-hopping and failure to reach threshold are described below.

Mode Hopping

A mode-hop is where the pair of modes next to the current pair move into alignment resulting in a change of one FSR in the signal and idler frequencies. If we assume that the original mode pair is exactly on resonance then by changing the cavity mode frequencies by a total amount equal to the mismatch in the free spectral ranges, ΔFSR there will be a mode hop. Thus the condition for a mode hop is given by

$$\frac{2\Delta L F_s}{\lambda_s} + \frac{2\Delta L F_i}{\lambda_i} = \Delta F \tag{4.1}$$

where λ_s and λ_i are the wavelengths of the signal and idler respectively, ΔL is the change in the cavity length. F_s, F_i and ΔF are the FSRs of the signal and idler and the FSR mismatch respectively. Hence for a DRO, the change in the cavity length required to obtain a mode hop, ΔL_{hop}, is

$$\Delta L_{hop} \approx \frac{\Delta F}{2F}\lambda_p \tag{4.2}$$

where λ_p is the pump wavelength.

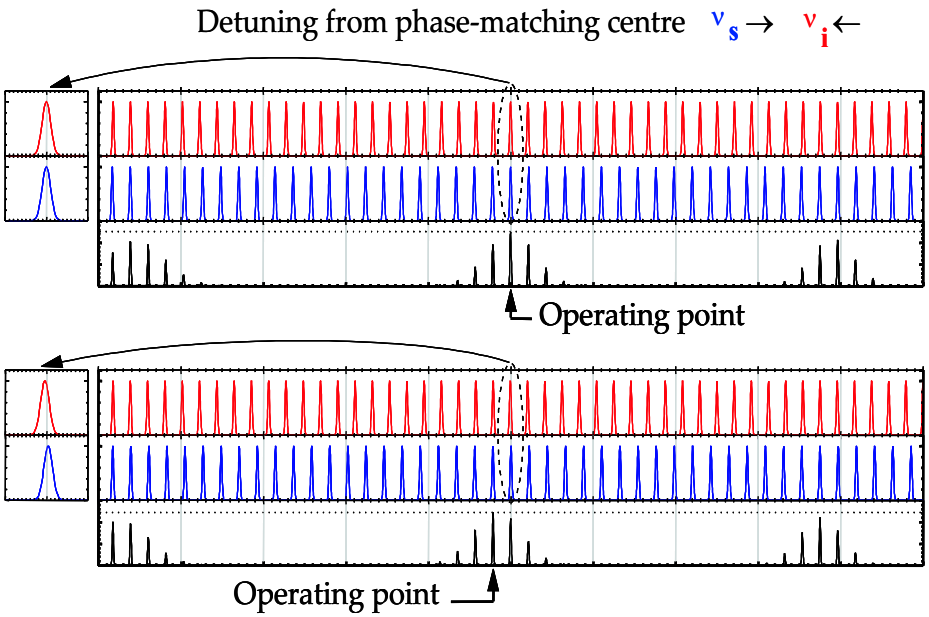

Figure 4.2: **Mode Hopping**
A small perturbation causes the OPO to shift its operating point to an adjacent mode pair. This is likely to occur when the difference in the FSRs of the signal and idler is close to zero. Where the FSRs are similar, a wide cluster spacing is likely.

Cluster Hopping

The second possibility is cluster hopping. In this case, ΔF between the signal and idler is larger than for the mode-hop case. The clusters that are adjacent to the central cluster suffer a smaller reduction in net gain due to an increase in the phase mismatch. As tuning occurs and the combs of modes slide over one another the next mode to attain the highest net gain is in a cluster adjacent to the original one. Further tuning results in the mode pair adjacent to the original pair coming into alignment and the OPO hops back to the central cluster, operating on the mode pair adjacent to that at which it started. The number of modes between the centre of one cluster and the centre of the next cluster is given by $\Delta F/F$. Thus from Equations 4.1 and 4.2 for the conditions for a mode hop, we can similarly obtain the amount of cavity length detuning, $\Delta L_{cluster}$, and pump frequency detuning, $\nu_{p-cluster}$, required for a cluster hop from the centre of one cluster to the centre of the next cluster:

$$\Delta L_{cluster} = \frac{\lambda_p}{2} \tag{4.3}$$

$$\nu_{p-cluster} = FSR \tag{4.4}$$

These quantities are equal to the interval between cavity resonances of the pump field within the OPO cavity.

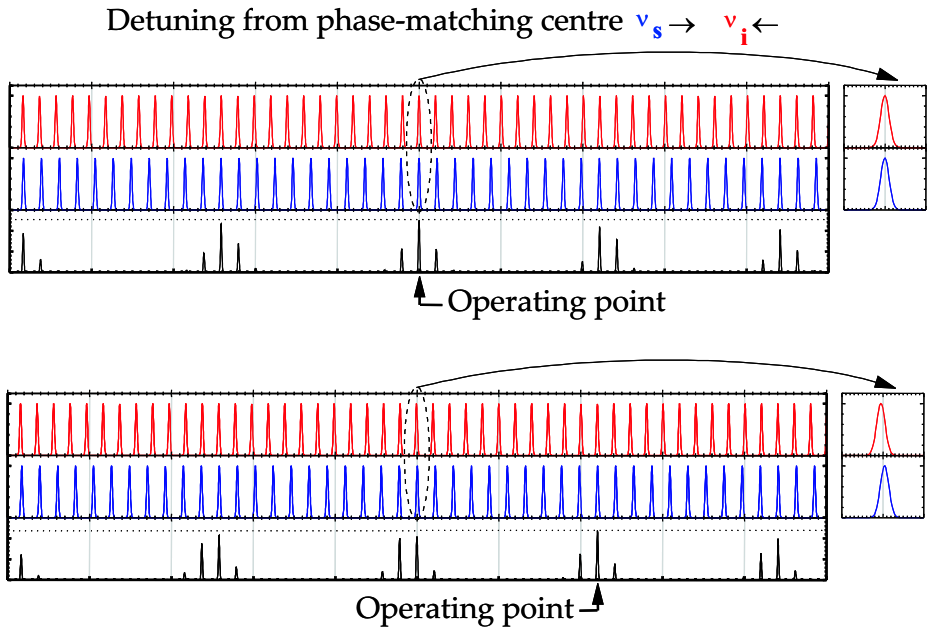

Figure 4.3: **Cluster Hopping**
A large perturbation cause the OPO operation to shift to a mode pair within another cluster. This is more likely to occur where the difference in FSRs of the signal and idler waves is large. This causes a smaller cluster spacing

The third possible outcome is when no mode pairs are sufficiently coincident, meaning that the DRO fails to reach threshold. In this case it ceases to operate until a mode pair come into sufficiently close alignment for threshold to be reached. Consequently, the DRO switches on and off continuously as it waits to attain threshold so there are large fluctuations in output power. The degree of phase-mismatch and loss in

the cavity varies with frequency, and consequently so does the threshold. The effect of this upon the mode and cluster hopping processes is to add additional frequency fluctuations.

It is these processes and effects that limit the practical use of DROs. However the much lower threshold power requirement for DROs motivates efforts to improve the stability and tuning of the DRO.

4.3 Diode Lasers as Pump Sources

For a laser to pump an OPO it should have sufficient output power, possess high spectral quality, have a diffraction limited output and be tuneable and stable. It is also desirable for the pump source to be efficient, inexpensive, compact, rigid and all solid state.

When considering the size and efficiency of a pump source, the ideal choice for a CW-OPO is a high power diode laser. Diode pumped OPOs were first demonstrated using injection locked diode laser arrays [8]. Diode lasers exhibit all of the desirable characteristics to make them excellent pump sources for a CW-OPO. One of the main advantages of diode pumping is the wide tunability of the pump wavelength. Semiconductor lasers are broadly tunable both by current and temperature. As described in Chapter 2, an external cavity diode laser (ECDL) offers lower operational threshold, less sensitivity to randomly phased feedback light, reduced sensitivity to unwanted injection current and temperature changes and wider mode-hop free tuning, making it a very promising candidate for pumping a CW-OPO. The ability to continuously tune the output of an ECDL provides a further means of tuning the output of a CW-OPO. The disadvantage the ECDL compared to the solitary diode laser is its lower output power, requiring a sufficiently low threshold for the OPO.

4.3.1 The Pump Source

The ECDL system used is configured in a standard Littrow external cavity configuration as discussed in Chapter 2. The two laser diodes used in this work were a Spectra Diode Labs (SDL) AlGaAs device operating at 810nm within a homebuilt Littrow external cavity configuration with a maximum power rating of 100mW. The violet diode with which we hope to eventually pump a DRO device is a Nichia GaN device operating at 405nm. A basic characterisation of the violet diode laser is given in Chapter 5. The threshold current of the IR laser when free running is 23.4mA. In ECDL configuration, threshold was reduced to 17.6mA. The temperature and current tuning characteristics were typical for a diode laser. The maximum output power in the external cavity was 90mW, a reduction from 130mW in free-running configuration.

4.4 The DRO System

Previous work had shown that a periodically poled lithium niobate (PPLN) crystal would be expected to give a minimum threshold of the order of milliwatts within typical cavity parameters [9]. By defining these cavity parameters, extensive Mathcad modelling based on modematching and gaussian beam propagation theory was carried out to set parameters for the experimental work. The aim was to construct a DRO pumped directly by a violet ECDL based exactly on the design of the mid-IR emitting OPO described here. By developing the OPO system using an ECDL it was anticipated that the stability of the DRO could be improved in part with a more stable pump source. As the ECDL provides a ready source of narrow linewidth, single mode output, the effect of the stability of the laser on the OPO operation is no longer an issue and introduces a new opportunity for implementation of active stabilisation.

The non-linear crystal is configured for propagation along the optical x-axis with all three interacting waves polarised along the z-axis. The dimensions of the crystal are

19mm by 11mm by 0.5mm. The manufacturers' standard configuration allows eight different grating periods to be poled adjacently along the y-axis.

The pump beam is guided through the optical system shown in Figure 4.4, ensuring sufficient isolation and the correct polarisation for use in the OPO.

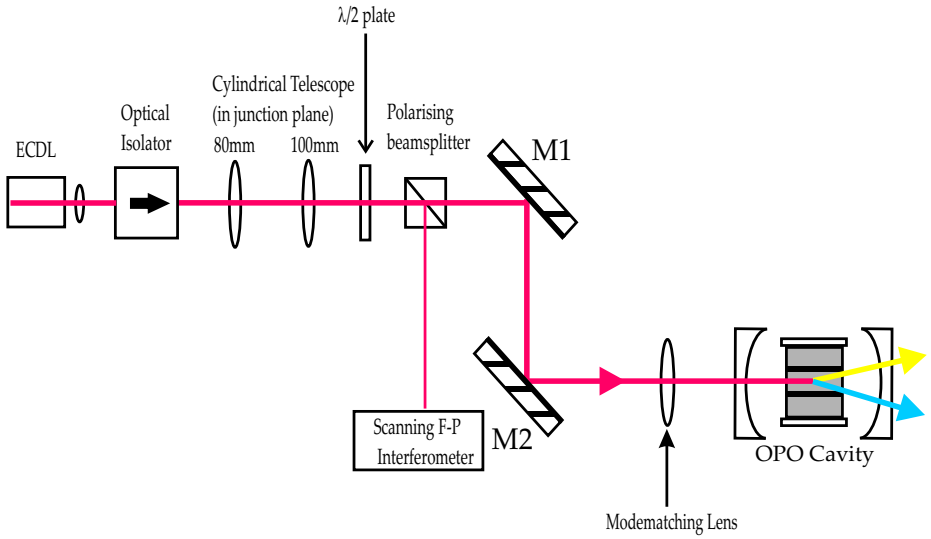

Figure 4.4: Schematic of the DRO Cavity Configuration
The pump wave (λ_p)is collimated through the modematching lens and enters the OPO cavity. This wave travels through the PPLN non-linear crystal and the signal and idler waves (λ_s, λ_i)are output.

A series of beam steering mirrors guide the beam into the OPO cavity. The isolator ensures that the laser is not destabilised by feedback effects. The cylindrical telescope that delivers a circular beam (same size of beam in horizontal and vertical planes) and beamsplitter cube and halfwave plate to form a variable beamsplitter. The beamsplitter is also used to split off a small portion of the beam to monitor the spectral behaviour of the laser through a Fabry-Perot interferometer.

4.5 Optical System Design

The design and configuration of an OPO cavity must satisfy certain requirements to give appropriate size and shape to the beam within the cavity. The cavity must be

stable and the field within the cavity retains a Gaussian intensity distribution. The divergent effects of the optical system on the Gaussian pump beam will affect the final beam waist position. The field at any point in the cavity can be described in terms of Gaussian beam parameters, primarily the radius of curvature of the wavefront R and the beam radius w that is perpendicular to the resonator axis. The point at which the radius is at its minimum, w_0, is the beam waist. At this point R is infinite (a plane wavefront) and the beam is said to be collimated. The beam waist is a crucial factor as this is the point where the beam irradiance, is greatest. This irradiance does not change significantly over a distance. Thus the lowest threshold operation for an CW-OPO occurs when the beam waists of all the resonant waves in the cavity are situated at the centre of the non-linear crystal. At the waist, the cross-sectional area of the beam (A) is πw_0^2. A certain distance from the waist the cross sectional area doubles to $2\pi w_0^2$. This distance at which this occurs is the Rayleigh range. The confocal parameter, b, is twice the Rayleigh range:

$$b = \frac{2\pi n w_0^2}{\lambda} \tag{4.5}$$

Here, n, is the refractive index of the medium that the beam propagates through and λ is the wavelength of the light. The confocal parameter is the distance over which the dimensions of the beam within the cavity remain approximately constant. For optimum focussing the confocal parameter is matched in size to the length of the non-linear crystal. The non-linear interaction is maximised when the beamwaist, w_0, is located at the centre of the crystal. This condition gives an expression for the beamwaist when Equation 4.1 is re-arranged where $b = L_x$:

$$w_{0,min,(confocal)} = \sqrt{\left(\frac{\lambda L_x}{2\pi n}\right)} \tag{4.6}$$

This equation gives a value for the beamwaist that will allow an estimate of the cavity length for minimum threshold. This analysis assumes that the beam dimensions

will remain constant throughout the length of the non-linear crystal. However a more detailed examination of the minimum pump threshold requirements concerning focussed Gaussian beams is given by Boyd and Kleinman [10]. This paper studies the case of a DRO, as we have in our situation, assuming that the confocal parameters of all three of the resonant beams within the cavity , the pump, signal and idler, are equal. In their analysis, Boyd and Kleinman apply a an extra multiplication factor $h_m(B,\xi)^{-1}$ to the expression for minimum pump threshold. The function $h_m(B,\xi)$ is defined by two beam parameters relating to the walkoff (B) and focussing (ξ). Where, as is the case here, quasi-phasematched materials are used, walkoff is not a factor so B=0. Therefore $h_m(B,\xi)$ has a maximum value (where the pump threshold is at a minimum) of 1.2 when ξ=2.84.

It is now possible to combine Equations 4.5 and 4.6 to obtain an expression for the minimum beamwaist. Using Equation 4.7 an estimate for the value of the beamwaist was obtained, and this value was used within an ABCD matrix cavity model to identify the required cavity length to deliver this beamwaist.

$$\text{Focusingparameter} = \frac{\lambda_0 L_x}{2\pi n_s (w_0)^2} \tag{4.7}$$

This is where the optimum focusing parameter = 2.84, $\lambda_0 = 1.2\mu m$, $n_s = 2.162$, $L_x = 0.019m$.

4.6 Cavity Modelling using ABCD Matrices

The position and size of the beam waist in the resonator cavity are crucial parameters in determining the cavity length and position of optical elements in order to achieve successful OPO operation. By modelling these parameters, the initial positions for the practical setup can be determined, making it easier to realise. The use of ABCD matrices is a well established technique for determining these parameters [11].

Firstly the length of the cavity must be determined, by imposing the condition for a stable cavity, which arises from the conditions that satisfy the propagation of a Gaussian beam. A stable cavity has a complex beam parameter, q , that is reproducible over a single round trip. This condition determines the waist, w , and the radius of curvature of the wavefront, R , at a reference point in the cavity. Therefore it is necessary to determine the dimensions of the cavity that will give a minimum beam waist at the centre of the crystal.

$$q = \frac{1}{r} - i\frac{\lambda}{\pi w^2}^{-1} \tag{4.8}$$

Applying a system matrix

$$\begin{pmatrix} A & B \\ C & D \end{pmatrix}$$

to the stability condition yields

$$q` = \frac{Aq + B}{Cq + D} \tag{4.9}$$

If we set $q` = q$ then the complex beam parameter is reproducible over a single round trip. When a system matrix for a particular resonator configuration is known, q, R and w can be calculated. The beam waist w_0 and the distance it is from the reference point z, can then be found using the following equations

$$w_0^2 = \frac{w^2}{1 + (\frac{\pi w^2}{\lambda R})^2} \tag{4.10}$$

$$z = \frac{R}{1 + \left(\frac{\lambda R}{\pi w^2}\right)^2} \tag{4.11}$$

Table 4.1 shows the ABCD matrices for some common optical elements.

Resonator Element	ABCD Matrix	Parameters
Free Space	$\begin{pmatrix} 1 & d \\ 0 & 1 \end{pmatrix}$	d=distance
Crystal	$\begin{pmatrix} 1 & \frac{L}{n} \\ 0 & 1 \end{pmatrix}$	L=crystal length, n=refractive index
Spherical Mirror	$\begin{pmatrix} 1 & 0 \\ \frac{-2}{R} & 1 \end{pmatrix}$	R=radius of curvature
Lens	$\begin{pmatrix} 1 & 0 \\ \frac{-1}{f} & 1 \end{pmatrix}$	f=focal length

Table 4.1: **Common ABCD Matrices**

Using these fixed parameters, the beamwaist is $w_0 = 24.31\mu m$. In addition, simple ABCD models are used to obtain the optimum position for the modematching lens outside the cavity once the parameters of the pump beam are defined. This is done by further modelling which defines the positions of the collimating lens after the diode laser and the separation of lenses in the cylindrical telescope. The system is a product of the various matrix elements that describe the propagation of the beam through one round trip of the OPO cavity. For one complete round-trip of the cavity, shown schematically in Figure 4.5, there are nine separate elements within the cavity stability matrix.

1. Beam starts at centre of crystal. Travels a distance $\frac{L_x}{2}$ to exit the crystal.
2. Travels through air from crystal edge to output cavity mirror.
3. Beam reflected from output mirror with radius of curvature of 0.025m.
4. Beam travels back from output mirror to the edge of the crystal.
5. Beam travels through full length of the crystal.
6. Beam propagates through air from the crystal edge to the input cavity mirror.

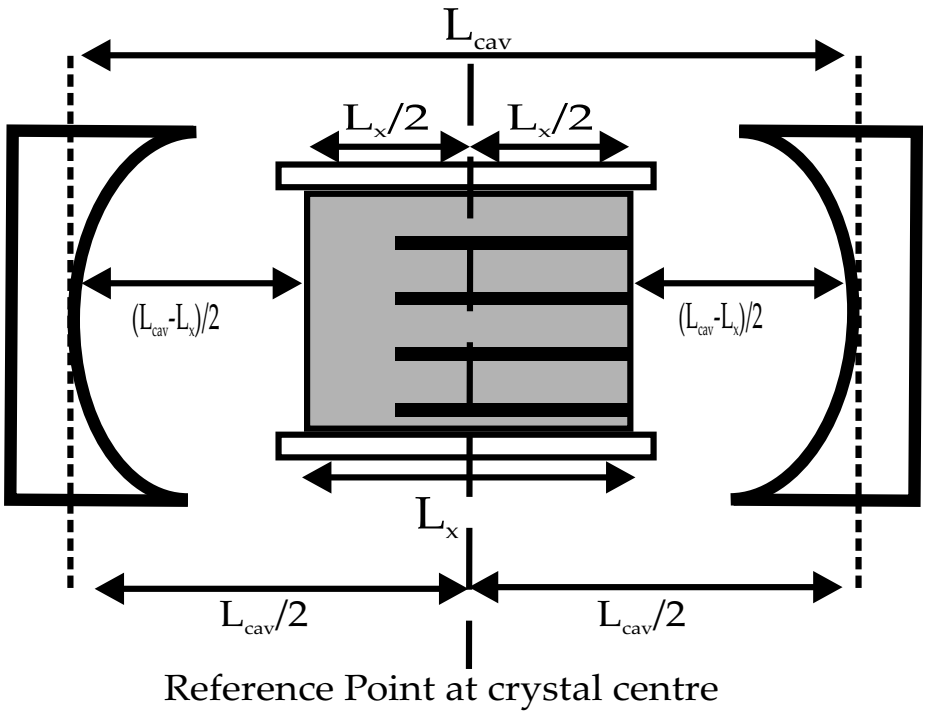

Figure 4.5: **Roundtrip of OPO cavity**
The diagram shows all the dimensions and elements used in an ABCD matrix analysis of a single round trip of a Gaussian beam propagating through the cavity.

7. Beam reflected from input through mirror with radius of curvature of 0.025.

8. Beam goes from input mirror to the crystal edge.

9. Beams travels from crystal edge back to the centre of the crystal completing one round trip of the cavity.

The dimensions used to model the round trip are given in Table 4.2. Figure 4.6 shows the modelling results for a stable cavity. The cavity stability condition is satisfied for a cavity length of 0.11m.

Having determined suitable cavity configurations defining the input beamwaists, the propagation of the pump beam throughout the entire system must be matched to this. To determine an appropriate focal length and position for the modematching lens another ABCD beam trace analysis is applied. The modematching lens focusses the incoming pump beam into the cavity. As stated earlier the beam waist must be

Cavity Element	Dimension(m)
Crystal Length L_x	0.019
ROC Cavity Mirror 1	0.030
ROC Cavity Mirror 2	0.050
Initial Cavity Length	0.090

Table 4.2: **Cavity Parameters for ABCD Matrix Calculation**

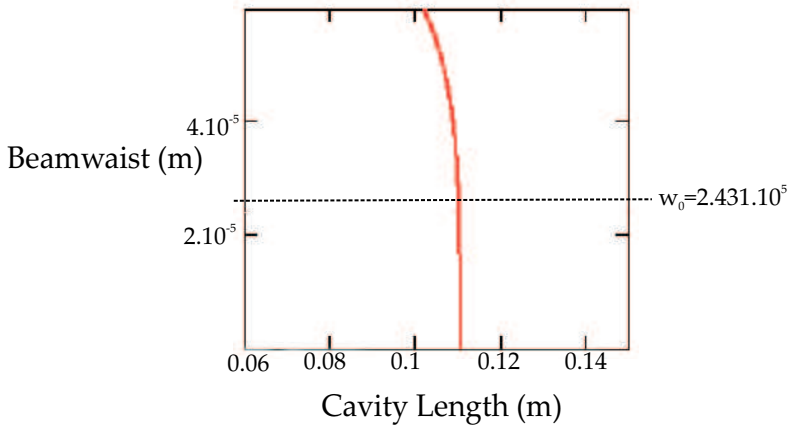

Figure 4.6: **Modelling Results for a Stable Cavity**
The graph shows that the minimum beam waist is achieved at the crystal centre for a cavity length of 0.11m

at the centre of the crystal. The ABCD analysis here must take into account the propagation of the beam through the optical elements from the output of the diode laser to the input mirror of the OPO cavity. The dimensions required for this analysis are shown in Figure 4.7 and their values give in Table 4.3.

The distances z and y were modelled using Mathcad to ensure a circular beam throughout the entire system. The dimensions for a stable cavity were included within the modematching analysis.

Figure 4.8 shows that the beamwaist is obtained when distance $L_m = 0.08m$. This is confirmed by the second graph showing that when the modematching lens is in this position, the confocal focussing requirement is satisfied.

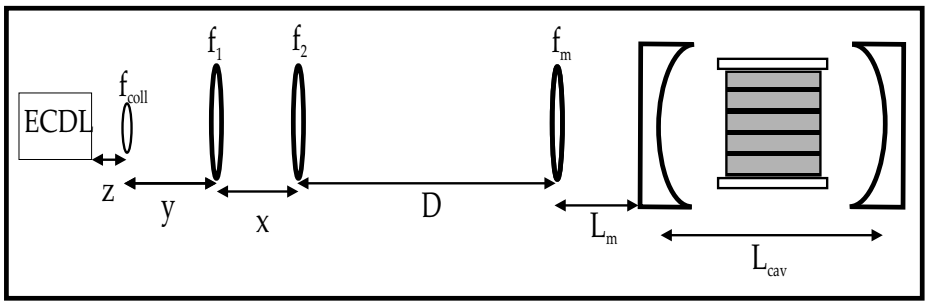

Figure 4.7: **Modelling for the position of modematching lens**
The diagram shows the parameters and elements used for an ABCD matrix analysis for the positon of the modematching lens from the cavity.

Cavity Element	Dimension(m)
Diode Laser to collimating lens (z)	0.0002
Collimating Lens to telescope (y)	0.2
Telescope Separation (x)	0.083
Telescope to modematching lens (D)	2.0
Cavity Length (L_{cav})	0.11
Focal Length of collimating lens (f_{coll})	0.002
Focal length of telescope lenses (f_1 and f_2)	$0.022, 0.060$

Table 4.3: **Cavity Parameters for Modematching Lens ABCD Matrix Analysis**

Double passing the pump wave should have the effect of reducing the threshold of the device further as shown in Chapter 3. A beamsplitter splits off the resonant waves and allows the pump wave to be reflected back into the cavity via a double passing mirror, shown in Figure 4.9. To account for the double passing of the pump, the cavity position needs to be realigned to provide for the focussing of the beam at the crystal centre. This is achieved again with the aid of Mathcad modelling where the cavity is redefined to include the input cavity mirror and the double passing mirror. The same basic model is used but the differences in the round trip travel, caused by the asymmetry of the cavity, is accounted for. Table 4.4 shows a summary of the

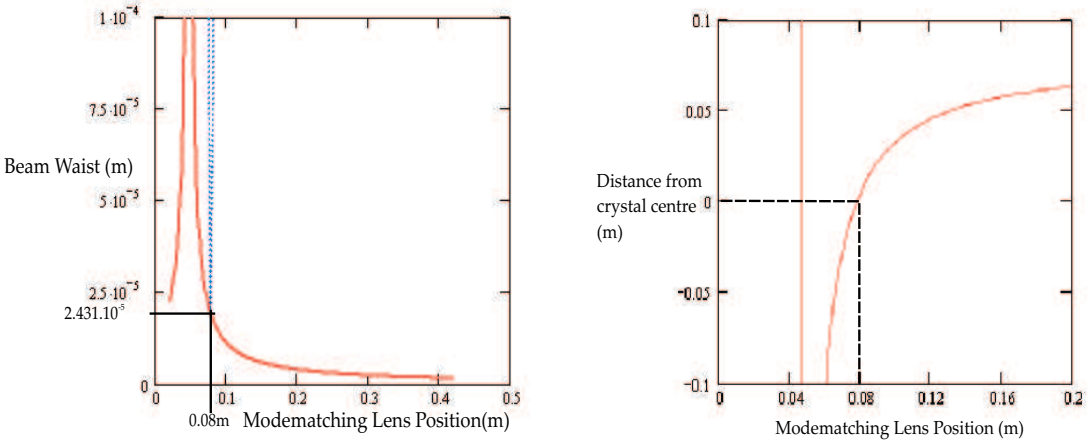

Figure 4.8: **Modelling Results for the position of the modematching lens** The graphs shows that the modematching lens gives the beamwaist at 0.08m from the input cavity mirror. The second graph shows that this position gives the beamwaist at the crystal centre.

modelling results for both single and double passing of the pump wave.

Cavity Configuration	Cavity Length(m)	Modematching Lens Position(m)
Single Pass Pump	0.011	0.08
Double Pass Pump	0.090	0.13

Table 4.4: **Summary of Mathcad Modelling Results**

4.7 OPO Operation

The PPLN crystal was poled with eight grating periods from $\Lambda = 21.0\mu m$ to $22.4\mu m$. This allows phasematching of the idler wavelengths from degeneracy to $5\mu m$ between room temperature and 200^oC when pumped at 810nm. The end faces of the crystal were coated to give R $< 0.2\%$ over the range $1.16 - 1.25\mu m$, R $< 0.8\%$ over $2.35 - 2.8\mu m$ and R=1.5% at 810nm. The mirrors were coated to have reflectivity at the signal and idler wavelengths and high transmission of the pump wavelength.

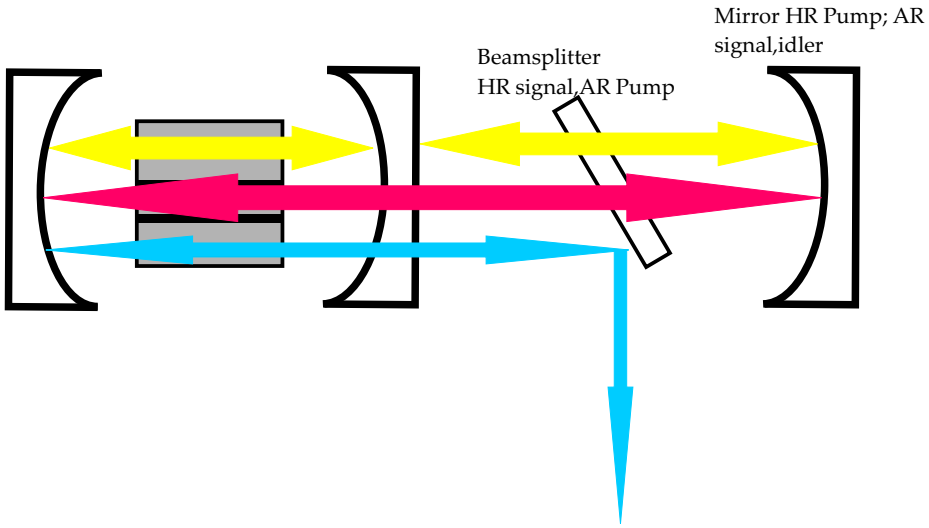

Figure 4.9: **Double Passing of Pump**
The DRO cavity is shown with the pump (red), signal (yellow) and idler (blue) waves. The cavity is assymetrical to account for the mirror that is used to double pass the signal through the cavity

OPO Threshold Measurements

The threshold of the OPO was reduced to its minimum value for both single and double pass operation. The output powers for the two cases are shown in Figure 4.10.

The threshold power of the OPO in single pass was measured as 41mW and the threshold in double pass was 21mW. These were the best values obtained and the factor of two reduction in the threshold as a result of double passing follows the theoretical pattern described in Section 3.4.2.

OPO Efficiency

Figure 4.11 shows a plot of the efficiency of the OPO for both single and double pass of the pump wave. The efficiency shown in these figures is that as measured after the output coupling from the cavity and is not a measure of the conversion efficiency of the non-linear process that would be measured within the cavity.

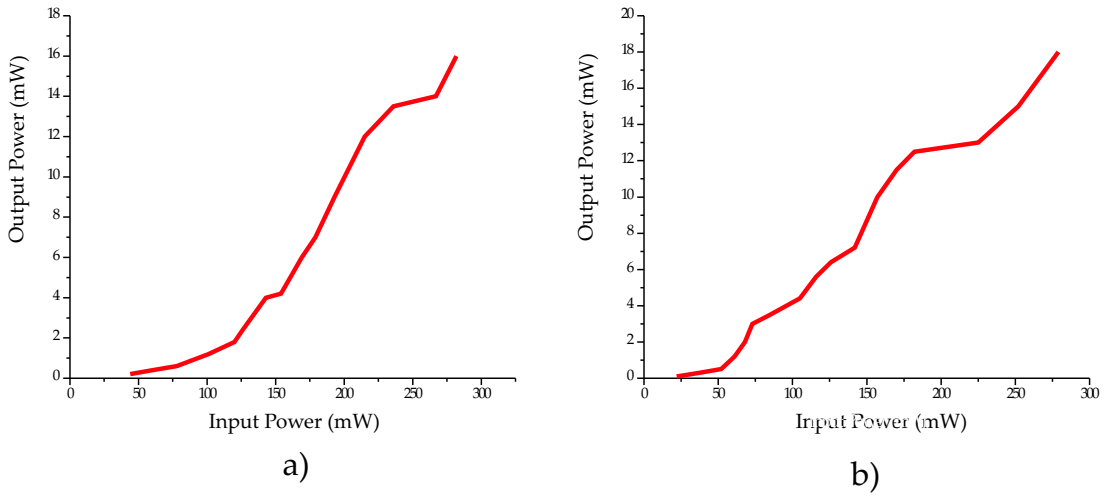

Figure 4.10: **Threshold of DRO**
Graphs of output power versus input power show the threshold of the OPO for single pass (a) and double pass (b) operation, where the slope of the graph suddenly increases signalling the start of parametric oscillation behaviour.

For the single and double pass of the pump the maximum efficiency is 5.5% and 7% respectively.

From these values it is possible to estimate the efficiency within the cavity and within the crystal, thus investigating the efficiency of the OPG interaction. The output mirror of the OPO has a reflectivity of 99% so using the following equations,

$$P_{output} = \left[\frac{a}{a+b}\right] P_{downconverted} \tag{4.12}$$

where a is the output coupling of the DRO cavity and b is the parasitic loss in the cavity. Parasitic loss can be attributed to a number of factors including absorption within the crystal, thermal effects and the reflectivity of the signal and idler from the cavity mirrors.

$$\text{Downconversionefficiency} = \frac{P_{downconverted}}{P_{input}} \tag{4.13}$$

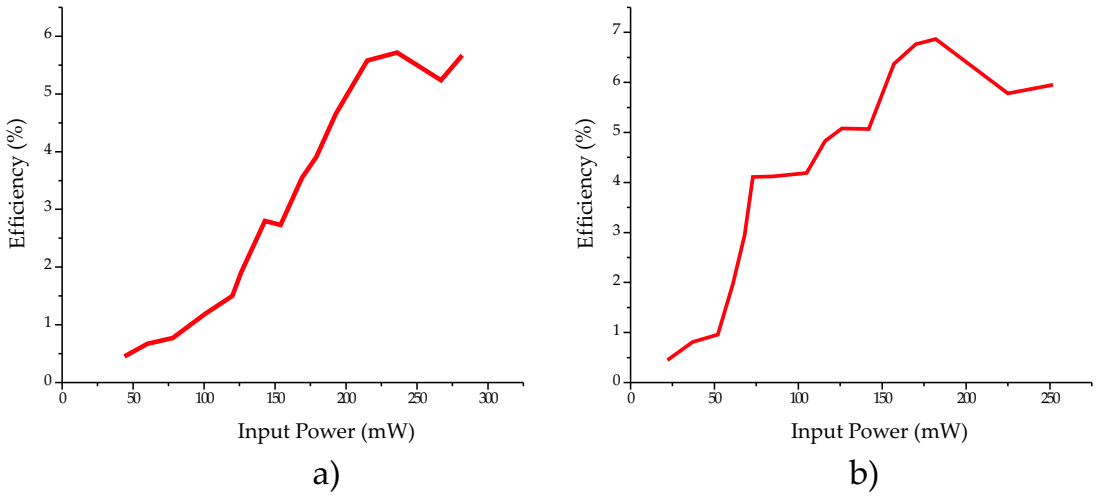

Figure 4.11: **Efficiency of DRO with for single and double pass of the pump wave**
The graphs show the efficiency at the output of the OPO for the single pass pumping (a) and double pass pumping (b)

To estimate the downconversion efficiency trends in Figure 4.11 are used along with an estimate of the parasitic loss within the DRO cavity. An estimate of the conversion efficiency will be made using a parasitic loss value of 10% of the input pump power. This value is chosen as for most OPO applications, parasitic loss values of greater than 10% of the pump power would characterise a cavity that is not operating at its optimum and would suggest that the design of the OPO cavity needs to be amended. Thus the figure of 10% of pump power is the maximum desirable parasitic loss in an OPO cavity.

For the single pass case the peak efficiency occured for an input power of 230mW. The output power of the OPO at this input power is 13.5mW, parasitic loss is 23mW and output coupling is 1% of the pump (2.3mW). Thus from these values the down-converted power is calculated from Equation 4.13 to be 148.5mW. Therefore the conversion efficiency for this interaction is 65%. Similarly for the double pass case, the peak efficiency occurs for a pump power of 175mA and output power of 13mW so the downconverted power is 143mW. Therefore the conversion efficiency is 82%.

Wavelength Temperature Tuning

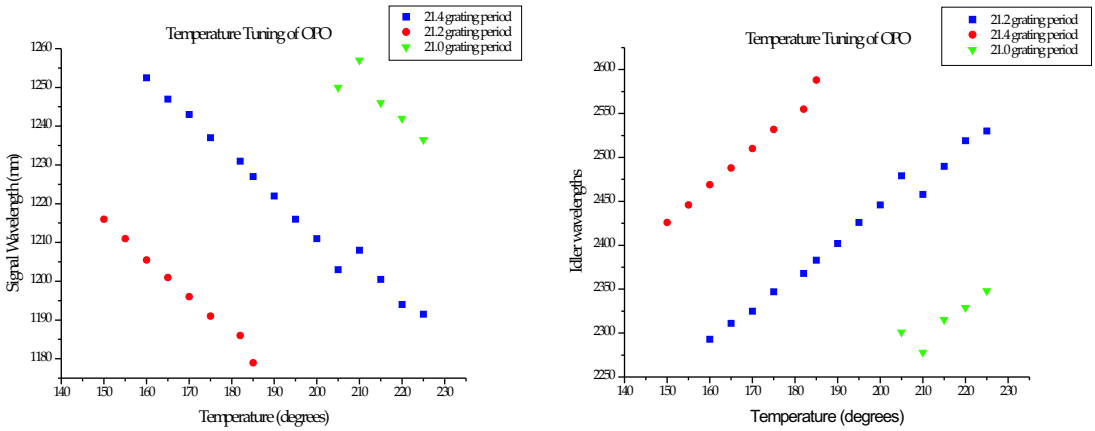

Figure 4.12: **Temperature Tuning of OPO for Signal and Idler Wavelengths** The variation in the signal and idler wavelengths as a result of changes in temperature of the non-linear crystal.

The OPO was tuned by alteration of the crystal temperature. The OPO was operated through three grating periods and the wavelengths of the output signal and idler waves were measured. Figure 4.12 shows the tuning of the OPO over three grating periods. For the 21.6μm grating period, the signal wavelength range was 61nm (5THz) which demonstrates the wide tunability of these devices. The wavelength range attainable over all three grating periods was 1.2μm to 1.23μm for the signal and 2.3μm to 2.6μm for the idler wavelengths. For a spectroscopic tool, the wavelength range of an OPO is better than any other device available, allowing spectroscopy on a wide choice of different elements.

4.8 Discussion

Although the results obtained from the working OPO were limited by time, there was sufficient data to allow some trends to be identified and future work to be proposed.

Temperature tuning was obtained over three grating periods of the crystal giving a

wide wavelength range for the device. Both single and double passing of the pump beam resulted in successful operation. By double passing the OPO, a lower threshold power was obtained, increasing the variety of pump sources available for this type of device. The threshold requirements for an OPO relax with shorter pump wavelengths so it is conceivable that for the violet OPO the threshold would be lower than 21mW, which is an output power that is attainable by a violet diode laser such as those characterised in Chapter 5. In addition, double passing the pump further restricts the number of potential oscillation conditions, thus providing a more stable output.

The development of the DRO system was attempted in order to obtain a source of continuous, stable tunable laser radiation of frequency and wavelength that is, with certain restrictions,user selectable. It was discussed earlier that the DRO is more prone to discontinuous frequency output than other cavity configurations. There has been extensive theoretical and experimental work carried out on the tuning of birefringently phase matched (BPM) DROs [12, 5, 6]. However, as yet, these phenomena have not been investigated for quasi-phase matched DROs. Lindsay [9, 13] examined these issues theoretically by modelling the tuning and stability behaviour of the DRO system described in this chapter. Based on experimental observations, Mathcad modelling and comparisons with the predicted and actual observed behaviour of BPM DROs, it appears that there are factors involved in the stability and tuning that are typical to quasi-phase matched materials (in the initial case periodically poled lithium niobate (PPLN).

Observation of the operation of the DRO showed that it exhibited strong cluster hopping behaviour resulting in no well defined points of simultaneous resonance as the cavity length was varied. This has significant implications for the stability of the device. The characteristics of the PPLN DRO could not be explained by simple mode-hopping behaviour. Close to degeneracy, the behaviour was similar to that exhibited by Type I BPM devices. However, results showed that the outer clusters have a similar threshold to the central cluster and that the phasematching bandwidth was not sufficiently narrow to exclude outer clusters. There were large increases in

the phasematching bandwidth of the DRO at degeneracy. For comparison, the cluster spacing was also calculated for the same parameters and then the ratio of the cluster spacing to the phasematched bandwidth was calculated. It was found that at these wavelengths there were 4 to 6 clusters within each phasematch bandwidth, many with a threshold close to minimum. This is in contrast to observations of BPM DROs where systems exhibited typically 3 and 1 clusters within the phasematch bandwidth.

Material	$\Delta\nu_{pm}$	$\Delta\nu_{cl}$	Number of clusters
Type 1 BPM	$5.6THz$	$1.62THz$	3
Type 2 BPM	$450GHz$	$260GHz$	1
QPM	$1.07THz$	$169GHz$	$4-6$

Table 4.5: **Clusters for different phase-matched materials**

The combination of the number of clusters and their thresholds being so similar gives rise to the competition between clusters and the cluster hopping behaviour. This problem appeared to be intrinsic to PPLN at these wavelengths.

The number of clusters within the phasematching bandwidth is independent of the length of the crystal and is solely dependent upon the refractive indices and frequencies of the signal and idler waves. The ideal situation is a large cluster spacing and small phasematch bandwidth in order to minimise the possibility of multiple clusters. From the expression for the ratio of phasematch bandwidth to cluster spacing, $\frac{\Delta\nu_{pm}}{\Delta\nu_{cl}}$, we want the conditions for where the phasematch bandwidth is minimum. Again the behaviour of the DRO in different conditions was modelled. At degeneracy $\Delta\nu_{pm}$ is always large. The cluster spacing is large when the refractive indices at the signal and idler are almost equal. From the modelling results it was seen that $\Delta\nu_{pm}$ remained large for pump wavelengths in the near IR region. Thus we conclude that, over this tuning range, we expect a small phasematching bandwidth for shorter pump wavelengths, i.e. those in the visible. To clarify this, $\frac{\Delta\nu_{pm}}{\Delta\nu_{cl}}$ as a function of

signal wavelength for various pump wavelengths was plotted as shown in Figure 4.13. This showed that the number of clusters at longer wavelengths is generally higher than for shorter wavelengths. Thus cluster selection is always a problem for pump wavelengths in the near IR.

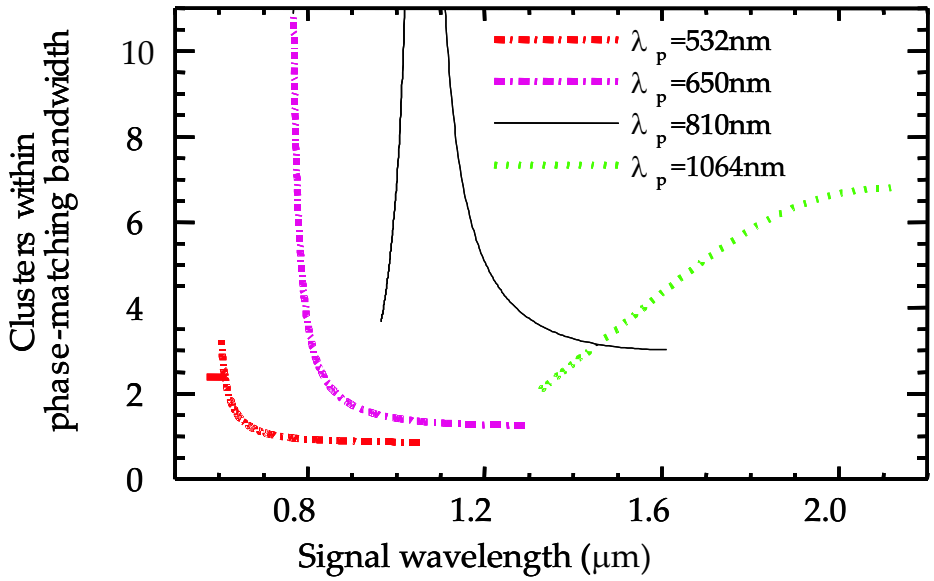

Figure 4.13: **Variation in number of clusters with pump wavelength** [13]

$\Delta\nu_{pm}$ is dependent upon the dispersive properties of the material. Therefore it was sensible to see if this trend still existed when other periodically poled QPM materials were used in the modelling. The materials used included PPKTA, PPKTP and PPRTA. The trends were similar regardless of the material as shown in figure 4.14. No material offered a significantly better ratio of cluster spacing to phasematch bandwidth than PPLN.

Following this work, potential solutions to the cluster hopping problem have been identified as described in the next section.

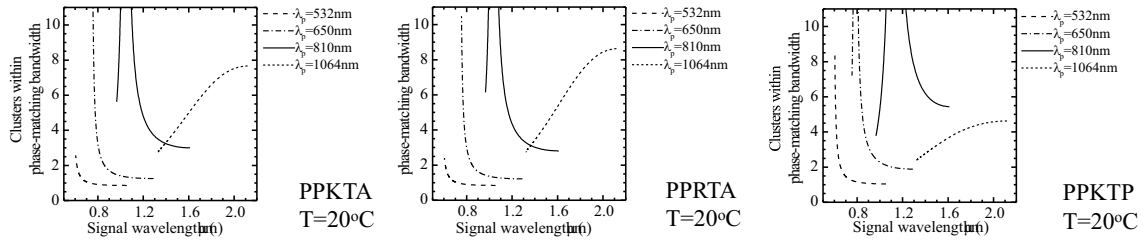

Figure 4.14: **Cluster numbers with different periodically poled materials** [13]

Frequency Selective Elements

An intracavity element such as an etalon will have the effect of suppressing the outer clusters within the phasematch bandwidth. The etalon will achieve this much faster than a reduction in the phasematch bandwidth. The etalon, if chosen to have a FSR larger than the phasematching bandwidth, can be positioned such that it only allows transmission of a cluster at a particular position. In this way, not only is the problem of cluster hopping overcome, there is a further element of selectivity introduced into the operation of the DRO. By adjusting the angle of the etalon, the cluster can be chosen.

Improved Locking Scheme

Side-of-fringe locking schemes have been used to good effect in various applications of stabilisation from solitary diode lasers to OPOs but creates further problems regarding cluster hopping. When side-of-fringe locking is used, the electronic locking circuit tries to keep the power of the OPO at a constant level. Therefore it is necessary to have a monotonic variation in the output power around the lock point. This occurs only in side-of-fringe locking. In contrast, the top of fringe locking technique has the output power decreasing in both directions away from the lock point. The top-of-fringe method is more complicated to implement than side-of-fringe as the electronic circuit cannot tell solely from the variation in power in which direction the cavity

length must change in order to bring the OPO back to the lock point. Improving the locking technique is a measure that can be employed to minimise the effect of the cluster hopping without actually preventing the occurence of the phenomenon.

In the context of cluster hopping the side-of-fringe method causes additional problems as overlap between clusters occurs at the side of the fringe. A small perturbation from the lock point will cause the locking electronics to see the power variation from the adjacent overlapping mode which it will then lock to. Also, because the 'opposite' side of the next fringe is overlapping with the original fringe, the response of the power to changes in cavity length will actually have the opposite sign and the locking electronics will accelerate the change in this direction until it reaches the other side of the new fringe. This means that it is very difficult to use the side-of-fringe method to reliably lock the OPO output where there are lots of overlapping modes and clusters. The top-of-fringe method does not experience this problem to the same extent, but if there is a sufficiently large perturbation the OPO could move away from the top of the fringe into a region where there is an overlapping fringe leading to the same problem.

Shorter pump wavelength (Visible pumping of OPO)

The mathematical modelling carried out by Lindsay [9] demonstrated that the use of a shorter pump wavelength yields a smaller phasematching bandwidth (Figure 4.13). Pumping a DRO with a visible laser would allow a practical investigation of the effects of a reduction in the pump wavelength on the tuning properties of the device. If the phasematching bandwidth was shown to reduce and the cluster hopping problem overcome, a potential solution to the stability problems of the DRO could be designed and implemented thus moving the DRO towards its goal of becoming a reliable working device. Thus a DRO pumped using a violet diode laser provides an opportunity to gain access to a previously unattainable region of the spectrum. the possibility for obtaining smooth tuning of a QPM DRO would be increased. In

addition, a reduction in the pump wavelength will also introduce a different range of generated signal and idler waves.

4.9 Summary

In this chapter the process of designing and obtaining parameters for a practical OPO system was described. A brief discussion on the stability and tuning issues so crucial to applying these devices was then followed by a detailed description of ABCD matrix modelling for the system design using Mathcad. A DRO was successfully built and operated with a threshold power as little as 21mW demonstrating the suitability of diode lasers as pump sources. Temperature tuning over three grating periods showed the wide range of wavelengths attainable by an OPO, indicating their potential as spectroscopic tools. A discussion of potential investigation to improve the spectral characteristics and stability of DROs was given, as well as the potential to pump the OPO using a violet diode laser.

The development of a smoothly tuning DRO based upon a quasi-phasematched material requires extensive investigation into the tuning properties of these devices. One solution that was identified was the use of a violet emitting pump diode laser with modelling having indicated that the shorter wavelength would yield conditions more suitable for smooth tuning. In addition there has been no previous demonstration of an OPO device that is pumped by a violet diode.

Much of this potential work is feasible however due to factors outwith of the laboratory I was unfortunately unable to continue with the OPO project and fully investigate the DRO system. To the best of my knowledge the tuning and stability issues still exist and an OPO pumped directly by a violet emitting diode laser has not yet been achieved. The development of a device such as this and its application to a spectroscopic investigation along with further investigation of the tuning properties of the device would be an interesting and worthwhile aim for a PhD project.

Bibliography

[1] Malcolm H. Dunn and Majid Ebrahimzadeh. Parametric generation of tunable light from continuous wave to femtosecond pulses. *Science*, 286(5444):1513–1517, 1999.

[2] J.A Giordmaine and R.C Miller. Tunable coherent parametric oscillation in $LiNbO_3$ at optical frequencies. *Physics Review Letters*, 14(24):973–976, 1965.

[3] R.G. Smith, J.E. Geusic, H.J. Levenstein, J.J. Rubin, S. Singh, and L.G Van Uitert. Continuous optical parametric oscillation in $Ba_2NaNb_5O_{15}$. *Applied Physics Letters*, 12(9):308–310, 1968.

[4] G.M. Gibson, M.H. Dunn, and M.J. Padgett. Application of a continuously tunable cw optical parametric oscillator for high resolution spectroscopy. *Optics Letters*, 23(1):40–42, 1998.

[5] A.J. Henderson, M.J. Padgett, F.G. Colville, J. Zhang, and M.H. Dunn. Doubly-resonant optical parametric oscillators: tuning behaviour and stability requirements. *Optics Communications*, 119:256–264, 1995.

[6] R.A. Tahtamoui, K. Bencheikh, R. Storz, K. Schenider, M. Lang, J. Mylnek, and S. Schiller. Long-term stable operation and absolute frequency stabilisation of a doubly resonant parametric oscillator. *Applied Physics B*, 66:733–739, 1998.

[7] M.Bode, P.K.Lam, I.Freitag, A.Tunnermann, H.A.Bachor, and H.Welling. Continuously-tunable doubly resonant optical parametric oscillator. *Optics Communications*, 148:117–121, 1998.

[8] B. Beier, J.-P. Meyn, R. Knappe, K.J. Boller, G. Huber, and R. Wallenstein. A 180mw Nd:LaSc3(BO3)4 single frequency TEM00 microchip laser pumped by an injection locked diode-laser array. *Applied Physics B: Lasers and Optics*, 58(5):381–388, 1994.

[9] I.D. Lindsay. *High Spatial and Spectral Quality Diode-Laser-Based Pump Sources for Solid-State Lasers and Optical Parametric Oscillators*. PhD thesis, University of St Andrews, 1999.

[10] G.D. Boyd and D.A. Kleinman. Parametric interaction of focussed gaussian light beams. *Journal of Applied Physics*, 39(8):3597, 1969.

[11] H. Kogelnik and T.Li. Laser beams and resonators. *Applied Optics*, 5(10):1550–1567, 1966.

[12] M.J. Padgett, F.G. Colville, and M.H. Dunn. Mode selection in doubly-resonant optical parametric oscillators. *IEEE Journal of Quantum Electronics*, 30(12):2979–2984, 1994.

[13] I.D. Lindsay, M.H. Dunn, and M. Ebrahimzadeh. Cluster selection in doubly resonant optical parametric oscillators based on quasi-phasematched materials. In OSA, editor, *Conference on Lasers and Electro-Optics Technical Digest Series*, page 159, Washington, May 2000.

Bibliography

[1] Malcolm H. Dunn and Majid Ebrahimzadeh. Parametric generation of tunable light from continuous wave to femtosecond pulses. *Science*, 286(5444):1513–1517, 1999.

[2] J.A Giordmaine and R.C Miller. Tunable coherent parametric oscillation in $LiNbO_3$ at optical frequencies. *Physics Review Letters*, 14(24):973–976, 1965.

[3] R.G. Smith, J.E. Geusic, H.J. Levenstein, J.J. Rubin, S. Singh, and L.G Van Uitert. Continuous optical parametric oscillation in $Ba_2NaNb_5O_{15}$. *Applied Physics Letters*, 12(9):308–310, 1968.

[4] G.M. Gibson, M.H. Dunn, and M.J. Padgett. Application of a continuously tunable cw optical parametric oscillator for high resolution spectroscopy. *Optics Letters*, 23(1):40–42, 1998.

[5] A.J. Henderson, M.J. Padgett, F.G. Colville, J. Zhang, and M.H. Dunn. Doubly-resonant optical parametric oscillators: tuning behaviour and stability requirements. *Optics Communications*, 119:256–264, 1995.

[6] R.A. Tahtamoui, K. Bencheikh, R. Storz, K. Schenider, M. Lang, J. Mylnek, and S. Schiller. Long-term stable operation and absolute frequency stabilisation of a doubly resonant parametric oscillator. *Applied Physics B*, 66:733–739, 1998.

[7] M.Bode, P.K.Lam, I.Freitag, A.Tunnermann, H.A.Bachor, and H.Welling. Continuously-tunable doubly resonant optical parametric oscillator. *Optics Communications*, 148:117–121, 1998.

[8] B. Beier, J.-P. Meyn, R. Knappe, K.J. Boller, G. Huber, and R. Wallenstein. A 180mw Nd:LaSc3(BO3)4 single frequency TEM00 microchip laser pumped by an injection locked diode-laser array. *Applied Physics B: Lasers and Optics*, 58(5):381–388, 1994.

[9] I.D. Lindsay. *High Spatial and Spectral Quality Diode-Laser-Based Pump Sources for Solid-State Lasers and Optical Parametric Oscillators*. PhD thesis, University of St Andrews, 1999.

[10] G.D. Boyd and D.A. Kleinman. Parametric interaction of focussed gaussian light beams. *Journal of Applied Physics*, 39(8):3597, 1969.

[11] H. Kogelnik and T.Li. Laser beams and resonators. *Applied Optics*, 5(10):1550–1567, 1966.

[12] M.J. Padgett, F.G. Colville, and M.H. Dunn. Mode selection in doubly-resonant optical parametric oscillators. *IEEE Journal of Quantum Electronics*, 30(12):2979–2984, 1994.

[13] I.D. Lindsay, M.H. Dunn, and M. Ebrahimzadeh. Cluster selection in doubly resonant optical parametric oscillators based on quasi-phasematched materials. In OSA, editor, *Conference on Lasers and Electro-Optics Technical Digest Series*, page 159, Washington, May 2000.

Chapter 5

Characterisation of Diode Lasers for Spectroscopy

Tunable diode lasers are readily adaptable for use in spectroscopic applications. In the work described in this thesis the diode laser output has been carefully set to suit the application. Basic information about the operating characteristics of the diode laser are crucial for success with experimental investigations. Here the violet and red diode lasers used in this thesis are described and the experimental data obtained is used to determine the parameters required for each device in the chosen application.

5.1 Introduction

In this chapter I present results of the characterisation of red and violet diode lasers to determine their spectral characteristics and tuning behaviour. For each laser the threshold current was found along with the temperature and current tuning characteristics. In addition information about the linewidth and tuning range of the lasers is presented; crucial parameters for spectroscopic applications. The lasers that are used include a Nichia violet diode laser at 405nm in both free running and home-built extended cavity operation, sutiable for pumping an OPO and red and violet microlensed diode lasers for use in sum frequency mixing to obtain UV light. Finally the properties of a commercially constructed violet extended cavity diode laser are investigated and then this laser is used to measure the hyperfine structure of indium, demonstrating a simple application of tunable diode laser spectroscopy. The absorption features of indium are then used as a frequency reference for use in stabilisation of the laser. The use of a hollow cathode galvatron source of indium atoms shows the first demonstration of the use of a blue diode for the spectroscopy of indium in such a source.

5.2 Basic Characterisation of Violet Diode Laser for pumping an Optical Parametric Oscillator

As described in Chapter 4, an OPO device that is pumped by a violet diode laser would be desirable, not only for accessing a previously unobtainable region of the spectrum with these types of devices, but also to allow investigations into the spectral properties of the OPO. The blue diode laser that is used here is a Nichia Corporation NLHV3000E device with the manufacturers' specifications detailing a nominal C-W output of 30mW at 405nm.

Figure 5.1 shows the response of the output power of the laser to a variation in the

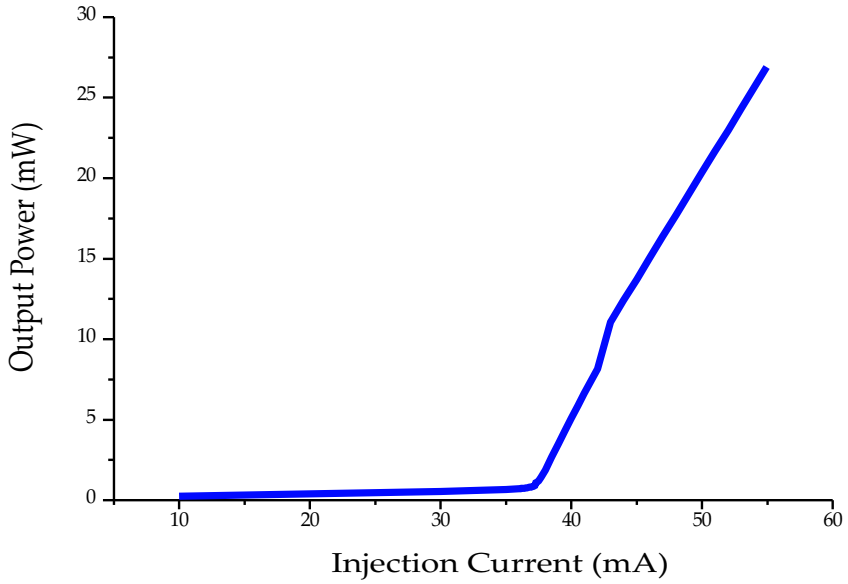

Figure 5.1: **Output Power versus input current for a free running Nichia violet diode laser**
The sharp change in the slope indicates the threshold injection current and marks the beginning of laser operation.

injection current. The injection current was increased whilst the output power was recorded using a Newport power meter. The threshold current for the laser is 37mA, and the maximum output power is 27mW. This output power was typical for blue diodes. Red and IR diode lasers typically have output powers greater than 100mW, but with generally higher threshold currents.

Figure 5.2 shows the wavelength tuning range for the Nichia violet diode. For a variation in injection current the change in the wavelength of the laser output was recorded. The operating current of the diode laser was fixed at 45mA. The range of wavelengths obtainable is over 1.4nm with the largest range of mode-hop-free tuning for the temperature variation between 17 and 20 degrees, where the wavelength is 406.5nm.

After characterisation in free running mode shown in figures 5.2 and 5.1, the laser diode was incorporated within a home built Littrow external cavity configuration

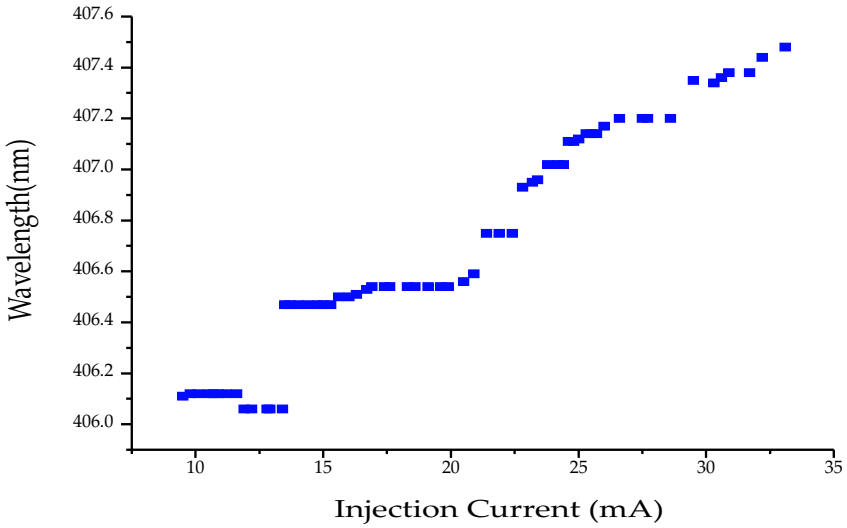

Figure 5.2: **Wavelength versus temperature for a free running Nichia violet diode laser**
Short continuous segments of similar wavelength values show the tuning of a single longitudinal mode as a result of varying the optical path length.

using a holographic UV grating (1800 lines/mm) and collimated over a large distance (∼4m). The diode was held within a standard mount and the grating contained within a machined holder which was mounted using a commercial 1 inch adjustable mirror mount which allowed the grating orientation to be altered in both the vertical and horizontal direction. The laser diode was temperature stabilised using a Peltier thermoelectric cooler (TEC) which was sandwiched using heatsink paste between the laser mount and an aluminium baseplate. At first the thermistor that provided the feedback to stabilise the temperature was placed at the top of the aluminium mount, however this was not sufficiently close to the laser diode for the feedback to the temperature controller to operate properly. To alter this the thermistor probe was then placed within the mirror mount, closer to the laser diode.

One of the benefits of introducing optical feedback within a laser diode device is a reduction in the threshold operating current. In order to obtain the lowest threshold current for the ECDL configuration, the first order diffracted beam from the grating

must be aligned with the diode output. This is achieved practically by placing the grating within a kinematic mount allowing orientation of the grating in the horizontal and vertical directions. In the alignment procedure, the laser is operated just below threshold and the second, diffracted, less intense beam is observed to return to the centre of the collimating lens. If this beam is observed separately to the main diode laser beam then not all of the diffracted beam is being coupled back to the diode, showing that the ECDL is not in perfect alignment. By careful adjustment of the grating, the two beams can be coincident upon each other, ensuring that the diffracted light passes through the centre of the collimation lens and couples back into the diode. Through careful alignment the threshold of the laser was reduced from 35mA in free running mode to 27.8mA in the external cavity mode, demonstrating the reduction in threshold as a result of using an external cavity.

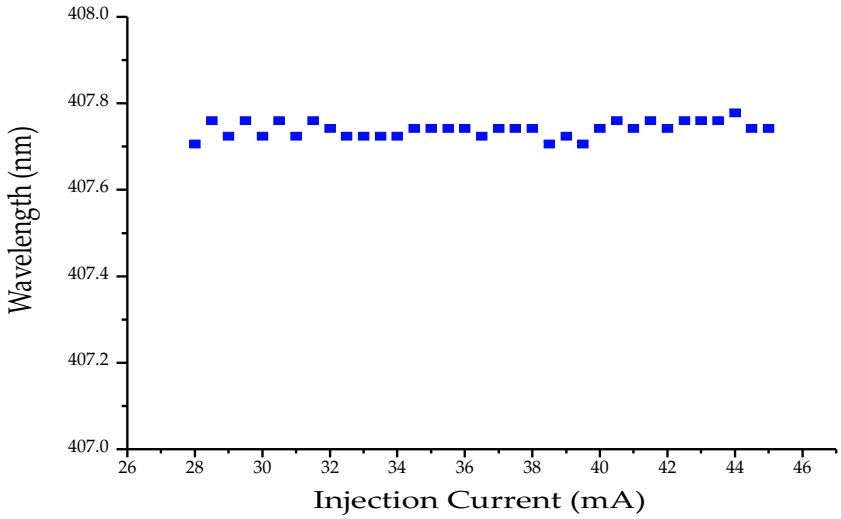

Figure 5.3: **Wavelength-Current Characteristic of a Nichia violet extended cavity diode laser**
The wavelength maintains a step function, but over a far smaller wavelength range

Figure 5.2 shows the wide tuning range and the 'step' characteristics of the wavelength of a free running diode laser. In contrast, Figure 5.3 shows the wavelength tuning range of the diode when operated in an external cavity configuration. The diode current was varied from 28mA to 45mA with the temperature stabilised at 20

degrees. The step function remains but the wavelength range has reduced considerably to 0.1nm which demonstrates that the laser oscillates preferentially on a single longitudinal mode.

To observe the spectral output from the diode laser both in free running and extended cavity configurations, the output from the laser diode was observed on an optical spectrum analyser (OSA). The laser light was aligned and coupled into the OSA via an optical fibre probe. The spectra recorded are shown in Figure 5.4.

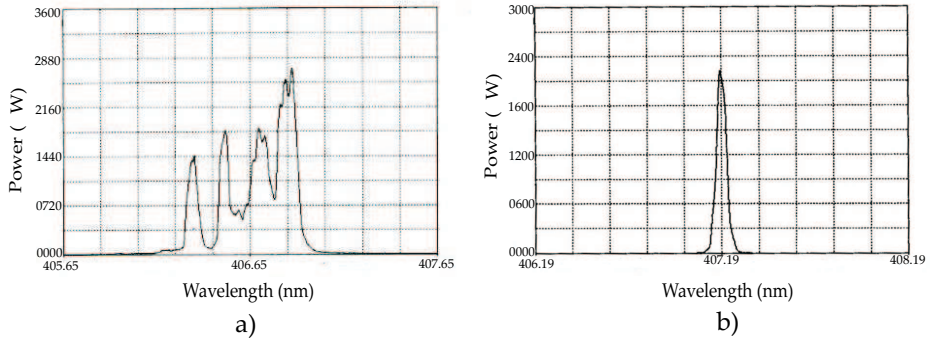

Figure 5.4: **Comparison of spectral output from the free running and external cavity diode laser**
The multimode output from the free running laser (a)and the single mode output from the ECDL (b) are clearly shown.

The spectral outputs shown in Figure 5.4 show the difference in the spectral output from the diode laser when operated free running and extended cavity. For the free running diode there are 4 modes shown and the laser supports oscillation at these four modes, over a wavelength range of 0.9nm. In contrast the ECDL oscillates on a single mode over a range of 0.2nm. The feedback introduced by the extended cavity encourages the single mode oscillation.

Phase continuous tuning of the diode laser was also attempted. Without the use of the electronic circuit, the mode hop free tuning range was 6GHz. An electronic circuit was used in a method similar to that described in [1]. The circuit is used to vary the length of the solitary and extended cavity within the same ratio. The mode hop free tuning range achieved was 16.5GHz shown in Figure 5.5.

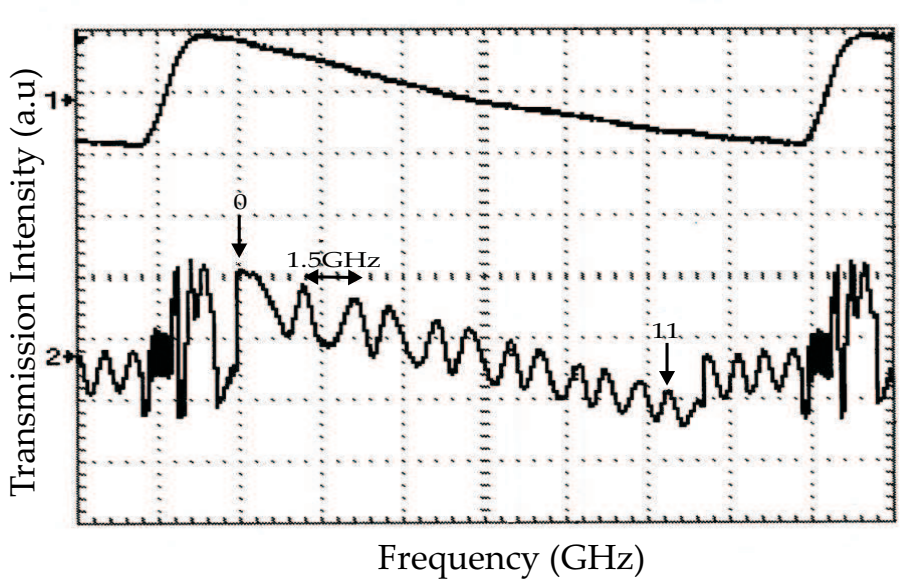

Figure 5.5: **16.5GHz Mode-Hop-Free Tuning of Nichia Violet ECDL**
Transmitted fringe pattern of the violet ECDL through a low finesse Fabry-Perot interferometer (FSR=1.5GHz) with a fixed length. There are 11 equally spaced fringes corresponding to 16.5GHz of mode-hop-free tuning. (Smooth tuning trace obtained by D. Gawron)

5.3 Characterisation of red and violet microlensed diode lasers

The red and violet microlensed diode lasers (MDLs) that are used with great success in the experimental work described in Chapter 6 have been characterised extensively in [11]. Here I give a summary of this characterisation and present some experimental data taken.

The MDLs were characterised both in free running and extended cavity mode with the goal to demonstrate that the quality of the output beams can be retained whilst maintaining good tuning and spatial characteristics. For the free running laser systems the microlensed diodes were placed within a collimation tube (Thorlabs UK LT230P-A), mounted on home built aluminium mounts, temperature stabilised to 10mK. In separate investigations the MDLs were placed within a Littrow external cavity configuration. For both lasers the polarisation was determined by observation

of the power transmission through a $\frac{\lambda}{2}$ plate whilst the diode laser head was rotated to find the orientation that delivered the maximum output power.

5.3.1 Red free running microlensed diode laser

The free running red diode (Blue Sky Research California, PS110) operates at 661nm with a maximum output of 50mW. The beam quality measurement gave M^2 values of 1.1 in the horizontal plane and 1.6 in the vertical plane [11]. The spectral output of the laser was monitored using a spectrum analyser with 300MHz free spectral range (FSR) and finesse of 500. The linewidth of the laser was 3 MHz. A continuous mode-hop free tuning range of 58GHz was measured using a spectrum analyser with FSR=2GHz. This was observed by variation of the current from 108.1mA to 119.1mA demonstrating a tuning rate of 4.8 GHz/mA.

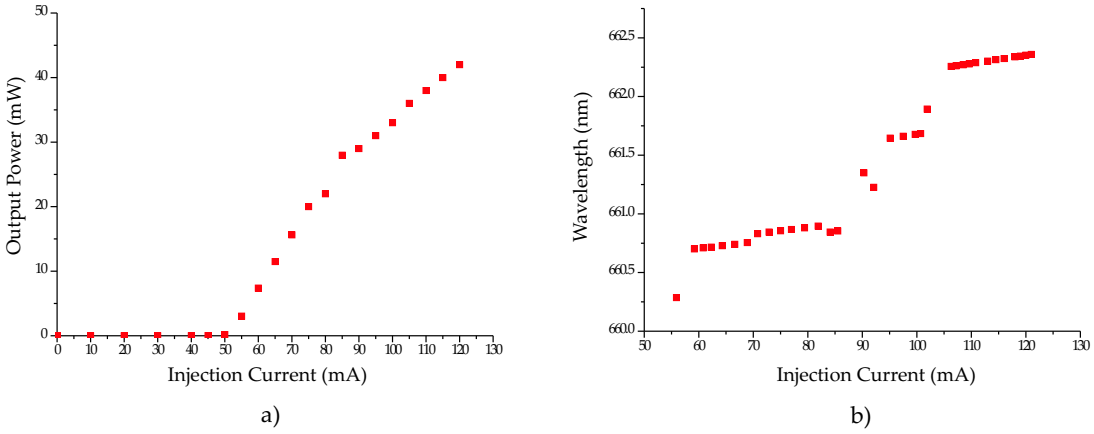

Figure 5.6: **Output power and wavelength characteristics for variation in injection current for the red microlensed diode laser**
The power output (a) and wavelength (b) of the red MDL was recorded for an increase in the injection current. The threshold of the laser is deduced from (a) as 50mA and the wavelength range in running mode is 2.25nm.

The threshold of the red MDL is 50mA and the maximum output power of the diode laser is 43mW. The wavelength range was obtained by observation of the wavelength of the output beam whilst the injection current was varied from the threshold to the

maximum operating current. The temperature of the laser was fixed at 21 degrees. The range of wavelengths from the laser at this temperature is from 660.25nm to 662.4nm.

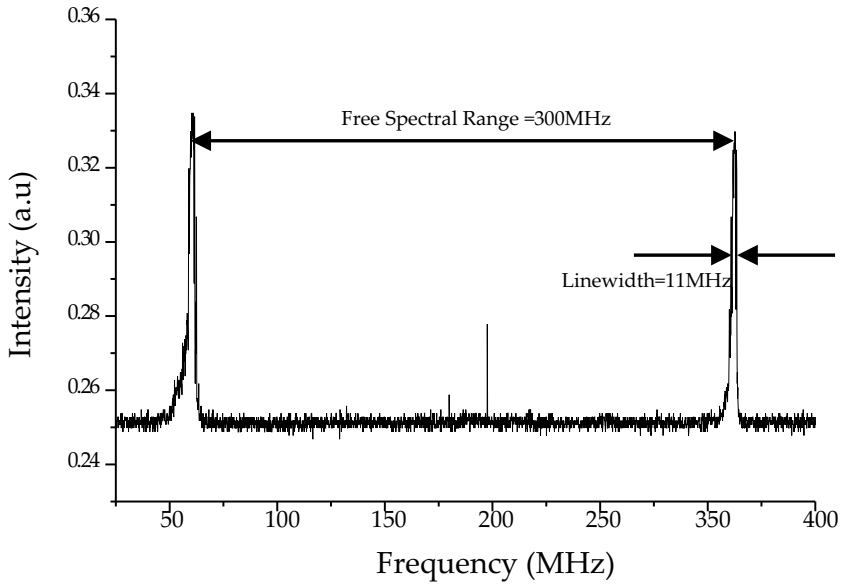

Figure 5.7: **Linewdith of Red Microlensed Diode Laser**
Linewidth (11MHz) and FSR (300MHz) of a free running red microlensed diode laser.

The spectral linewidth of the red MDL was measured by observing the output from the laser through an Fabry-Perot etalon, controlled via an optical spectral analyser which provides a high voltage input to the etalon and allows the amplified output from the etalon to be observed on an oscilloscope. The linewidth is measured at the full width half maximum (FWHM) of the mode and is calculated as a ratio of its FWHM to the frequency spacing between adjacent modes given by the FSR of the etalon, which in this case is 300MHz. For use in the mercury spectroscopy application described in Chapter 6, smooth mode-hop-free tuning of the red MDL was obtained over 58GHz without any need for enhancement of the tuning range via electronic control. The injection current of the laser was set at 114mA. This tuning range was obtained without any further electronic control of the temperature and current. The wide continuous tuning range demonstrated by the MDL lasers shows their ability to

run in single longitudinal mode in contrast to standard diode lasers. This is attributed to the use of a microlens.

The characteristics of the red MDL when operated in external cavity are given in [11].

5.3.2 Violet microlensed diode laser in ECDL configuration

The free running violet diode (Blue Sky Research (California) VPSL-0450-N5B) operates at 413nm with a continuous output of 25mW. Measurements of the beam quality yielded M^2 values of 1.3 in the horizontal plane and 1.5 in the vertical plane [11]. The laser output was observed directly on a spectrum analyser with a FSR of 1GHz and finesse of 500. The linewidth of the diode was less than 22GHz and a continuous tuning range of 40GHz, scanning from 51.8-62.7mA giving a tuning rate of 5.06GHz/mA.

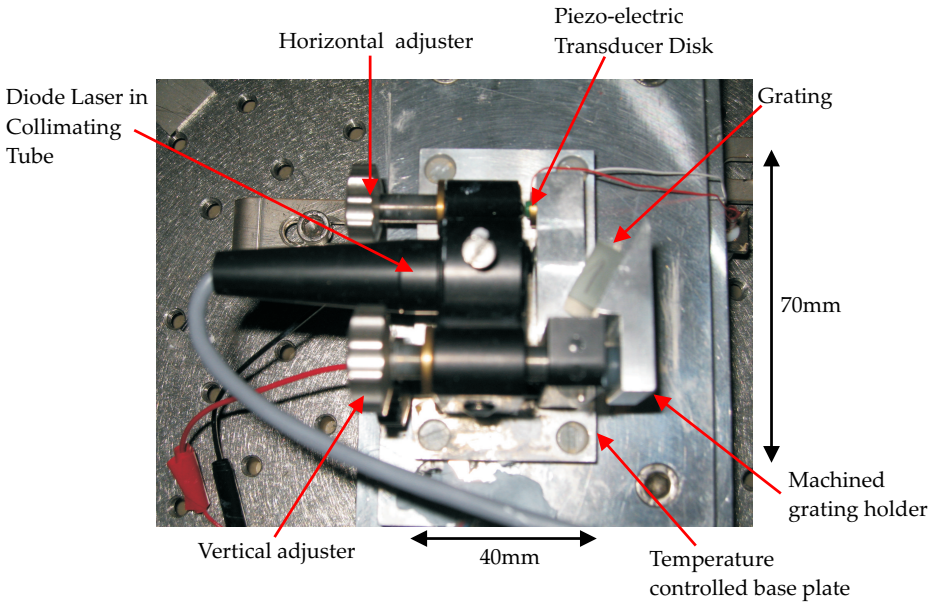

Figure 5.8: **Photograph of violet microlensed ECDL**
A homebuilt Littrow external cavity diode laser showing the optical and mechanical elements used within a Littrow extended cavity configuration.

The diode was placed within a home-built ECDL system based upon a Littrow configuration. Figure 5.8 shows a photograph of the home built system. The laser is mounted upon an aluminium plate under which the TEC is sandwiched between this

plate and a larger aluminium base. The grating holder is machined at a specific angle to allow the correct orientation of the grating to allow the first order diffracted beam to be returned to the laser diode. This holder is then attached to the mirror mount with a screw, allowing the coarse adjustment of the orientation of the grating using the horizontal and vertical adjusters. The piezo-electric transducer disk allows fine tuning of the length of the extended cavity and can be used to optimise the tuning characteristics.

The threshold of the ECDL was reduced to its minimum value by careful alignment of the diode output with the grating back reflected spot as described earlier.

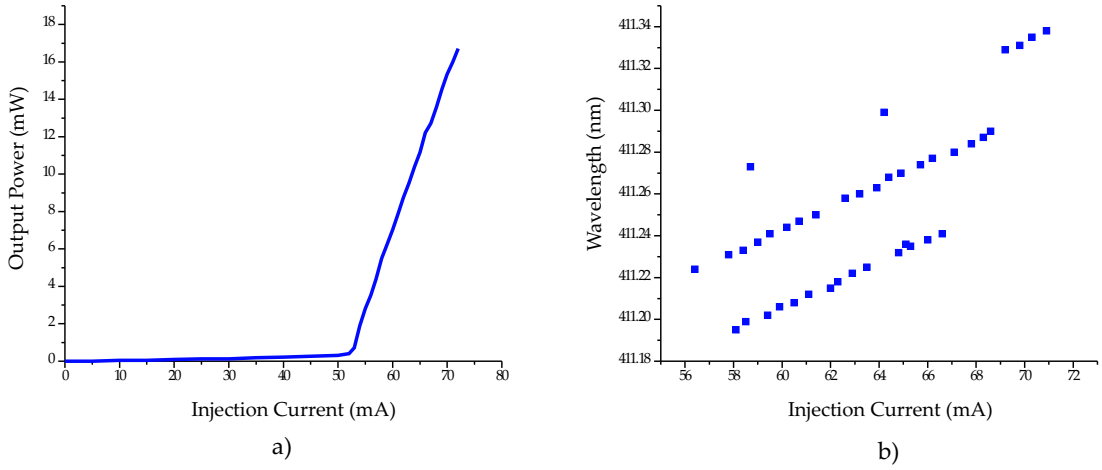

Figure 5.9: **Output power and wavelength characteristics for variation in injection current for the violet microlensed ECDL**
Variation of power (a) and wavelength (b) with injection current for the violet microlensed diode laser in ECDL configuration. The threshold of the laser is 53mA and the maximum output power is 16mW.

The grating is a HoloUV grating with 2400 lines per mm which was found to yield maximum output power, largest tuning range and narrowest linewidth [11]. The maximum output power from the violet MDL was 16mW and the threshold was 53mA. The output power is similar to that of a normal diode with an elliptical output beam, as shown in the characterisation of a commercial violet ECDL. The wavelength response of the diode laser was measured at a constant temperature of 12 degrees. The wavelength tuning of the diode laser showed very few regions of smooth

tuning, demonstrated by the observation of a mode-hop-free fine tuning range of less than 3GHz. The wavelength range of the ECDL is very narrow however, with a variation of 0.15nm. For use within the mercury spectroscopy application, the violet MDL is current and temperature tuned to deliver the correct wavelength light for sum frequency generation of UV light.

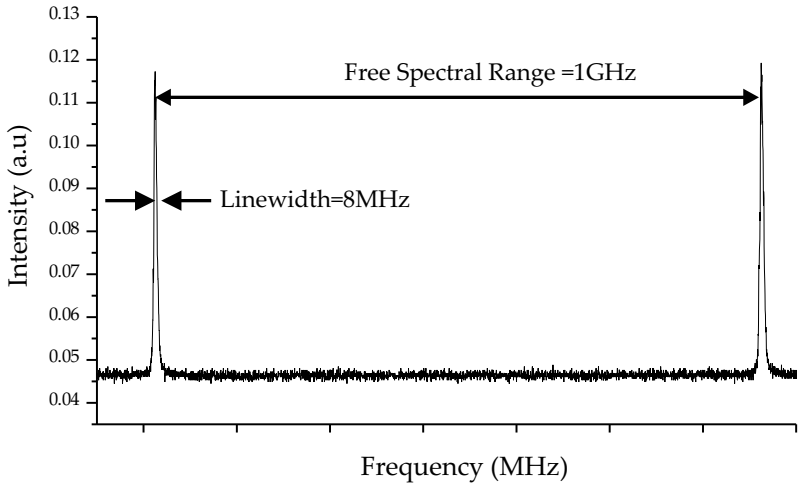

Figure 5.10: **Linewidth of Violet Microlensed Diode Laser in Extended Cavity**
Linewidth (8MHz) and FSR (1GHz) of a violet microlensed diode laser in an external cavity configuration.

The linewidth of the violet MDL was measured by observation of the spectral output of the laser using a Fabry-Perot etalon with a FSR=1GHz and finesse of 500. Figure 5.10 shows the linewidth of a single longitudinal mode with respect to the spacing between adjacent modes.

5.4 Characterisation of T-Optica Laser

Here, a commerical GaN external cavity diode laser (T-Optica Photonics AG DL100) based on a Littrow geometry is characterised. The use of this laser within a spectroscopic application is described later in this chapter.

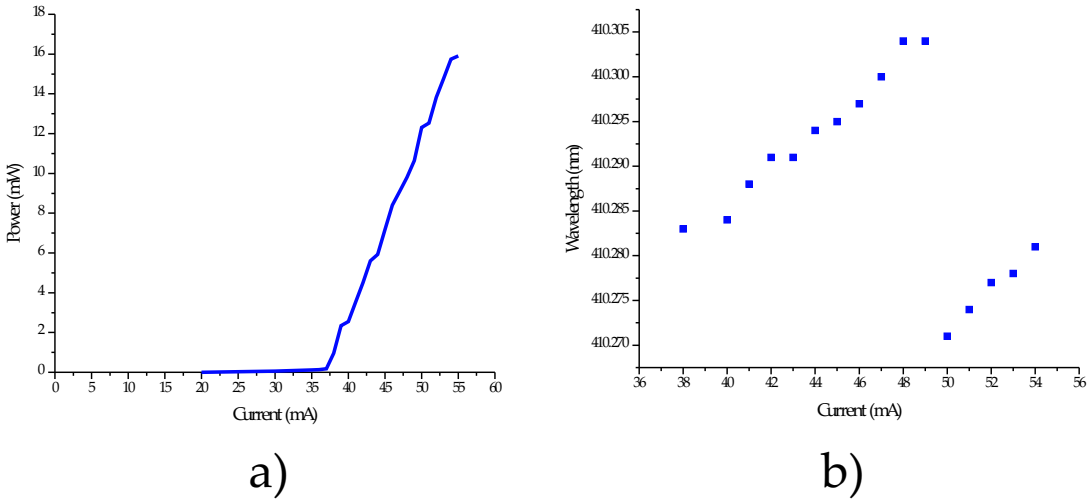

Figure 5.11: **Power and wavelength characteristic for variation in injection current for commercial ECDL**
Variation of output power (a) and wavelength (b) with injection current for T-Optica violet ECDL.

The threshold of the laser is 37mA and the maximum output power is 16mW. The temperature was fixed at 20°C. The wavelength range obtained demonstrated the step function and clearly shows a mode jump where the laser operation switched to a lower wavelength.

The linewidth of the laser was determined by observing the output on a Fabry-Perot spectrum analyser with a FSR of 1GHz and finesse of 500. The linewidth of the laser was found to be 7MHz as shown in Figure 5.12.

For most spectroscopic applications a large mode-hop-free tuning range is desirable. To successfully resolve all the features of the indium transition within a single scan of the laser a mimimum mode-hop-free tuning range of 20GHz was required. A

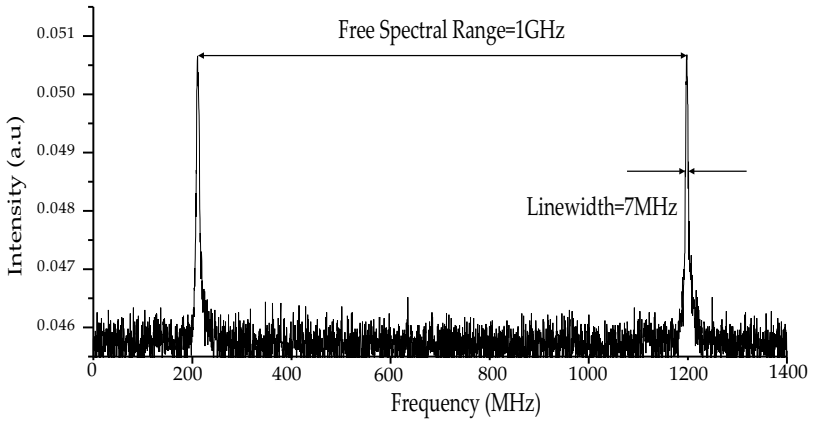

Figure 5.12: **Linewidth and Free Spectral Range of Commercial Violet ECDL**
Linewidth (7MHz) and FSR (1GHz) of T-Optica commercial violet diode laser in external cavity.

Littrow ECDL can be tuned smoothly by means of adjusting the injection current and grating angle. This tuning range is limited, however, as the adjustments of the two parameters are difficult to match. However a wider range could be obtained by employing a feed-forward loop where the PZT voltage and the injection current are adjusted within a ratio maintaining constructive interference, increasing the mode-hope free tuning range. This method is widely used within spectroscopic applications. For the configuration described here, the output of the laser was enhanced by using an integrated scanning control box (Scan 110). A frequency calibration of the laser scan was performed using a confocal Fabry-Perot etalon with a free spectral range of 1GHz.

The characteristics of the laser highlighted its suitability as a source for spectroscopy on Indium. The linewidth (7MHz) is much smaller than the full width at half maximum (FWHM) of the narrowest absorption peak of the indium profile (5 GHz).

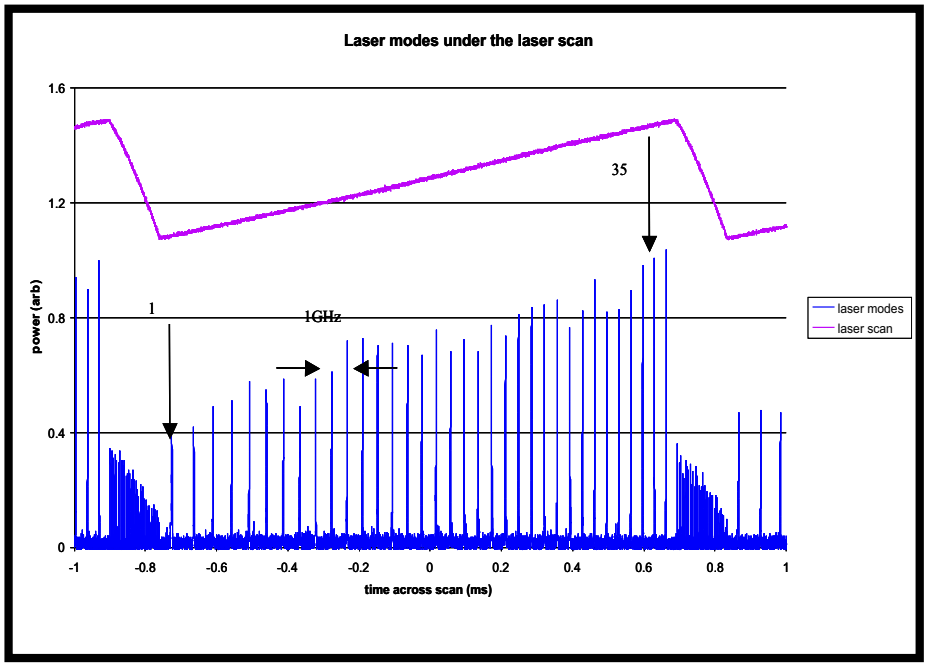

Figure 5.13: **35GHz Mode-Hop-Free Tuning**
35GHz mode-hop-free tuning of T-Optica violet laser measured using an Fabry-Perot etalon with FSR of 1GHz.

5.5 Indium

Indium has a strong $5^2P_{1/2} - 6^2P_{1/2}$ transition at 410nm. This line has already been used in high resolution spectroscopy for hyperfine structure measurement and has proved a fruitful application for violet diode lasers. One of the major applications for the use of indium is in atom lithography, allowing the deposition of atoms to grow semiconductor structures to obtain photonic bandgap structures [3]. Hildebrandt *et al* used a violet diode laser to detect the absorption spectrum of indium vapour within a cell [4]. The cell was heated to 1300 degrees and was used to resolve the transitions from F=4,5 to F'=4,5. In addition, well resolved Lamb dips were observed. Leinen *et al* [5] provided information about the structure from spectroscopy on an atomic beam of indium produced by a heated vapour cell. They were able to resolve individual isotopes in the atomic beam. Hult *et al* have measured the hyperfine structure of indium and observed the fluorescence of indium atoms induced by a violet diode laser within a pressure flame [6]. Rasbach *et al* [7] applied the techniques of high resolu-

tion saturation and polarization spectroscopy to indium vapour contained within a sapphire cell heated to 600 degrees. The sapphire is used because of its sensitivity to high temperatures, crucial when the cells are heated within the experimental setup. They performed measurements using both a violet diode laser and then also with a violet light generated at 451nm by a frequency doubled Ti:Sapphire laser.

Here, I describe the use of a hollow cathode lamp source of indium atoms for the spectroscopy of indium using a violet diode laser. The use of hollow cathode lamp could provide a simple and effective source of indium to produce an atomic beam suitable for use within nanofabrication applications. For atomic transitions that are narrow or weak high sensitivity techniques are required to detect the features. This is the case for indium where vapour cells must be heated to increase the density of the atoms. A hollow cathode galvatron provides a high density vapour of indium atoms. The HCL obviates the need for heating apparatus for a vapour cell, simplifying an experimental setup. For these reasons HCLs have been used in many laser spectroscopy applications [8, 9, 10]

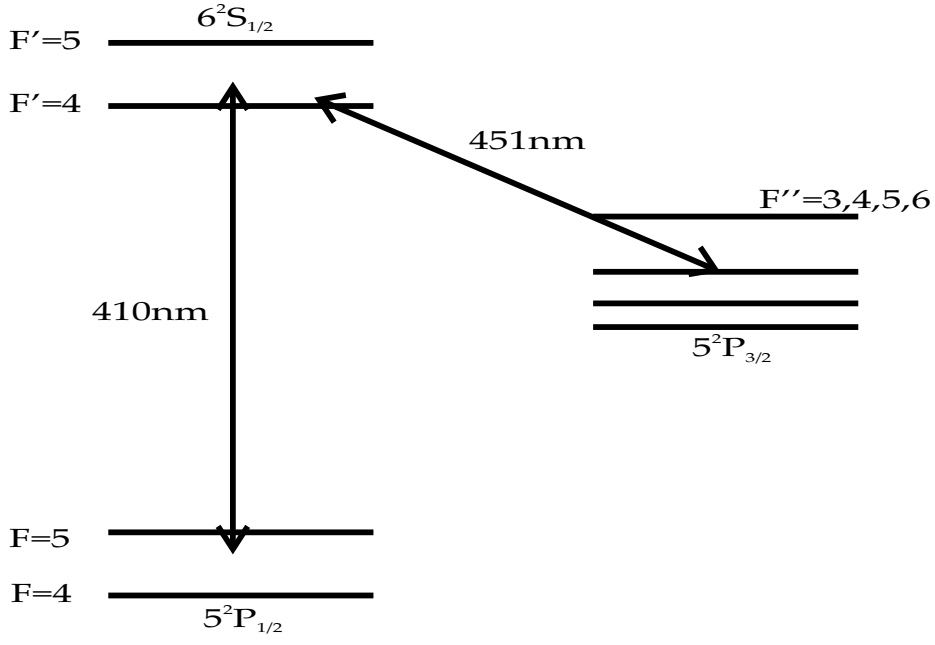

Figure 5.14: **Indium Energy Level Scheme**
The energy level scheme of atomic indium corresponding to the F=4,5 to F'=4,5 transition.

The absorption spectrum and hyperfine structure were obtained using a source of neutral indium atoms in a hollow cathode galavatron (HCL) (Hamamatsu series L2783-31 In). This is the first demonstration of laser spectroscopy of indium using a hollow cathode lamp.

In a galvatron, shown in Figure 5.15, a discharge plasma is generated in the hole through the cathode. Laser light is incident upon the cathode and propagates through the hole. When the absorption wavelength of the atoms in the discharge plasma is resonant with the laser light, the electronic properties of the discharge plasma are altered, delivering an optogalvanic signal. When the laser wavelength and the absorbed wavelength are resonant, the strongest optogalvanic signal is obtained. As the wavelengths go off resonance the signal becomes much smaller.

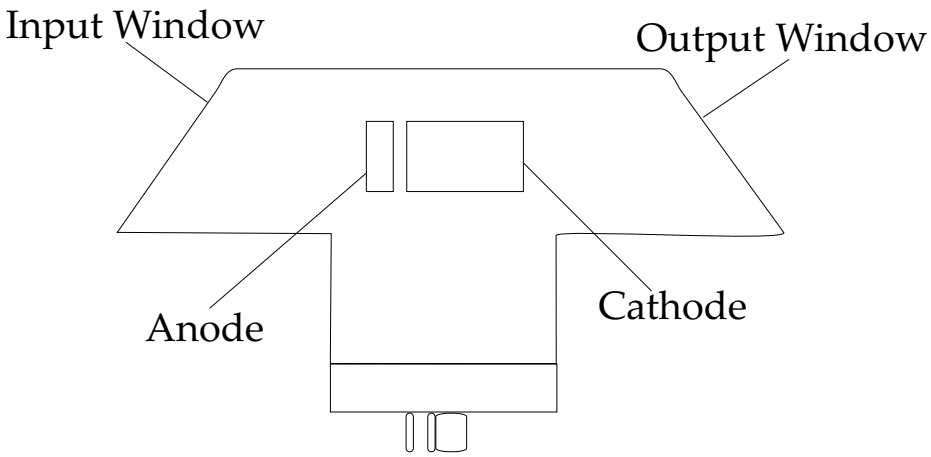

Figure 5.15: **Construction of Galvatron**

The transparent cathode is a 15mm long hollow cylinder with a 3mm inner diameter. The maximum current for the galvatron is 10mA. Indium atoms are sputtered from the surface of the cathode by energetic ions produced in the xenon buffer gas. There are advantages of using a hollow cathode discharge instead of the more commonly used vapour cells. For experiments using indium cells it is necessary to heat the cells to over 1000^{o}C, however HCL experiments can be performed at room temperature. However, the lifetime of a HCL is limited due to its method of operation which leads to degradation of the lamp and reduced production of the trace element.

5.6 Absorption Spectroscopy of Indium

For this application a commercial T-Optica violet ECDL, characterised earlier, was used. The experimental setup for the absorption spectroscopy is shown in Figure 5.16. A polarisation beamsplitter is used to divide the laser beam. One portion was incident on a photodiode as a reference. The other beam was used for the absorption spectroscopy and is passed through both the anode and cathode of the HCL. The beam coming out of the HCL is split further to enable simultaneous diagnostic measurements of the wavelength and tuning of the laser with interaction of the indium atoms. The absorption is detected as a difference in intensity between a reference beam and a beam that has interacted with the indium atoms. Both detected signals are displayed on a digital oscilloscope (Tektronix TDS 520A).

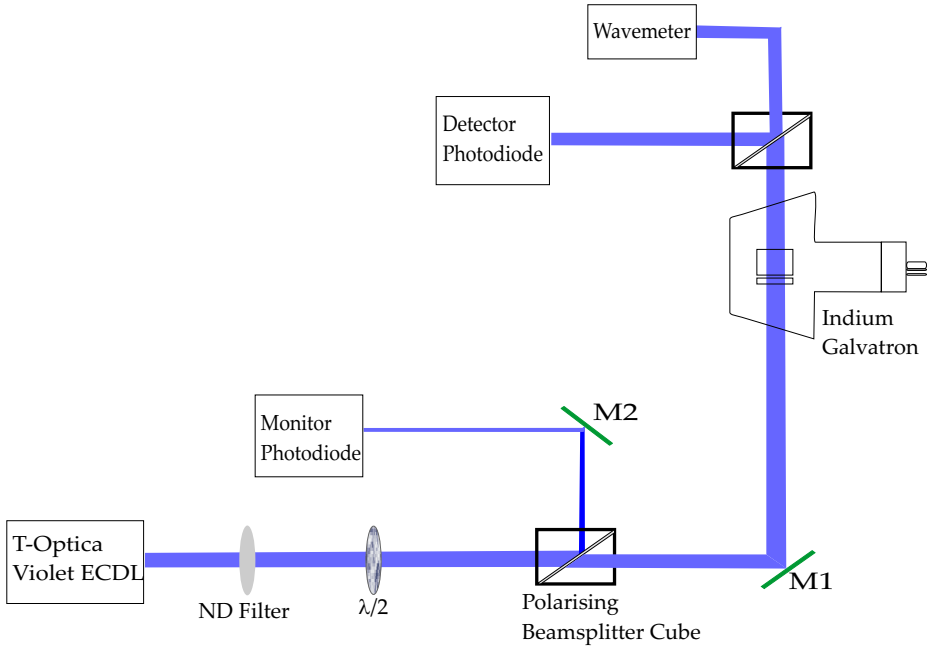

Figure 5.16: **Experimental Setup for Indium Spectroscopy**
The violet diode laser is aligned through the hollow cathode lamp using mirror M1. The beam interacts with the indium atoms and the output beam is detected by the detector photodiode. The polarising beamsplitter cube allows a portion of the laser beam to be split off and aligned using mirror M2 to the monitor photodiode. The wavelength of the laser is ascertained by the wavemeter.

To obtain the indium spectrum, the HCL was powered using a current of 10mA

and the laser wavelength scanned through the line to observe any depletion in the power output from the galvatron, indicating the presence of indium. The laser was temperature and current tuned to give output at 410.176nm, the given wavelength for the indium line on the NIST database [11]. We were, however, unable to resolve the indium line despite extensive refinements of the setup. However, by examination of published work in this area the indium line was quoted at 410nm and only one reference gave an indication of the line being at 410.3nm. In order to find the line a searching process was initiated whereby the laser was temperature tuned from 410.33nm downwards and the difference between the two signals was observed at each wavelength range until depletion indicating a single peak was observed at 410.297nm. Subsequent tuning to 410.293nm delivered all four of the hyperfine features within a single scan shown in figure 5.17.

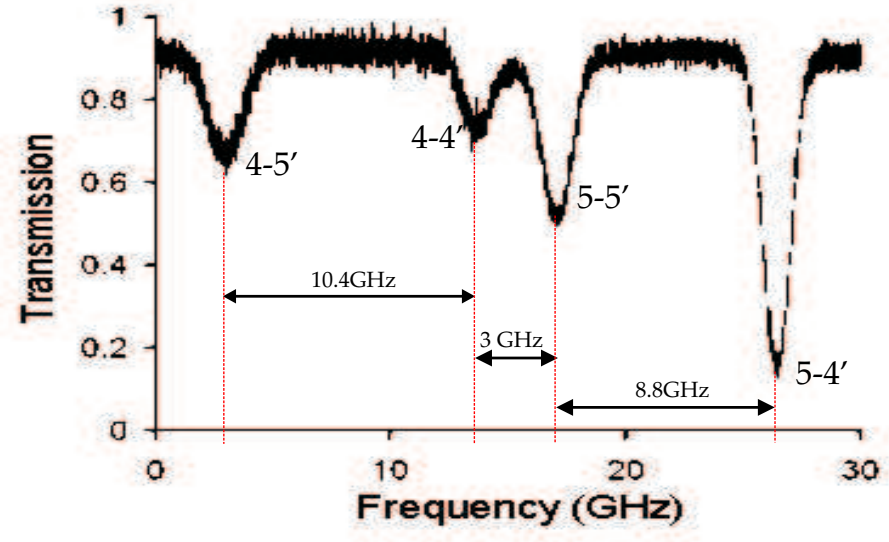

Figure 5.17: **Hyperfine structure of indium at 410nm**
The spectrum shows the features corresponding to the F=4,5 to the F'=4,5 transition in indium. The spectral separation between the features are indicated.

The frequency separations between the features are in good agreement with the hyperfine measurements shown in work by Leinen, Hildebrant and Hult [4, 5, 12].

5.6.1 Locking to the Indium Line

The principles of active stablisation and the locking of a laser to a frequency reference through use of electronic feedback circuits was described in Chapter 2. Absorption features are appropriate frequency references and here the use of an indium absorption feature to stabilise the violet diode laser is described.

The strongest absorption feature was chosen as the reference feature. The output of the laser was monitored by observing the spectral modes of the laser through a Fabry-Perot etalon. The signal that interacts with the trace species was detected using a photodiode and the output of the photodiode was fed into the locking circuit. The locking electronic box (T-Optica PID100) was used to zoom in on the feature and the reference point was set at the side of the fringe. The procedure for fine tuning of the stabilisation feedback loop was performed by adjusting in turn the proportional (P), integral (I) and differential (D) controls on the locking electronic circuit. The systematic procedure for this type of stabilisation was given in Chapter 2. In side-of-fringe locking the size of the feature is important with a larger fringe providing a bigger region over which the frequency change is less dramatic, allowing the stabilisation feedback loop to operate properly and providing a longer term lock. The lock point can be set at a point in the centre of the fringe, far away from any rapid changes in the frequency where the fringe gradient is steeper for example near to the top of the fringe.

Achieving stabilisation was initially non-trivial as the reference indium feature was weak, a result of degradation of the galvatron. The drift of the laser was much greater than would have been expected for this type of stabilisation scheme. However, observation of the spectral output from the laser, observed using a Fabry-Perot etalon, indicated a significant difference in the laser output for locked and unlocked operation. Figure 5.18 shows a significant difference between the spectral output the drift of the locked and unlocked laser. Trace 5.18(a) shows the output from the laser when the negative feedback circuit is not used. Over 15 minutes the laser drifts by 357MHz

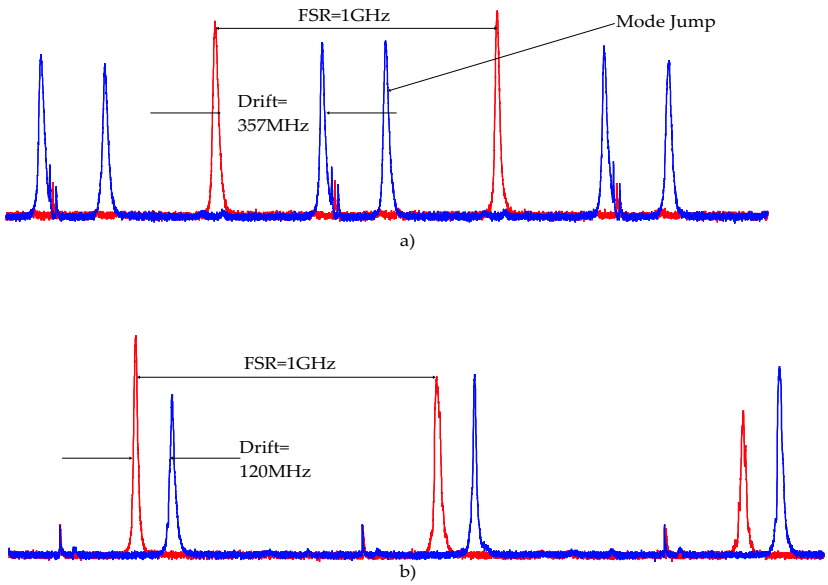

Figure 5.18: **Frequency Stabilisation of Violet ECDL over 15 minutes**
Trace (a) shows the unlocked behaviour of the laser where there is a larger drift and a a mode jump. Trace (b) indicates laser stabilisation.

and there is a clear mode jump, which indicated that the laser switched its operating point. In contrast Trace 5.18(b) shows the effect upon the laser spectrum when the feedback circuit is employed. The drift of the laser frequency is 120MHz and the laser continues to oscillate on the same mode.

The effect of the stablisation scheme is further confirmed by examination of the behaviour of the error signal. Figure 5.19 shows the effect on the error signal when the lock is on and off. When locked the error signal is at zero, indicating a zero error between the reference and signal, but when unlocked the error signal drifts from the zero point.

The stabilisation results indicate that with a stronger absorption feature, such as those obtained with the initial detection of the spectrum, then the stabilisation would be much more successful. When unlocked the drift of the laser is 333MHz and there is clearly a mode hop indicated by the extra mode. For the locked trace there is no mode-hop and the drift is only 120MHz. This result demonstrates the use of the feedback loop to keep the laser operating at the pre-determined reference frequency.

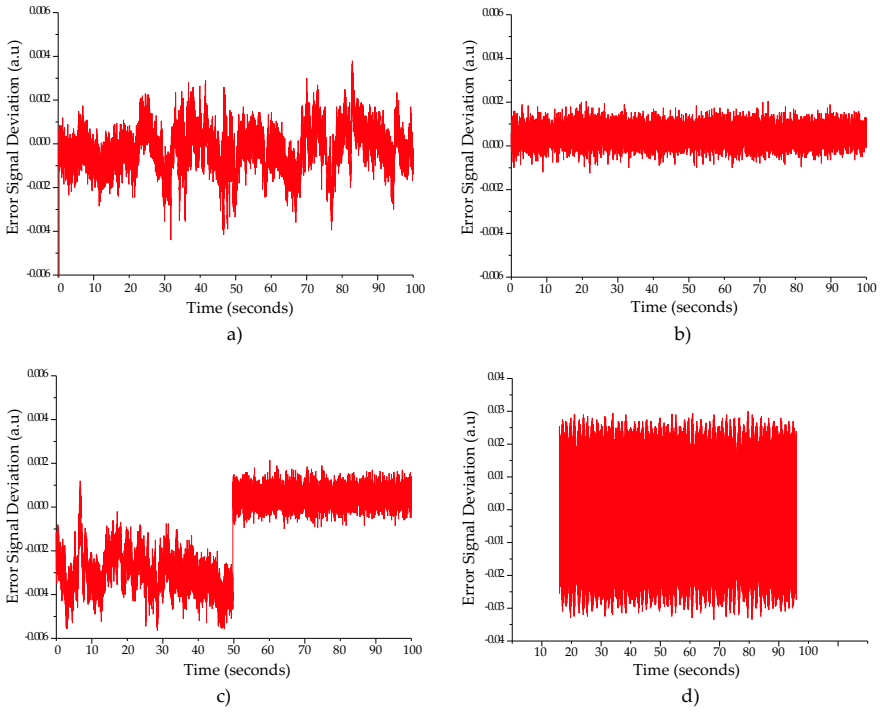

Figure 5.19: **Effect of the stabilisation upon the error signal**
Traces (a), (b) and (c) shows the effect of the lock upon the behaviour of the error signal. Trace (d) shows the effect on the error signal when the feedback loop has too much gain. In Figure (a) the error signal is recorded over 100s without the use of the lock. Figure (b) shows the effect upon the error signal over 100s when the lock is implemented. In Figure (c) the difference in the error signal when the lock is implemented after 50s is shown.

5.7 Summary

In this chapter the characteristics of diode lasers used were given and are summarised in Table 5.1.

Laser	Threshold (mA)	Power (mW)	Tuning (GHz)	Linewidth (MHz)	Application
Nichia (FR)	35	27	–	–	–
Nichia (EC)	27	17	7	–	OPO
Red MDL	50	42	58	11	SFG
Red MDL (EC)	–	26	6	6	SFG
Violet MDL	–	24	40	22	SFG
Violet MDL(EC)	53	15	3	8	SFG
T-Optica (EC)	37	16	37	7	Indium

Table 5.1: **Summary of Diode Laser Characterisation**

The output powers of violet diode lasers were found to be much lower than those demonstrated by their longer wavelength counterparts and they have much shorter smooth tuning characteristics. This is due to their structure, a result of the effects of confinement of carriers that had for so long prevented short wavelength diode lasers from being of any practical use. The use of a microlens within a diode laser assembly creates an extended cavity effect with a small amount of feedback to the diode from the back facet of the lens. This gave a degree of stability to the laser output as demonstrated by the large mode-hop-free tuning range (58GHz) from the free running red MDL.

The use of a violet diode laser for the spectroscopy of Indium at room temperature allowed all of the features in the hyperfine structure to be resolved. This simple application of tunable diode laser spectroscopy demonstrated the versatility of these devices in these applications. Although the results for the stabilisation of the com-

mercial ECDL to an indium absorption feature were inconclusive, the technique used was appropriate. The behaviour of the error signal indicated that the feedback loop was working and further refinement of parameters along with stronger indium features would be most appropriate to obtain convincing laser stabilisation. Further investigation on this method of stabilisation would hope to have a stronger feature and thus a larger side-of-fringe locking range to choose. It is conceivable that stabilisation of the laser with a drift of less than 1MHz would be possible. In addition the opportunity exists for comparisons of this stabilisation method with top-of-fringe locking and locking to an external stable reference cavity.

Bibliography

[1] C.Petridis, I.D.Lindsay, D.J.M Stothard, and M. Ebrahimzadeh. Mode-hop-free tuning over 80GHz of an extended cavity diode laser without antireflection coating. *Review of Scientific Instruments*, 72(10):3811–3815, 2001.

[2] A.E. Carruthers, T.K. Lake, A. Shah, J.W. Allen, W. Sibbet, and K. Dholakia. Microlensed red and violet diode lasers in an extended cavity geometry. *Review of Scientific Instruments*, 75(10):3360–3362, 2004.

[3] D. Meschede and H. Metcalf. Atomic nanofabrication: atomic deposition and lithography by laser and magnetic forces. *Journal of Physics D: Applied Physics*, 36(–):R17–R38, 2003.

[4] Lars Hildebrandt, Richard Knispel, Sandra Stry, Joachim R. Sacher, and Frank Schael. Antireflection-coated blue GaN laser diodes in an external cavity and doppler-free indium absorption spectroscopy. *Applied Optics*, 42(12):2110–2118, 2003.

[5] H. Leinen, D. Glässner, H. Metcalf, R. Wynands, D. Haubrich, and D. Meschede. GaN blue diode lasers:a spectroscopist's view. *Applied Physics B: Lasers and Optics*, 70(4):567–571, 2000.

[6] Johan Hult, Iain Stewart Burns, and Clemens Friedrich Kaminski. Measurements of the indium hyperfine structure in an atmospheric-pressure flame by use of diode-laser-induced fluorescence. *Optics Letters*, 29(8):827–829, 2004.

[7] U. Rasbach, J. Wang, R. dela Torre, V. Leung, B. Kloter, and D. Meschede. One- and two colour laser spectroscopy of indium vapour in an all-sapphire cell. *Physical Review A*, 70(–):33810–33817, 2004.

[8] H. Scheibner, S. Franke, Samir Solyman, J.F. Behnke, C. Wilke, and A. Dinklage. Laser absorption spectroscopy with a blue diode laser in an aluminium hollow cathode discharge. *Review of Scientific Instruments*, 7(2):378–382, 2002.

[9] R.L. Cavasso-Filho, A. Mirage, A. Scalabrin, D. Pereira, and F.C. Cruz. Laser spectroscopy of calcium in hollow-cathode discharges. *Journal of the Optical Society of America B*, 18(12):1922–1927, 2001.

[10] O.M. Marago, B. Fazio, P.G. Gucciardi, and E. Arimondo. Atomic gallium laser spectroscopy with violet/blue diode lasers. *Applied Phyiscs B Lasers and Optics*, 77(8):809–815, 2003.

[11] National Institute of Standards and Technology. Atomic spectra database. http://physics.nist.gov/PhysRefData/ASD/index.html.

[12] Iain Stewart Burns, Johan Hult, and Clemens Friedrich Kaminski. Spectroscopic use of a novel blue diode laser in a wavelength region around 450nm. *Applied Physics B - Lasers and Optics*, 79(4):491–495, 2004.

Chapter 6

Wavelength Modulation Spectroscopy with Diode Lasers

Modulation spectroscopy techniques improve the signal to noise of recorded spectra, allowing refinement and improvement in the acquisition of experimental data. Often features within trace species are weak and not easily identifiable with direct detection methods. A diode laser based spectroscopy system that is able to detect and distinguish spectral lines that are broadened with a direct detection system is a powerful tool which can be applied to a variety of media as demonstrated here with mercury vapour detection and Raman spectroscopy of biological samples.

6.1 Introduction

Tunable diode lasers are ideal for optical spectroscopy because of their narrow linewidths, large tuning ranges and stable outputs. They are more compact and rugged than many other laser sources and have enabled spectroscopic methods to be used outside the laboratory as well as within. Applications of diode laser spectroscopy include remote sensing, trace gas detection and process monitoring. They can be used to monitor environmentally important species. High power semiconductor diode laser sources and high-efficiency frequency doubling have enabled the generation of narrow-band tunable radiation for UV spectroscopy. Recent widespread availability of blue diode lasers has allowed frequency conversion techniques to access the UV region. The use of modulation spectroscopy techniques serves to improve the signal to noise [1] and may be implemented with tunable diode laser spectroscopy [2, 3, 4]. Direct absorption techniques are attractive because of the ease of interpretation of the results and the simplicity of the experimental parameters. However for applications that require greater noise rejection and lower detection limits, wavelength modulation methods are a promising solution. Broadened spectral features are difficult to resolve with direct absorption measurements where the method is sensitive to the magnitude of the intensity of the feature. In contrast modulation spectroscopy is a derivative method that is sensitive to the curvature of the lineshape of the spectrum. This difference in the measurement principle is demonstrated in this work, where wavelength modulation spectroscopy (WMS) allows resolution of individual isotopes with a natural mix of mercury giving a level of insight unattainable with the direct technique.

The $6^1S_0 - 6^3P_1$ intercombination line of mercury at 253.7nm is one of the most studied lines in atomic physics. There are many spectral features of interest with the natural mercury vapour combining isotope transitions with the hyperfine structure. Although innovative techniques and enhancements to vapour discharge lamps have allowed some improvement in experimental precision, the resolution has until rela-

tively recently been limited by an unresolved hyperfine isotope structure. Recently, spectroscopic investigations on this line using two diode lasers has been able to resolve these features. The $6^1S_0 - 6^3P_1$ intercombination line in mercury, has been accessed by Jacobs *et al* [5] who frequency quadrupled a 1016 nm semiconductor laser in a bulky, multi-pass, two-stage process to deliver 150 mW of 254 nm light and obtained a scan width of 40 GHz. Alnis et al [6] were able to generate 0.9 nW of UV light using sum frequency mixing of a 5 mW, 404 nm, extended-cavity diode laser and a 30 mW single mode 688 nm diode laser. This had an optical to optical efficiency of 2.57x10^{-6}%. However, they were reliant upon a combination of multiple adjacent scans over 80GHz to see the all of the mercury absorption features. In comparison, in this chapter I present a compact, all diode laser based system that demonstrates over 50nW of UV light output and resolution of the absorption features of mercury at 254nm within a single, 58GHz scan, with an efficiency of 2.54 x10^{-4} % [7]. In addition a system to allow wavelength modulation spectroscopy of WMS is also described. The results presented show a far more detailed investigation than had previously been attempted [6], involving the use of low modulation frequencies and extensive investigation into the optimum parameters for WMS of the mercury vapour. The design of the SFG system is presented along with details of the methods used to maximise the non-linear conversion in the crystal, resulting in high generated UV power. The spectra of mercury ressolved using pressure cells at both atmospheric and low vapour pressure are given, the latter allowing resolution of individual features within the mercury natural isotope mix. The spectral features are then also identified using a low frequency wavelength modulation spectroscopy (WMS) technique where the rapid detection allows clear isotope separation within the natural mix to be identified. In addition direct and WMS spectra were recorded for a low vapour pressure source of the ^{198}Hg isotope of mercury. All of these results were obtained within a single scan of the system, obviating the need for complicated combinations of multiple scans to observe all of the spectral features. Absorption signals were recorded for direct detection and WMS techniques. In each case an accurate frequency spacing between features is given and a comparison between the two techniques is shown. Efforts to

optimise the parameters for WMS are described along with investigations into the effects of modulation amplitude, modulation frequency and harmonic detection. These results demonstrate the sensitivity and power of the WMS over the direct detection technique and show a very detailed investigation into the properties of the mercury line at 253.7nm.

The WMS detection method was also applied to Raman tweezers laser spectroscopy for investigations on polymer spheres and biological cell samples. The WMS method demonstrates the first use of this type of detection system using tunable diode lasers. The system shows a clear improvement in the signal to noise, shorter acquisition times for spectra and effective rejection of the background fluorescence which hinders the determination of spectral features within the sample.

6.2 Mercury

Mercury has seven naturally occuring isotopes, ^{196}Hg, ^{198}Hg, ^{199}Hg, ^{200}Hg, ^{201}Hg, ^{202}Hg and ^{204}Hg. Even isotopes have integer spin and nuclear spin of zero; odd isotopes have half integer nuclear spin. The spin of the isotope contributes to the spectral features of the vapour. Zero nuclear spin results in individual isotopic shifts in the spectral lines whereas integer spins causes splitting of the energy levels forming hyperfine structures which coincide with the ^{204}Hg, ^{198}Hg and ^{196}Hg isotope shifts, shown in Figure 6.1. The resolution of these features within the mix is shown with five individual spectral features. The spectral features occur as a result of the nuclear spin coupling with the angular momentum of orbiting electrons [8]. Typical background concentrations of mercury in air are a few ng/m^3. Environmental pollution monitoring systems based on Zeeman absorption and LIDAR techniques have already been used to identify mercury in air [9, 10]. The LIDAR systems are mobile but not compact. Here, a powerful, compact, diode laser based alternative is presented.

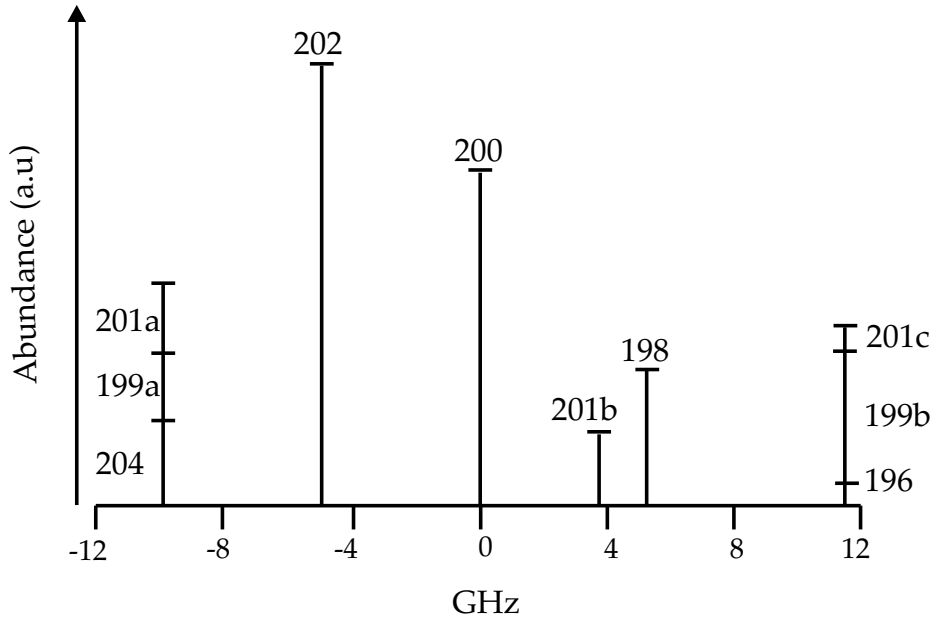

Figure 6.1: **Naturally Occuring Mercury Isotopes**
The even isotopes make single contributions to the absorption line structure. The two odd isotopes contribute to the structure, combining with the even isotopes.

6.3 Absorption Spectroscopy of Mercury

6.3.1 Generation of 254nm light

An explanation of the $\chi^{(2)}$ interaction that causes second order non-linear optical interactions was presented in Chapter 3. Sum Frequency Generation (SFG) is a specific case of this interaction, where two fundamental waves interact within a non-linear crystal to generate a single, higher frequency wave. This phenomenon is described in more detail in Section 3.12.

To generate light at 254nm a frequency conversion system based upon SFG was assembled from scratch, using a free running microlensed diode laser (MDL) at 662nm and an MDL within a Littrow external cavity configuration using a holographic UV diffraction grating for single mode operation at 411nm. The two lasers were wavelength matched to deliver sum frequency generated light in the UV. The properties of the two microlensed lasers are summarised in Table 6.1 and presented in more detail

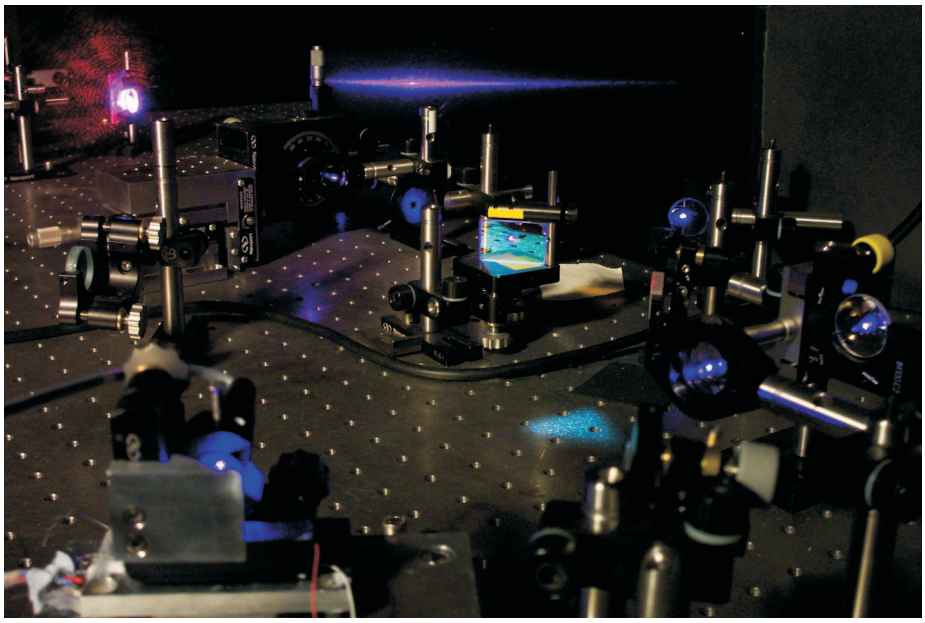

Figure 6.2: Photograph UV Generation

in [11] and in Chapter 5. The system was initially setup by A. Carruthers who successfully obtained the broadened mercury spectrum shown in Figure 6.5. Following on from this work, I led the assembly of the system in an alternative configuration, and after generating the maximum UV power from the system, resolved the fine structure features using a low vapour pressure mercury cell manufactured by the School's departmental glass blower.

Wavelength(nm)	Output Power (mW)	Linewidth(MHz)	Continuous Tuning(GHz)
662	50	11	70
411	14 (ECDL)	4	6

Table 6.1: **Properties of microlensed diode lasers for generation of 254nm [11].**

Figure 6.3 shows the practical set-up for the generation of UV light.

The two laser beams were brought together by using beam steering mirrors (M1 and M2 for the red beam; M3 and M4 for the violet beam) and combined by a dichroic

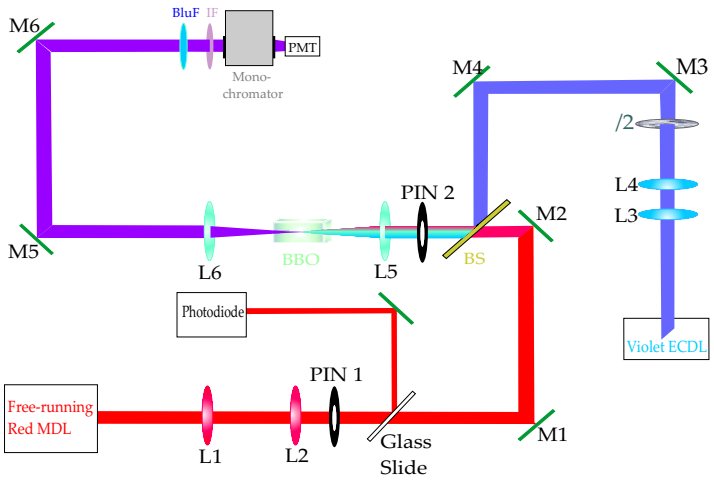

Figure 6.3: **Sum Frequency Generation of UV**
Experimental setup for generating 253.7 nm. M1-M6 are mirrors, L1-L6 are lenses. PMT is the photon multiplier tube, IF is the interference filter, PIN 1 and PIN 2 are the pinholes, BBO is the non-linear crystal, BS is the dichroic beam splitter, the glass slide is marked Glass and $\lambda/2$ denotes the halfwave plate.

beamsplitter (BS). Both the beams were then aligned through two pinholes (PIN 1 and PIN 2) to ensure good beam overlap through propagation within the non-linear crystal. A lens system (L5 & L6) was introduced to focus the combined beams into the crystal. L5 was an uncoated, 50mm focal length lens that focussed the red and blue beams into the crystal. L6 focusses the output from the crystal onto the first UV mirror. L6 is coated for maximum transmission of blue and UV and recollimates the beam out of the crystal. To minimise the harmful effects of back reflection into the red diode laser, the lenses were anti-reflection coated. The non-linear crystal was a β-barium borate (BBO) crystal, cut at $\theta = 49.3^o$ and $\phi = 0^o$ with dimensions of 3mm by 3mm by 8mm. The crystal was coated on the front face for transmission at the input wavelengths and the back face coated for transmission at the up-converted wavelength. The crystal was mounted on stage that permitted rotation through 360 degrees and then also onto an X-Y-Z translation stage, allowing precise alteration of the crystal orientation to ensure maximum non-linear conversion. The position of the crystal was determined crudely at first, with the alignment achieved by aligning the back-reflected red beam back to the pinhole, PIN 2, slightly left of centre. In this orientation, the generated beams were aligned using the two UV mirrors that were used to guide the

beam onto the photomultiplier tube (PMT) through a monochromator ensuring that only UV light at 254nm was detected. To fine tune the alignment the output from the PMT was observed on a oscilloscope and adjustments made accordingly to maximise the gain. Firstly the crystal mounting was adjusted to obtain maximum gain, firstly coarsely and then with further fine adjustment using the X-Y-Z actuators on the mounting. There was little need to adjust the crystal rotation as this had already been optimised for SFG in the previous application of this system using the atmospheric vapour pressure cell. Once the position of the crystal had been set, further fine adjustment was used to yield the maximum gain. This involved adjustment of the UV mirrors (M5 and M6) to ensure optimum alignment onto the PMT and then slight adjustment of the red and blue beams to perfect the alignment through the crystal. At various stages during this alignment system the PMT became saturated and filters (BluF and IF) were introduced to allow further detection of generated light.

To maximise non-linear frequency conversion the beam sizes of both lasers were collimated using cylindrical lens systems, (L1 & L2 and L3 & L4) The beams can be shaped to match their size to either their beamwaists, w_0, or the confocal parameter, b, of the BBO crystal. In Section 3.5 an expression for the theoretical SFG power was given. For the case of different matched parameters this expression can be adapted. For the case where the beamwaists of the two fundamental beams are the same, but the confocal parameters are different, m, given in equation 3.x. can be simplified using $1/w_3^2 = 1/w_1^2 + 1/w_2^2$. For equal beamwaists, $w_1 = w_2$ so m is further simplified to $w_3 = w_{1,2}/\sqrt{2}$. Thus the conversion efficiency η for the SFG process as described in [12, 13] can be given by

$$\eta = \frac{P_3}{\sqrt{P_1 P_2}} = \frac{2 d_{eff}^2 l^2 \omega_1 \omega_2 \sqrt{P_1 P_2}}{\pi \varepsilon_0 c^3 n_1 n_2 n_3 w_{1,2}^2} \tag{6.1}$$

In contrast the generalised expression can also be adapted for optimum phasematching and thus for matched confocal parameters. To account for Gaussian beam focussing and walk off the Boyd-Kleinmann multiplication factor is introduced.

$$P_3 = \frac{2d_{eff}^2\omega_1\omega_2 P_1 P_2 l k_0 h(B,\xi)}{n_1 n_2 n_3 c^3 \varepsilon_0 \pi} \tag{6.2}$$

For matching the confocal parameters of the two beams to the length of the non-linear crystal (b=8mm), the theoretical UV power that should be generated by this system is 83nW [7], based upon the assumption that the red and violet laser beams are overlapped optimally within the non-linear crystal and that their dimensions remain constant within the crystal and the confocal parameters are matched for both beams. To satisfy these conditions the beamwaists for the two beams would be different, (17.6μm for the violet and 22.5μm for the red). This means that the waist of the red laser must be increased thus reducing the amount of power from the laser available for non-linear conversion. With the initial system used, there was no further beamshaping using lens relays, the beamwaists were matched to 20μm resulting in a generated UV power of 6.5nW. Although a significant improvement on the previous reported best (0.9nW), the theoretical power suggested that if the system parameters were optimised, the system would yield more power.

Conventionally, for non-linear conversion, matching the beamsize to the confocal parameter ensures stability and maximum efficiency. However, here theoretical modelling indicated that matching the beamwaists rather than the confocal parameters would deliver the best overlap between the two beams [14]. As the beam diameter of the red laser is larger than that for the violet laser within the crystal a substantial amount of the red laser power is not used for conversion. Ruffing *et al* [15] during investigations into the parametric generation of violet light, showed that the most efficient non-linear conversion is obtained for a situation where the beamwaists of the lasers are matched, utilising all of the available laser power within the non-linear interaction. By matching the beamwaists of the two lasers to $40\mu m$ the power available for SFG is increased [7].

Table 5.2 shows that significantly higher powers were obtained for matching the beamwaists. Matching the beam parameters is achieved by choosing the correct lens

relay and improvements in the output power when the beamwaists were matched to $40\mu m$ by finding the most appropriate combination of lenses.

Matched Parameter	Lens Relay(Red)	Lens Relay(Blue)	UV Power (nW)
b= $8mm$	$100 + 50$	$50 + 40$	17.8
w_0=20 μ m	None	None	6.5
w_0=40 μ m	$100 + 50$	$100 + 50$	50.3 [14]

Table 6.2: **Lens Systems used to maximise UV output**

The UV beam power was measured using the photomultiplier tube (PMT) with filters to ensure only the UV light was detected and prevent saturation of the PMT. The PMT is sensitive to blue and UV light only, so a chopper was used to exclude the red to provide a simple check of the light being generated and allow this to be maximised. The measurement of the UV power at the back facet of the crystal was calculated by determining the power at the PMT and then accounting for the transmission properties of the different optical elements within the system after the crystal.

Once the PMT had been saturated a more direct measurement of UV was taken using an optical power meter. Although the power meter can be used to directly measure power at a certain set wavelength, its response time is much slower than that of the PMT and so initially the PMT was used to maximise the UV power. The power meter was placed after the monochromator and the UV mirrors and a glass slide was used to differentiate between generated UV light and background noise. The output UV power of 50.3nW was over an order of magnitude greater than that previously reported [6], a direct result of the improvement in SFG conversion efficiency, described in Section 3.5, and [7]. This improvement in efficiency is attributed to the use of microlensed diode lasers as the circular output beam allows more of the direct diode output to be used for non-linear conversion and reduces the requirement for lossy beamshaping optics within the system.

6.4 Direct detection absorption spectroscopy of mercury

To access the mercury line the sum-frequency system described was used to generate light at 253.7nm. The red and violet diode lasers were temperature and current tuned to set their wavelengths at 662.3nm and 410.3nm respectively. To detect the mercury absorption line, the experimental setup was adapted, as shown in Figure 6.4, to include a lens relay to focus the UV beam into the mercury cell and the output focussed onto the PMT with interference and blue filters used as before.

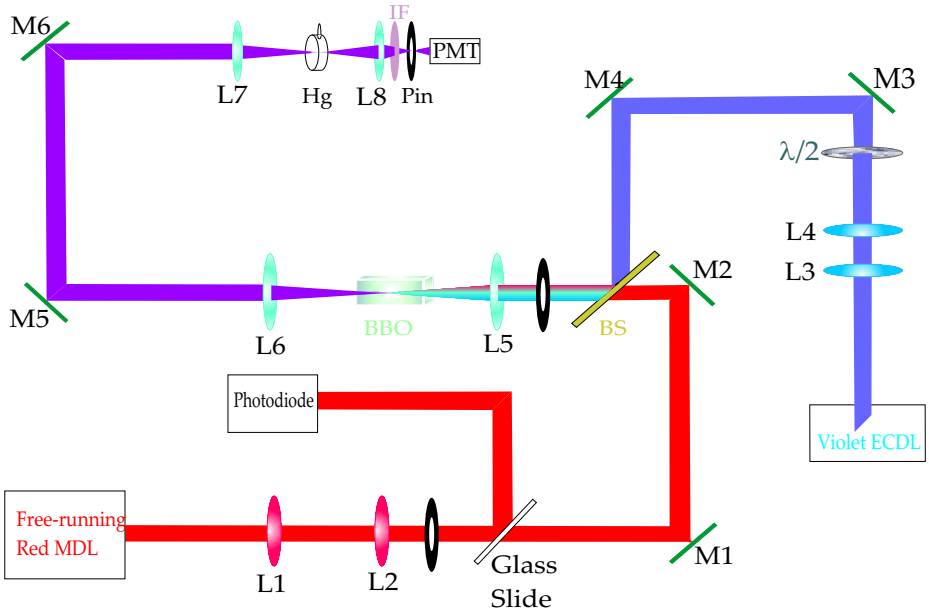

Figure 6.4: **Experimental setup for absorption spectroscopy of mercury** Experimental setup for spectroscopy of mercury. A lens relay is used to focus the UV beam into the mercury cell. The UV light is then detected,using the PMT.

To minimise the effect of scatter a pinhole is placed at the beam focus immediately before the PMT. To monitor the sweep of the laser, a glass slide is used to pick off a small amount of the light from the red laser to ascertain that the tuning is mode-hop-free. The red laser was current and temperature tuned to deliver a large (58GHz) mode-hop-free scan and a corresponding wavelength shift of 662.268nm - 662.354nm. This wavelength shift was measured using a Burleigh laser wavemeter. The frequency

scan was clarified by use of a Fabry-Perot etalon with a free spectral range of 2GHz. This was matched with a coarse tuning of the violet ECDL to access the mercury absorption line. The long smooth scan of the red laser allowed all of the features of the mercury absorption line to be resolved within a single scan of the red laser.

The fine structure of mercury was only obtained with a low pressure mercury cell due to the effects of pressure broadening. The spectra obtained with high and low pressure cells are shown in Figure 6.5. The lower pressure spectrum shows clearly resolved transitions that fit with the broadened features from the measurement at atmospheric pressure. The hyperfine structure aligns with the pressure broadened scan, with the frequency separation of the two traces and the resolved features matching in shape and size. Figure 6.6 shows an accurate frequency calibration of the mercury features. This calibration was obtained using an accurate 58GHz scan, measured using a Fabry-Perot etalon with a FSR of 2GHz. Using this etalon and observing the modes on an oscilloscope allows a measurement of the frequency scan to be $\pm$1GHz . The spacing between features was determined by zooming in on the separations. This allowed a more precise determination of the spacings between the individual features accurate to $\pm$0.5GHz.

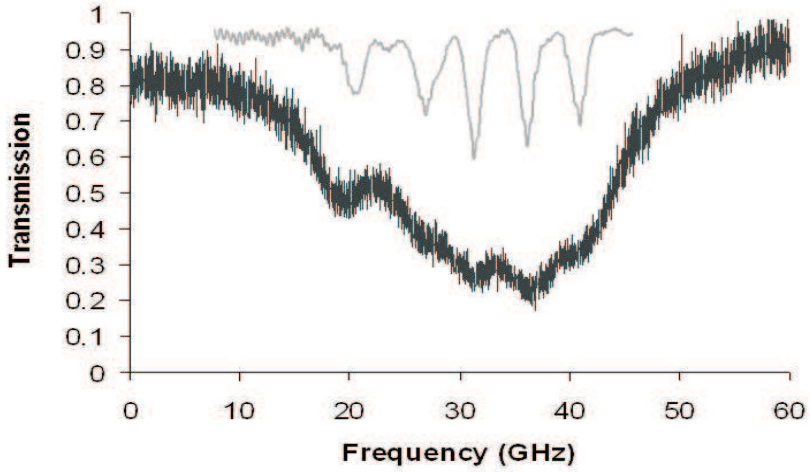

Figure 6.5: **Absorption Spectrum of Mercury**
Mercury absorption signal from an atmospheric pressure cell (black) and from a low pressure cell(grey) with a natural isotope mixture, taken at room temperature normalized to account for the power variation over the scan. (Signal from atmospheric pressure cell obtained by A. Carruthers)

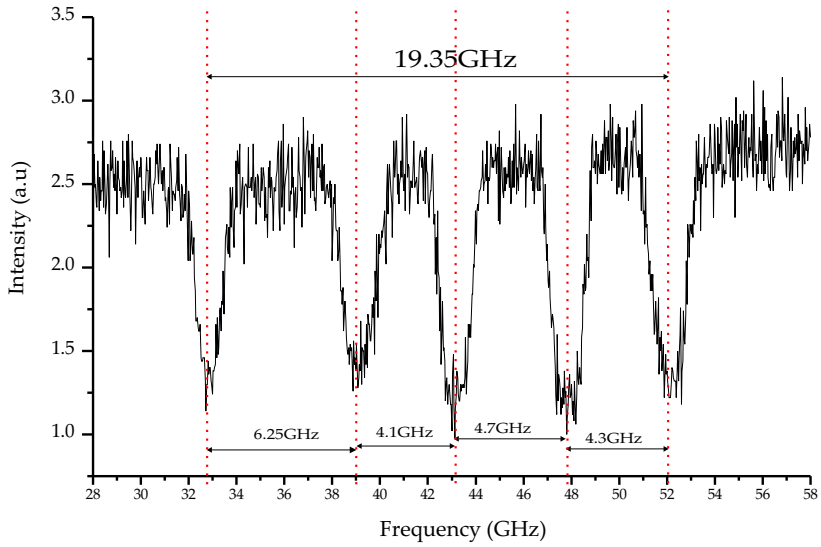

Figure 6.6: **Frequency Calibration of Absorption Spectrum of the Natural Mix of Mercury Vapour**
The trace shows the frequency separation between the fine structure features of mercury. The frequency span of all the features is 19.35GHz and the separation between the individual fine structure features are 6.25GHz, 4.1GHz, 4.7GHz and 4.3GHz.

6.5 Modulation Spectroscopy techniques for trace gas detection

When techniques for tunable diode laser spectroscopy are adapted to include modulation of the laser wavelength the detection sensitivity is vastly improved, delivering a powerful and highly precise spectroscopic tool without the need for complicated alterations to a direct detection method. Diode lasers are especially well suited for high sensitivity absorption spectroscopy because it is possible to tune their emission wavelengths over the whole absorption profile by changing the temperature of the laser and modulating the drive current. This results in simultaneous intensity and frequency modulation of the emitted light.

6.5.1 Review of Modulation Spectroscopy

The benefits of employing modulation techniques have been explored extensively resulting in a huge number of gas sensing publications. This section gives a brief review of some of the notable work carried out in this area.

Song and Jung [1] give an excellent review of wavelength and frequency modulation spectroscopy (WMS and FMS) techniques as well as other modulation techniques, Two-Tone Frequency Modulation Spectroscopy (TTFMS) and the sweep integration method. Bomse et al applied gave a comparison between FMS and WMS when applied to detection of absorption of N_2O using a lead-salt diode laser [16]. A theoretical description of the two methods is given by Supplee et al [17].

Diode lasers have been used within modulation spectroscopy systems to detect caesium [2] water vapour, oxygen [18] and have been used to assist with the characterisation of a laser [19]. The technique has been used in the spectroscopy of cesium to generate a frequency standard for diode laser stabilisation [20]. The technique has been used with blue diode lasers to detect trace gases: Alnis *et al* applied wavelength

modulation to the detection of potassium [3] and mercury [6]. However they were unable to see any discernible difference between this method and direct absorption for mercury. In contrast the results presented here show a more detailed investigation into the WMS technique, using a much lower modulation frequency and show the resolution of features that are not visible through direct detection.

6.5.2 Theory of Wavelength Modulation Spectroscopy

Modulation spectroscopy with diode lasers involves applying a sinusoidal modulation to the drive current at a frequency f whilst the operating wavelength of the laser is slowly tuned across the absorption line under investigation. There are two major techniques in modulation spectroscopy, wavelength modulation (WMS) and frequency modulation (FMS). The techniques are essentially the same but they are applied in different frequency regimes. Wavelength modulation spectroscopy employs modulation frequencies that are much smaller than the half width of the absorption feature of interest, $\omega_{1/2}$. By defining a parameter, x_m, the differences between the two techniques can be explained simply. If $x_m = \frac{\omega_m}{\omega_{1/2}}$ then for WMS, $x_m < 1$, whereas for FMS $x_m > 1$. The signal resulting from the applied modulation is then demodulated by a phase sensitive detector at the modulation frequency or at harmonics of this.

Wavelength modulation spectroscopy is a commonly used method in trace gas detection applications and involves the use of modulation frequencies $\sim$ kHz. There are several reasons why WMS can provide benefits to laser-based absorption techniques: Analysis of samples by absorption techniques are based upon the difference between two large signals which is observation of the detector signal in the presence and absence of the target species, similar to detecting the signal on and off resonance respectively. This is accomplished by continuously tuning the wavelength over the resonance which can be readily achieved with diode lasers. The other reason is that a smooth modulation of the wavelength at f, followed by the detection of the signal at f and higher harmonics, shifts the signal to a higher frequency where the $1/f$ noise

of the detector, which can dominate at lower frequencies, is significantly smaller. $1/f$ noise is most commonly associated with the noise of the detector and can be a significant problem with laser light detectors. The optimum harmonic is not necessarily n=1 and is dependent upon the degress of deviation away from the central frequency and the effect of the noise at lower modulation frequencies.

Figure 6.7 shows a typical absorption spectrum and a wavelength modulated absorption spectrum. In WMS, as the wavelength is scanned across the atomic transition, the wavelength modulation is converted to amplitude modulation (AM) giving rise to a modulation in the optical absorption of a sample at the same frequency. As the scan continues across the absorption profile, the amount of FM to AM conversion varies.

The conversion of FM to AM is dependent upon the slope (or derivative) of the absorption at that frequency. It is often referred to as 'slope conversion'. Essentially the lock-in amplifier measures an AC voltage (or current) of a particular frequency and gives output in the form of a DC voltage proportional to the value of the AC signal being measured. The amplifier is termed 'lock-in' because it locks to and measures signals at the particular frequency of interest ignoring all other signals at the input. The heart of the lock-in amplifier is a phase sensitive detector, sometimes known as the demodulator. It is this part of the instrument which demodulates the signal of interest and it should be noted that its output is a function of the relative phase angle between the input signal and the associated reference signal. It follows therefore, that the lock-in amplifier can also be used to measure the relative phase of two signals of the same frequency.

Near to the point of maximum absorption (i.e the bottom of a power depletion dip, marked **C** in Figure 6.7) the conversion of FM to AM is very small at frequency f(zero at the line centre). As one moves from the low frequency to the high frequency side of the peak the phase relationship between AM and FM is reversed (the differences in the AM signals marked at **B** and **D** in Figure 6.7. If the scan is continued away from

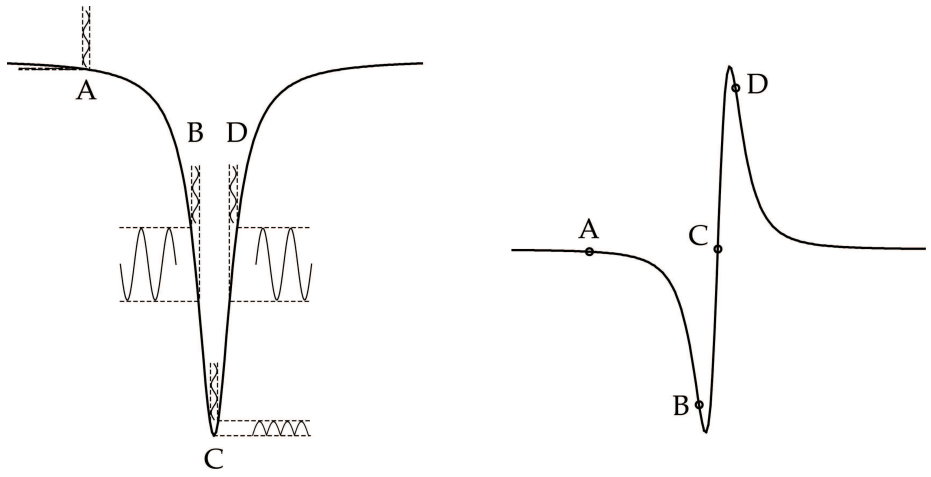

Figure 6.7: **Frequency Modulation to Amplitude Modulation**
The figure shows the effect of modulation upon a feature and the conversion from a direct to a derivative feature.The letters A-D indicate the different effects of the slope of the feature upon the conversion of FM to AM [21].

the absorption (i.e away from the power depletion) AM disappears because of lack of absorption and a near zero slop (point **A** in Figure 6.7). It is possible to plot the ratio of AM to FM versus the laser frequency and the phase inversion of the signal is represented by the sign change. The curve is thus the derivative of the absorption profile.

There are three frequencies that are associated with FM signals. The carrier frequency ω_0 is the centre frequency of the signal. The second frequency is the frequency deviation $\Delta\omega$ which is a measure of how far the instantaneous frequency departs from the carrier frequency. The third frequency is the modulation frequency ω_m which measures how quickly the instantaneous frequency varies about ω_0. We can define the wavelength modulation index,M, as the maximum deviation of the laser from the carrier frequency in terms of the frequency half width:

$$M = \beta x_m \tag{6.3}$$

where β is the FM index defined by $\beta = \frac{\Delta\omega}{\omega_m}$.

6.6 Wavelength Modulation Spectroscopy of Mercury

Modulation techniques have peviously been applied using a similar system on the same mercury line previously by Alnis *et al* [6]. Their method used a high modulation frequency of 5MHz and they were unable to see any discernible difference between the direct and modulation detection methods. Here I demonstrate low frequency WMS, and detailed investigation into system parameters. There is a considerable reduction in the noise contribution with the WMS spectra compared to the absorption spectra. In addition the WMS spectra were all obtained within a single scan of the system. Furthermore the investigations into the single isotope source indicated the presence of other isotopes, features that were not visible with the direct detection system. The improved technique described here is a direct consequence of the increased UV power obtained as a result of using microlensed diode lasers in the SFG system [22] and the detailed refinement of the system parameters to yield the clearest spectra. Figure 6.8 shows the setup for the WMS experiment.

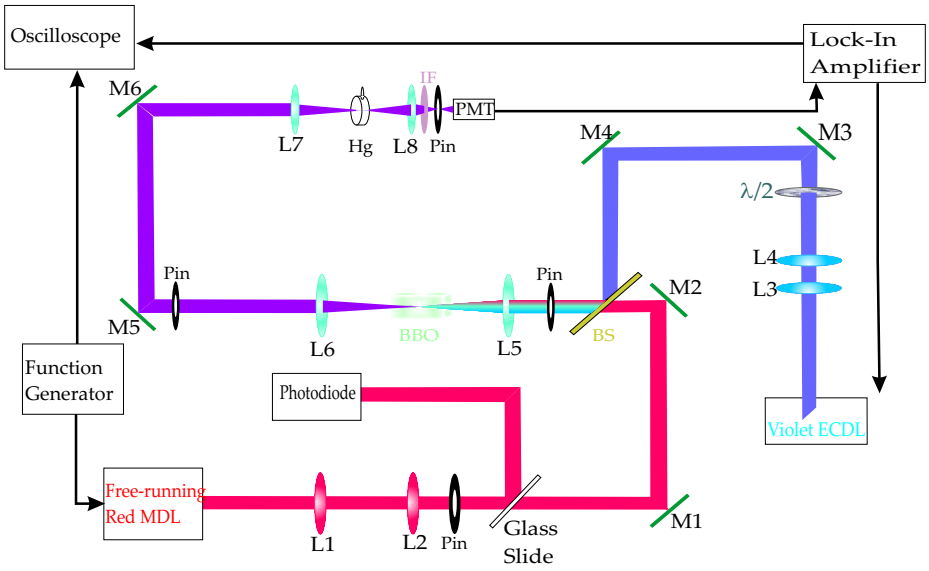

Figure 6.8: **Setup for Wavelength Modulation Spectroscopy**
The output from the PMT is fed to a lock-in amplifier which demodulates the signal. A small current modulation is applied to the diode laser from the lock-in amplifier.

The direct detection absorption system is adapted so that the output from the photomultiplier tube is input into a digital lock in amplifier (Stanford Research Systems Model 830). Harmonic detection requires that a sinusoidal modulation be imposed on the laser wavelength for modulation spectroscopy while the laser wavelength is scanned continuously. This modulation was generated in the digital lock-in amplifier. The frequency and amplitude of this modulation can be altered to suit the best parameters for the system. Initially, a sine wave modulation of frequency 1KHz with amplitude of 48mV was applied to the blue external cavity diode laser that was temperature and current tuned to deliver an emission wavelength of 410.29nm. The modulation transfer function of the diode laser is given by the manufacturer as $20mV/1A$. The smooth scan of 58GHz that is used here was obtained over a variation in injection current of 11mA, therefore gives a value for the transfer function of $105MHz/mV$ thus implying that an applied modulation with an amplitude of 1mV will apply deviation to the laser from its centre frequency of 105MHz. A function generator gives an adjustable ramp at 0.8Hz, applied to the red laser in the same way as in the direct absorption measurement, again providing us with 58GHz of mode hop free tuning. The time constant of the lock-in amplifier was set to 10ms, providing a sufficient amount of signal averaging for good signal to noise. Our system provided flexibility with the ability to modulate both lasers. When modulating the red laser a home built mixer circuit is used to apply the sweep and dither concurrently. Figure 6.9 shows the difference in the modulation spectra obtained when the modulation is applied to each laser.

For both cases the modulation system was able to detect signals where the corresponding spectra were able to resolve the features of the mercury vapour. However the signal to noise was significantly improved when the modulation was applied to the red laser concurrently with the sweep. For all subsequent measurements the modulation was applied to the red laser and the violet ECDL was temperature and current tuned to deliver the correct wavelength (411.3nm) to access the mercury line at 253.7nm.

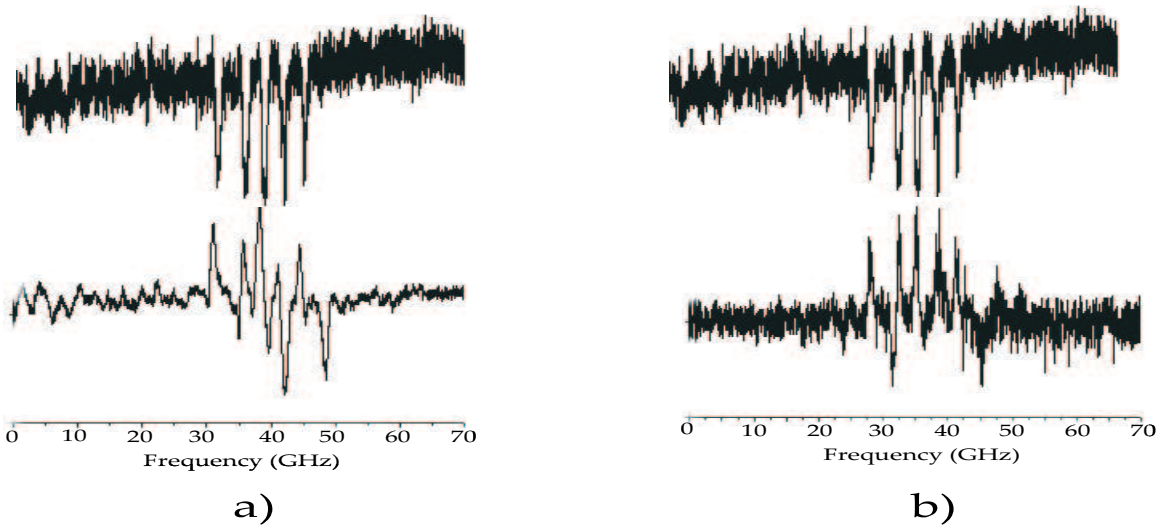

Figure 6.9: **WMS spectra with the current modulation applied to both the red and violet lasers**
A comparison of wavelength modulated spectra when applied to different lasers within the SFG system. Figure a) shows the modulation when applied to the free running red laser. Figure b) shows the spectrum when modulation is applied to the violet ECDL.

The amplitude of the applied sinusoidal modulation is a crucial parameter when performing WMS experiments. If the amplitude is too large then the resolution of the spectrum is compromised and eventually causes distortions in the lineshape of the feature. The ^{198}Hg single isotope source is contained within a glass cell at low atmospheric pressure. Figure 6.10 shows the effect of varying the amplitude of the modulating sinusoidal signal on the resolution of the detected features. The results show that if the deviation of the laser is increased then the there is a broadening effect upon the detected features, decreasing resolution and introducing distortion. It is a crucial parameter in allowing us to identify and resolve spectral features. If it is too large the resulting spectrum will be broadened and the clarity of the spectrum is lost. The initial modulating amplitude of 48mV is shown to be unsuitable, resulting in broadening of features.

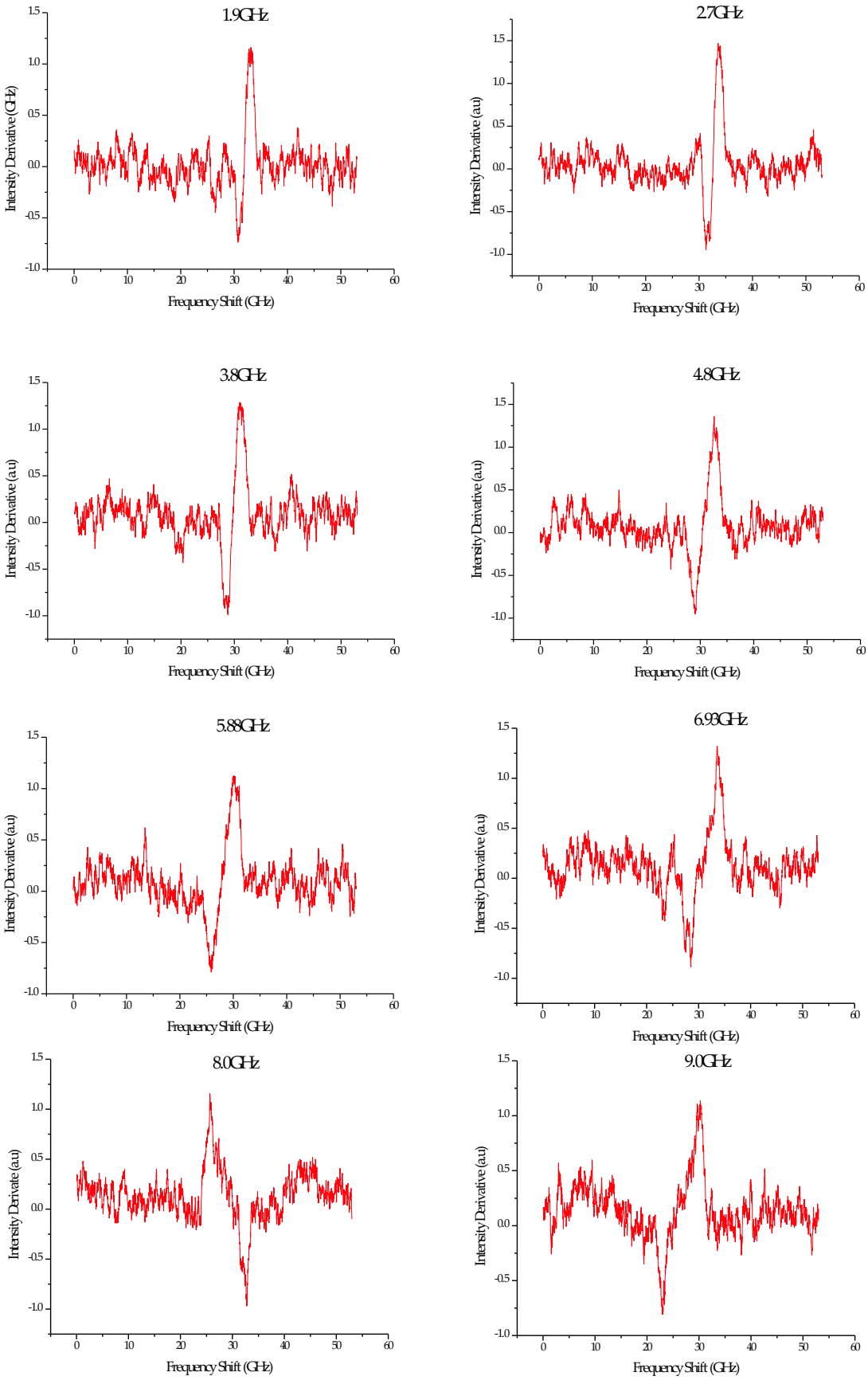

Figure 6.10: **Spectra recorded for detection of the ^{198}Hg isotope with a variation in modulating amplitude**
The figures show the effect of increasing the amplitude of the applied sinusoidal modulation upon the resolution of the detected features. The frequency deviation of the laser corresponding to the applied modulation is given with each figure.

6.6.1 Detection at different harmonics

For a system with significant detector $1/f$ noise, a harmonic detection system can be used effectively to shift the detection to higher harmonics where this noise effect is diminished and there can be a significant improvement in the signal to noise ratio (SNR). Pin diodes are commonly used detectors and have a relatively high $1/f$ noise at the frequencies used for modulation [23]. In our system, a photomultiplier tube is used which only displays $1/f$ noise at very low frequencies [24], much lower than the kHz regime of frequencies used in this work.

Detection of the signal by the lock-in amplifier can occur at different harmonics of the modulation frequency, nf, which influences the signal to noise ratio and in turn the clarity of the output spectra. The Stanford lock-in amplifier can detect harmonics up to n= 19999 as long as nf does not exceed 102KHz. In order to find the optimum detection parameters for this system, spectra with detection at harmonics n=1,2,4 for modulation frequencies of 1kHz at a constant modulating amplitude of 4mV shown in Figure 6.11.

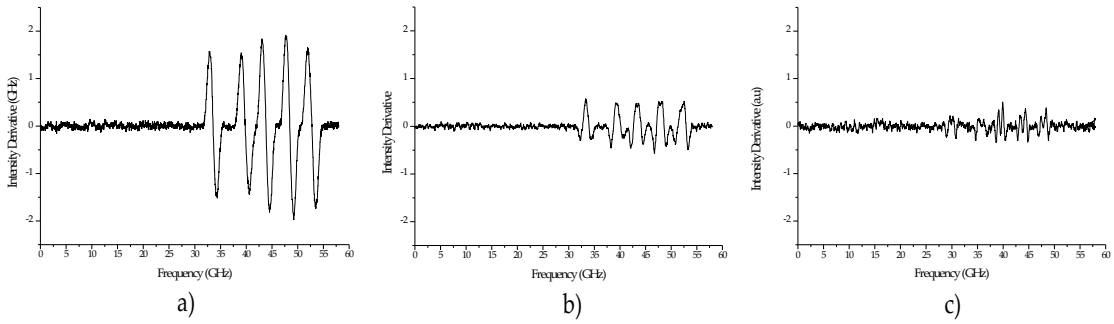

Figure 6.11: **Harmonic detection spectra for 1KHz modulation frequency**
The spectra recorded at f, 2f and 4f are shown in figures (a), (b) and (c) respectively.

In the published literature, detection has tended to occur at higher harmonics [2, 16, 18]. The results obtained here showed no improvement in the spectral resolution and signal to noise when the detection was shifted to a higher harmonic. This was is believed to be in a large part due to the very low $1/f$ noise present in photomultiplier

tubes. However, the low modulating amplitude used here is also a major factor. The amplitude of the applied sinusoidal modulation affects the deviation of the laser from its centre frequency and the amount of conversion from FM to AM. To explain this, it is necessary to consider the frequency spectrum of the FM signal. When FM signals are generated the instantaneous frequency at any time t can be given by

$$\nu(t) = A_0 sin(\omega_0 t + \beta sin\omega_m t) \tag{6.4}$$

where ω_0 is the carrier frequency, A_0 is the amplitude of the carrier, t is the time, and β is the FM modulation index

The Fourier series expansion of Equation 6.4 is given by:

$$\nu_0(t) = J_0 A_0 sin\omega_0 t + \tag{6.5}$$

$$2A_0(J_2(\beta)sin2\omega_m(t) + J_4(\beta)sin4\omega_m t + ...)sin\omega_0 t \tag{6.6}$$

$$+2A_0(J_1(\beta)cos\omega_m t + J_3 sin3\omega_m t + ...)cos\omega_0 t \tag{6.7}$$

The spectrum of a sinusoidally modulated FM wave consists of an infinite number of sidebands at higher frequencies on each side of the carrier frequency. The coefficients of the Fourier series expansion, $J_n(\beta)$ are Bessel functions of the first kind of order n and argument β and give the amplitude of the sideband corresponding to the nth harmonic of the modulation frequency ω_m. The series of Bessel functions are shown in Figure 6.12. Odd harmonics are only significant at higher amplitudes where there is considerable distortion of the lineshape.

The functions characterise the frequency component of the modulated light spectrum [17, 21, 25]. For a given modulation index there are certain upper and lower sidebands that will affect the FM spectrum. As the modulation index increases the number of sidebands increases. From Figure 6.12 we can see that for any given modulation index, there are a finite number of Bessel functions whose value is considerably different to

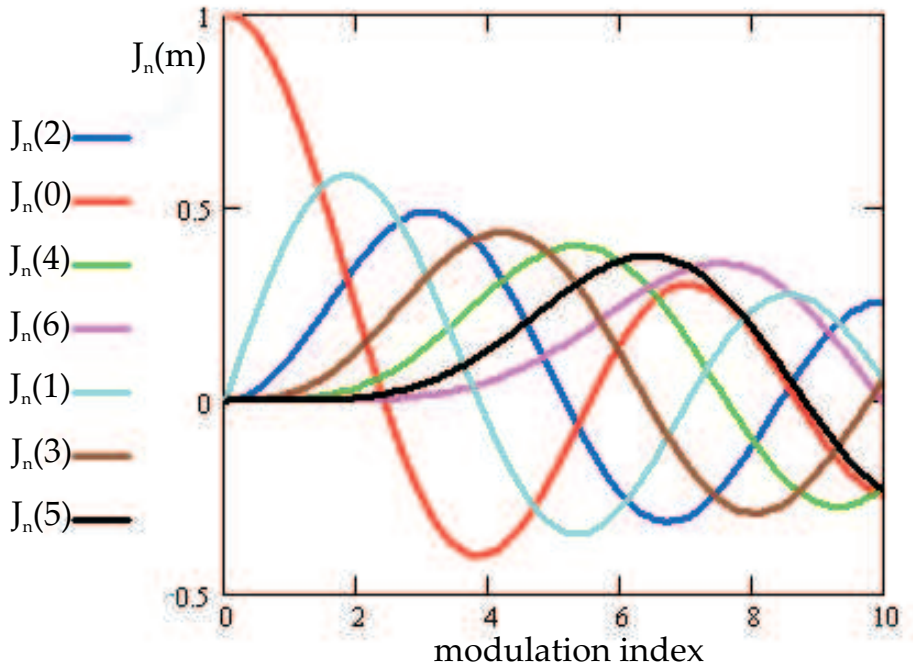

Figure 6.12: **Bessel Functions**
The Bessel functions shown are of order 0-6 with argument m. They provide a measure of the amplitude of the sidebands generated by a sinusoidally modulated FM signal.

zero. As such only the corresponding number of upper and lower sidebands contribute to the FM spectrum.

As the deviation of the laser from the carrier frequency increases, the number of sidebands that contribute to FM spectrum increases and the division of strength of the carrier frequency amongst the sidebands is not linear. The effect of those sidebands that contribute less than 1% of the magnitude of the initial carrier is considered negligible. The contributions from sidebands varies so it can be preferable to move the detection to higher harmonics where the SNR of the sidebands at further deviation from the carrier frequency is better. From this it is simple to deduce that for systems where $1/f$ noise is significant, detection at higher harmonics (where the deviation of the laser is larger and the number of detected sidebands increases) can be a more useful detection method. The contribution made by these sidebands to the spectrum will only be detected when their magnitude exceeds the noise level. The influence on

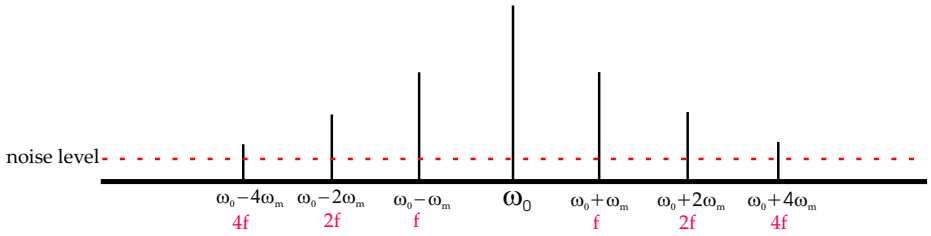

Figure 6.13: **Plot of the frequency spectrum of an FM signal**
The sidebands that are shown arise from the different frequency components of the FM spectrum. As the amount of deviation of the laser frequency increases the detection of those sidebands at higher harmonics is possible

the modulation index also is dependent upon the lineshape. Doppler, Lorentzian and Voigt fitted lineshapes will all respond differently to different amplitude variation due to the difference in the curvature of the lines resulting in a difference in the AM contributions. There has been detailed examination of the optimum wavelength modulation index, M, for these lineshapes at different harmonics [26, 27].

These effects were observed by measuring the peak signal height at different harmonics for a variation in the modulation index. For n=1,2,4,6 the peak height of the most abundant isotope, ^{202}Hg was recorded for variation in the amplitude of the sinusoidal modulating signal from 0.004V to 0.036V shown in Figure 6.14. The signal output at even harmonics modulation index follows a Bessel function at low indices that characterise the frequency modulation of signals. The results show that by operating the system at 1kHz and detecting at the first harmonic yields the best result for this system. The amplitude can be increased to 0.012V to get the best signal output without compromising the resolution of the features. At this modulating amplitude, the wavelength modulation index is 1.58. The corresponding Bessel function of the first order $J_1(\beta)$ has its maximum value at 1.78. For comparison the signal outputs at odd harmonics n=3 and n=5 were also recorded, shown in Figure 6.15.

It should be the case, because only even harmonics occur within the Fourier series expansion, that detection at odd harmonics should only occur if there is a distortion in the lineshape. The corresponding Bessel function $J_3(\beta)$ in Figure 6.12 shows that

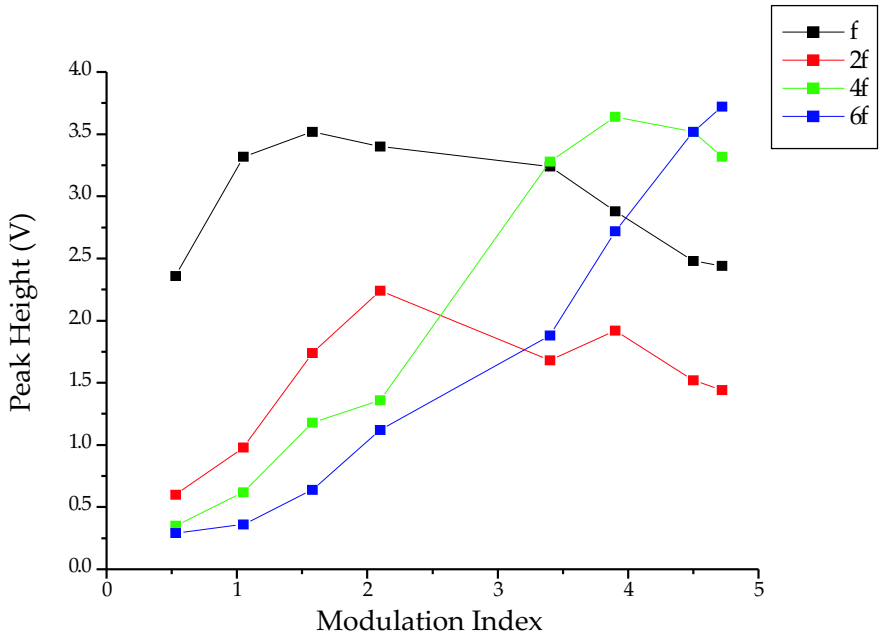

Figure 6.14: **Output signal at even harmonics for variation in modulation index**
The graph shows the magnitude of the WMS signal when the degree of laser deviation from the carrier frequency is varied. A comparison at different harmonics is shown. The maximum signal for the first harmonic is obtained a modulation index 1.58. The contributions of the signals detected at higher harmonics are not significant at this amount of deviation of the laser from its centre frequency.

there is a slow rise in this function, whereas the rise in the $3f$ signal in Figure 6.15(a), is very steep, not following the Bessel function pattern. The other odd harmonic $5f$ also does not follow the corresponding Bessel function J_5. This is due to a large deviation in the laser frequency caused by a large modulating amplitude. For the $3f$ and $5f$ signals to be significant there must be a distortion in the lineshape of the absorption feature, usually an indication of overmodulation. As shown in Figure 6.15, at the points where the odd harmonic contributions start to become significant the deviation of the laser caused by the applied modulation is sufficiently high to cause distortion and broadening effects as shown in Figure 6.10.

At low modulation indices, there is only a significant contribution from the first harmonic. The optimum SNR for the 1st harmonic occurs at a modulation index of

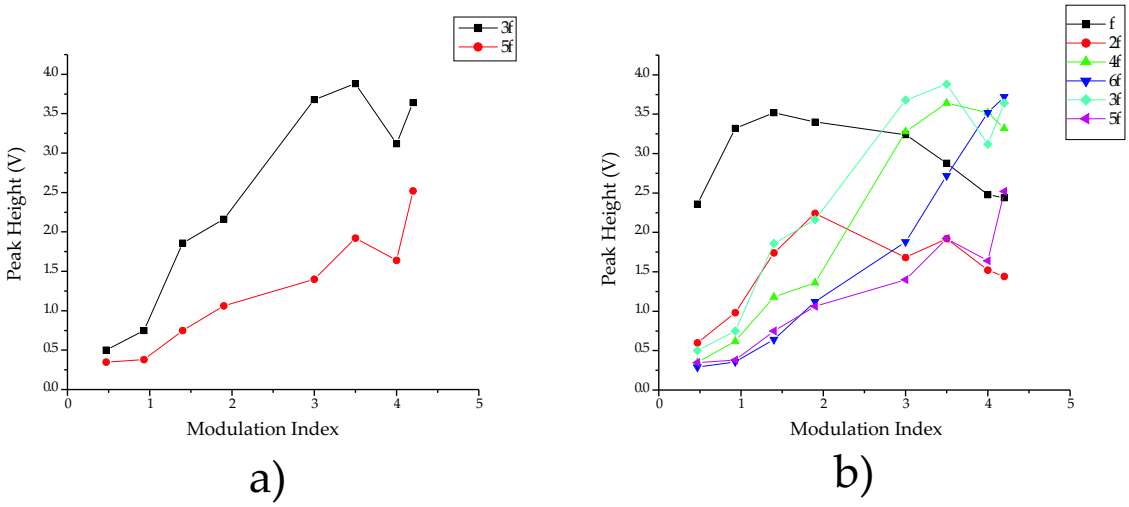

Figure 6.15: **Output signal at different harmonics for variation in modulation index**
The graph shows the magnitude of the WMS signal for variation in the modulation index for detection at odd harmonics (a) and then for harmonics n=1-6 (b). The odd harmonics are only significant at modulation indices that indicate large deviations in the laser frequency from the carrier, implying that the lineshape is distorted.

1.58. The peak of the 1st order Bessel function is at 1.78. At small deviations where there is some contribution from the second harmonic, the first harmonic contribution is still much greater. At higher indices where $2f$ is significant, third harmonic signals are also significant which indicates distortion of the lineshape, which is confirmed by the size of the modulating amplitude corresponding to this modulation index. Figure 6.15 shows that odd harmonic contributions are significant at higher modulation indices which implies distortion, over modulation and risks modulation that causes a deviation of the laser that is greater than the linewidth of the feature of interest.

Shifting detection to the second harmonic can be done in two ways, either detecting at $2f$ or increasing the modulation frequency to 2kHz. However, as shown significant $2f$ signals are only obtained where there is lineshape distortion. If ω_m is increased to 2kHz then the risk occurs that the relaxation time of the system will not be quick enough to allow for the quicker modulation.

This analysis shows that for this system there is no advantage gained by shifting the

detection to the second or higher harmonics. The $1/f$ noise contribution from the PMT is negligible at the frequencies used here.

6.6.2 Measurement of Isotope Separation in Mercury

The parameters for the WMS system were a modulation frequency of 1kHz with a corresponding modulation amplitude of 0.004V. With this system I was able to resolve all of the features within the natural mix with the WMS system shown in Figure 6.16. The features are separated by the zero crossing points which align with the absorption features, thus confirming that the WMS is a representation of the mercury features. From this spectrum the frequency separation between the isotopic features has been measured and found to match the separations measured from the direct detection spectrum in Figure 6.6.

The frequency separation between the individual features are shown in Figure 6.16. The frequency span of all of the features is 19.2GHz, compared to 19.35GHz for the direct detection method. The estimate of the accuracy of the spacings is as for the direct measurement. The points at which the signal returns to zero are clearly evident in the WMS spectrum, clearly indicating where there was the presence of mercury. The very low noise on the trace allows a more accurate discrimination between the features.

Figure 6.17 shows a comparison between the two techniques for spectroscopy on the single source of ^{198}Hg.

Figure 6.17 shows the results when the modulation system was applied to a single isotope source of mercury. The details of the purity of the source were not available and the resolution of extra features within the mix suggests that some other isotopes were present. The WMS system shows clearly the resolution of features that are not visible with the direct detection system. This is due in large part to the improvement in signal to noise with the WMS method. The location of these features and the

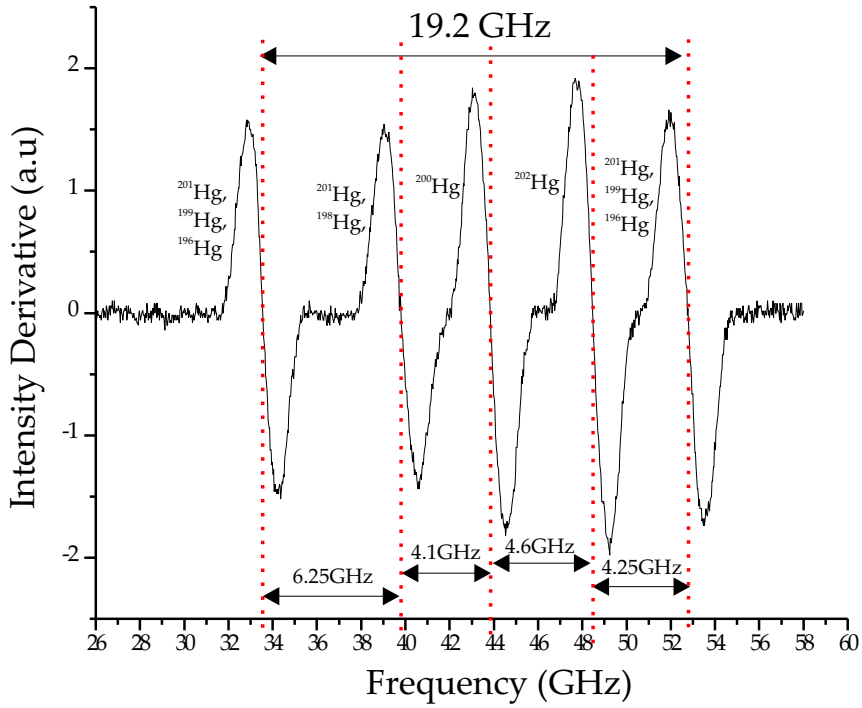

Figure 6.16: **Wavelength Modulated Spectrum for the Natural Isotope Mix of Mercury Vapour**
Resolution of isotopes within the Mercury vapour. The individual features are discriminated by the zero line (red dashed) and the frequency separation between the individual features are given.

frequency separation between them suggests the presence of other mercury features that, according to the frequency spacing, can be tentatively assigned to ^{201}Hg or ^{199}Hg. However due to the limited information regarding the source and the limits of the WMS system (these measurements were taken at the lowest modulation amplitude) further investigation into these features was not possible.

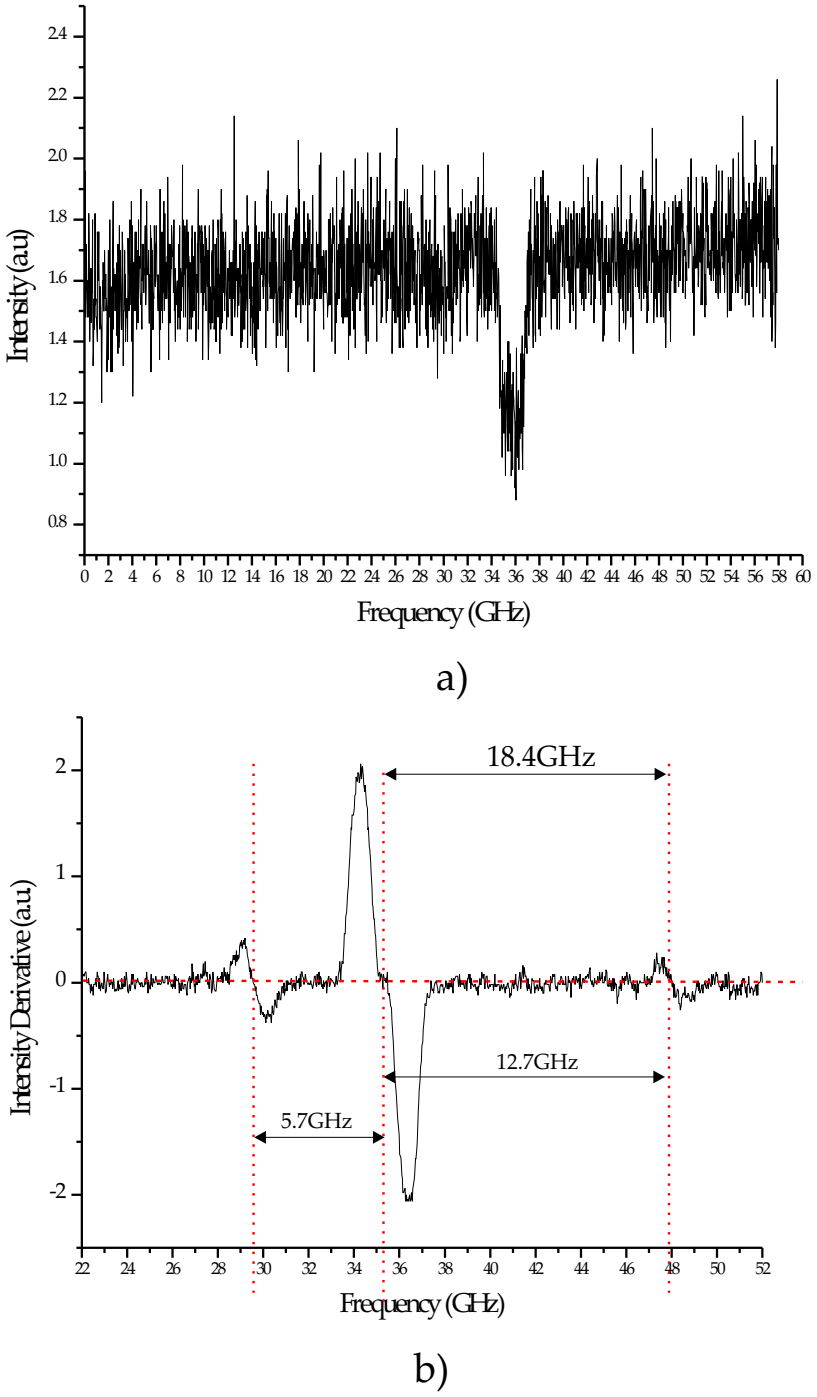

Figure 6.17: **Comparison of direct and WMS techniques for absorption of ^{198}Hg isotope**
The spectra from a single isotope source taken with direct detection (a) and wavelength modulation (b). The resolution of features within the wavelength modulation spectrum indicates the presence of features that are visible because of the reduction in signal to noise with the WMS technique. The frequency spacings of these 'new' features suggest that these are mercury and they can be tentatively assigned to residual ^{201}Hg or ^{199}Hg

6.7 Wavelength Modulation Raman Spectroscopy

6.7.1 Introduction to Raman spectroscopy

When light interacts with matter the photons can be absorbed, scattered or pass straight through without any interaction with the material. If the energy of the incident photon matches the energy gap between the ground and excited state of a molecule, the photon can be absorbed and the molecule is elevated to the higher energy state. This is the principle behind absorption spectroscopy which detects the reduction in energy of the incident light caused by the absorption within the media.

When a photon scatters as a result of interaction with a molecule, its energy does not need to match that of the difference between the energy levels of the molecules. Scattered photons can be detected at an angle to the incident light beam providing their is no simultaneous absorption within the material by electronic transitions similar to that of the incident light. Most scattered photons retain the energy and thus wavelength of the incident photons. This is known as elastic scattering. However, a small portion of the incident light is scattered at different (usually lower) energies, known as inelastic scattering. This inelastic scattering phenomenon was first observed by Raman and Krishnan in 1928 [28] and has since been referred to as Raman scattering. Raman scattering occurs due to a change in the vibrational or rotational energy within a molecule. It is the change in vibrational energy that can provide insight into the chemical composition of a sample. Spectroscopy based upon the phenomenon of Raman scattering is widely used to detect vibrations in molecules that will provide information on the chemical composition of a sample. The energy difference between the incident and Raman scattered photons is equal to one of the vibrational bond energies contained within the scattering molecule. A Raman spectrum is therefore a plot of the molecule bond energies against their relative scattering intensities.

The energy difference between the incident and scattered photons are shown by the arrows in Figure 6.18. Raman spectroscopy is normally characterised in wavenumbers

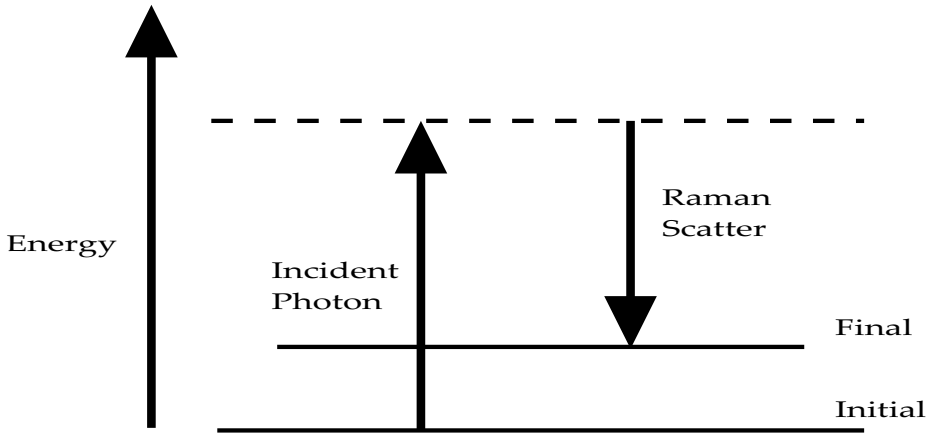

Figure 6.18: **Raman Scattering**

and is related to the energy difference between the initial and final vibrational levels. The wavenumber $\bar{\nu}$ is given by:

$$\bar{\nu} = \frac{1}{\lambda_{incident}} - \frac{1}{\lambda_{scattered}} \tag{6.8}$$

which characterises a frequency difference $\Delta\nu$ given by:

$$\Delta\nu = -\frac{c\Delta\lambda}{\lambda^2} \tag{6.9}$$

where c is the speed of light, λ is the excitation wavelength and $\Delta\lambda = \lambda_{incident} - \lambda_{scattering}$, the wavelength difference between the inital and final vibrational levels.

6.7.2 Raman Tweezers Spectroscopy

Raman tweezers spectroscopy is a combination of Raman spectroscopy and optical tweezing [29, 30, 31]. The tweezer is used to trap particles under investigation for the duration of the spectroscopic investigation. This combination of techniques allows the study of important biological systems that were previously very difficult to observe.

Raman spectroscopy has shown great potential in biomedical applications. It can be

applied to samples of varying sizes from single cells to intact tissue. Investigations into single cells are greatly improved with the ability to hold a cell in place whilst spectroscopic measurements are taken. Without the use of tweezers cells can move from the focal position during the acquisition time, required for a Raman spectra, due to the effects of Brownian motion or cell mobility. The use of optical tweezers within a Raman spectroscopy system allows a cell to be trapped whilst it is excited to obtain the Raman signal. The trapping laser combines the necessary power to induce Raman excitation whilst simultaneously trapping a single particle under investigation.

The setup is very similar to that of a typical optical tweezer, however the use of the beam splitter allows sampling of the collected Raman signal. Often a confocal arrangement is used to reduce the background signal collected from the sample. Finally a holographic notch filter is used to provide a very narrow blocking band that reflects the on axis Rayleigh scattered light but the reflectance band is so narrow that they allow the Raman signal to pass through.

One of the major challenges of Raman spectroscopy is the very weak signal. In materials such as biological tissue the Raman features are often obscured because of the strong background fluorescence. Additionally, the intensity of the signal is limited by the neccessity of operating at excitation intensities sufficiently low to prevent damage to the biological sample. A Raman signal can be enhanced by increasing acquisition time of the spectra. However, in the case of live cells, this can cause damage due to extended irradiation by the Raman excitation laser. In addition, a Raman signal can be obtained from the environment that surrounds the sample, and the fluorescence of the laser making it difficult to distinguish the molecular features within the sample.

Thus the Raman spectroscopy technique can be improved in three major ways:

1. Shorter acquisition time

2. Rejection of background fluorescence

3. Increased signal to noise

There is considerable effort focussing on the enhancement of signal to noise, rejection of background and faster acquisition times. The use of silicon-based charged-coupled devices (CCD) in the measurement of Raman spectra have significantly improved the technique due to the high sensitivity and low noise in these detectors. A wavelength modulation detection system appears to address all of these issues together with little need for complicated alterations to the experimental setup and relatively simple data processing.

Wavelength modulation techniques have been applied to the detection of Raman features previously [32]. This system used a dye laser to detect Raman features in methyl alcohol. Since this study there was relatively little investigation into the technique, but the problems of background fluorescence and weak signals were still investigated and remain a vital problem that must be overcome for Raman detection to be used practically. A derivative system was used to investigate biomembranes with the specific intention of improving the signal to noise. In this case a dye laser was used to provide the excitation [33]. This work yielded a factor of two improvement in the signal to noise over the direct technique. All previous examples of Raman modulation spectroscopy have used a photomultiplier tube as a detector which although effective, is not efficient for detection of signals over the frequency range that is required for Raman spectroscopy. The CCD allows large frequency ranges to be sampled with ease and thus in combination with a modulation system proves to be extremely powerful.

To date wavelength modulation or derivative Raman spectroscopy has not been performed using diode lasers, or upon trapped cells.

Acquisition Time

The weak nature of the Raman scattering leads to spectra that are characterised by their relatively long acquisition times. It is necessary to sum the contributions

of repeated spectra to obtain features of sufficient magnitude. This brings many problems including the potential damage to cell samples from prolonged excitation with laser light. In addition, the long time precluded this method from being adopted for *in vivo* studies on patients. The long acquisition times that arise, because of the need to obtain spectra with sufficiently large signal to noise have so far prevented the Raman technique from being used for in-vivo studies of human tissue. Acquisition time is important for different reasons - firstly fluorescence is a slower event than the Raman scattering and appearance of Raman features. If acquisition times can be improved, the effect of background will become less of a factor in analysis.

Background fluorescence

Fluorescence interference is a significant problem that affects the ability to measure the resonance of Raman spectra. Fluorescence intensity is generally of the order of mW whereas good chemical Raman signals are much weaker ($\sim 1000s$ photons) and Raman signals from biological samples are much weaker still ($\sim 10s$ photons). This problem arises from the absorption of the excitation light within the sample and is intrinsic to the technique.

Principle component analysis (PCA) is an important and commonly used analysis method for the detection of Raman features. PCA models are developed to quantify differences between Raman data sets and have become widely used to examine biological tissues particularly in the field of cancer diagnostics. To ensure that there is parity between a model and a real diagnostic measurement the background effect must be identical for both cases. If not, then the diagnosis may be affected by the differing background effect and lead to misdiagnosis. If the effect of background in negated then a PCA model can be used reliably to yield information about samples.

The background fluorescence can be eliminated via a shifted excitation Raman difference spectroscopy (SERDS) technique. This is a widely used technique that slightly shifts the frequency of the diode laser, resulting in Raman features that follow the

shifted excitation frequency whilst the background remains unchanged. This allows the two spectra to be subtracted yielding a spectrum that is derivative like with the background eliminated. Integration of this type of spectra then gives a spectrum from which Raman features can be identified clearly. This technique has proved very effective in rejecting the effect of background fluorescence. The principles of SERDS are particularly appropriate for the wavelength modulation technique which inherently includes a shift within the laser frequency. The reduction in acquisition time with a WMS technique means that this type of analysis is more efficient and allows more than 2 spectra to be compared to yield the Raman features.

Signal to noise

As described earlier in this chapter modulation spectroscopy techniques enhance the signal to noise, which can be of benefit when identifying spectra. A reduction in noise can make previously unseen features more visible, particularly those that are of smaller magnitude that had resulted in them being obscured by noise. For the case of Raman spectra where the features are inherently weak and the number of features within biological spectra are numerous and in some cases unknown, methods that can help to unobscure features assist with the identification of the sample.

The work here shows that the wavelength modulation of the exciting light has improved the Raman spectra. In addition this work is still in its elementary stage and there are many opportunities to develop this technique in the future. There is much scope for development of the technique with more careful investigations into the parameters of the modulation. There is a significant impact on results when the amplitude and frequency of the modulation is adjusted and optimisation of the technique will require more detailed study.

6.7.3 Experimental Setup

Here I present results demonstrating the use of a wavelength modulated diode laser system in Raman tweezers spectroscopy of polymer microspheres and SiHa cervical cancer cell line. The work here was carried out with colleagues Phillip Jess and Michael Mazilu who were crucial in the experimental realisation and interpretation of the experimental data.

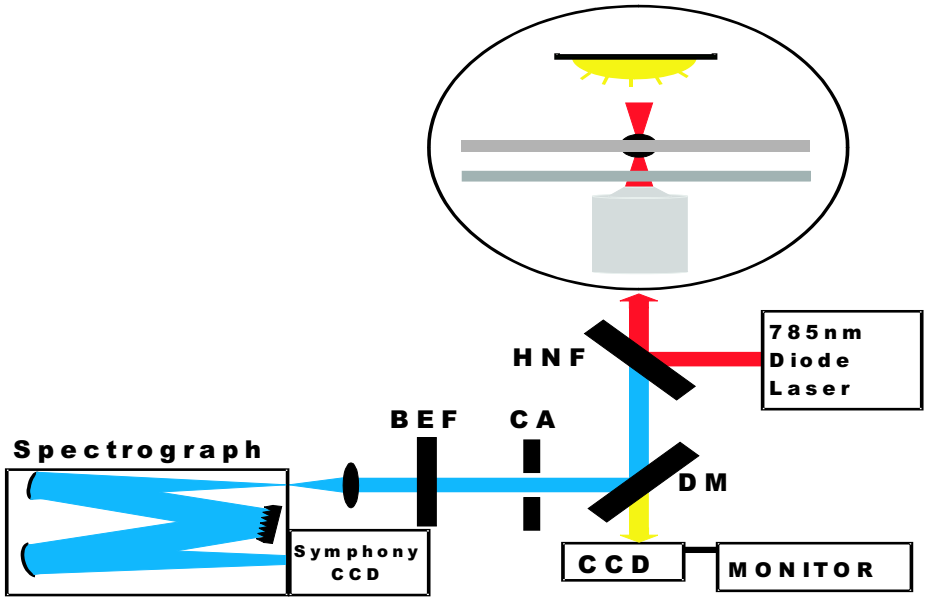

Figure 6.19: **Experimental Setup for Raman Tweezers Spectroscopy**
HNF: Holographic Notch Filter; DM: Dichroic Mirror; BEF: Band Edge Filter; CCD: Charged Coupled Device; CA: Confocal Aperture;(Figure courtesy of P Jess)

The experimental setup for Raman tweezers spectroscopy can be seen in Figure 6.19.

The diode laser is a commercial (Sanyo DL-7140-201) free running diode laser emitting at 785nm with an output power of 80mW. The laser has a dual role, both in trapping the sample of interest and providing the Raman excitation. The laser wavelength is modulated by applying a sine wave generated within a lock-in amplifier (Stanford Research Systems Model 830). The amplitude and frequency of the current modulation is altered to suit the characteristics of the different samples used. The demodulation of the spectral information in this instance is done via a Mathematica

modelling programme which processes the data collected at the CCD in the same way as a lock-in amplifier.

The laser beam is brought into the system, via a holographic notch filter (HNF, Tydex notch-4), to the inverted optical tweezers geometry and interacts with the sample contained within a chamber via a Nikon E-Plan x100 NA 1.25 oil immersion objective. The backscattered Raman light is collected by the same objective and passed through the HNF. The Raman signal is imaged onto a confocal aperture. The Raman signal is reflected by the dichroic mirror (DM) onto the spectrograph (Triax 550 Jobin Yvon). This spectrograph uses a CCD camera (Symphony OE STE Jobin Yvon) for detection of the Raman singal. The signal is imaged onto the CCD by a lens (f=80mm) placed in front of the slit of the spectrograph. The sample of interest is help within a chamber that is illuminated by white light to aid observation. The sample is observed through a CCD and on a monitor which allows the trapped particle to be chosen and observed, ensuring that the cell remains trapped throughout. The chamber is formed of a vinyl spacer (80μm) placed between two quartz coverslips (120μm). Quartz coverslips are used as they provides better rejection of any extraneous signals that can hinder the resolution of the Raman features, a problem that was identified with the use of standard glass (BK7) slides. The samples placed within the chamber are immersed in a diluting solution.

6.8 Results

In this study, the Raman spectra obtained through direct detection and then through modulation techniques were recorded and then compared. Firstly spectra were recorded for polymer microspheres. Individual spheres were trapped using the tweezers and then held within the chamber whilst spectra were recorded over 2 minutes for the direct detection technique and then over shorter periods of time for the modulation technique. This was to observe any benefit of using the modulation technique in reduction of integration time, improvement in signal to noise in the shorter time

and rejection of the effects of background fluorescence. A similar study was then performed on cervical cancer cells.

6.8.1 Polymer Spheres

The frequency and amplitude of the sinusoidal modulation applied to the laser were 0.5Hz and 3V respectively. Figure 6.20 shows the Raman spectra for a polymer sphere for both detection methods.

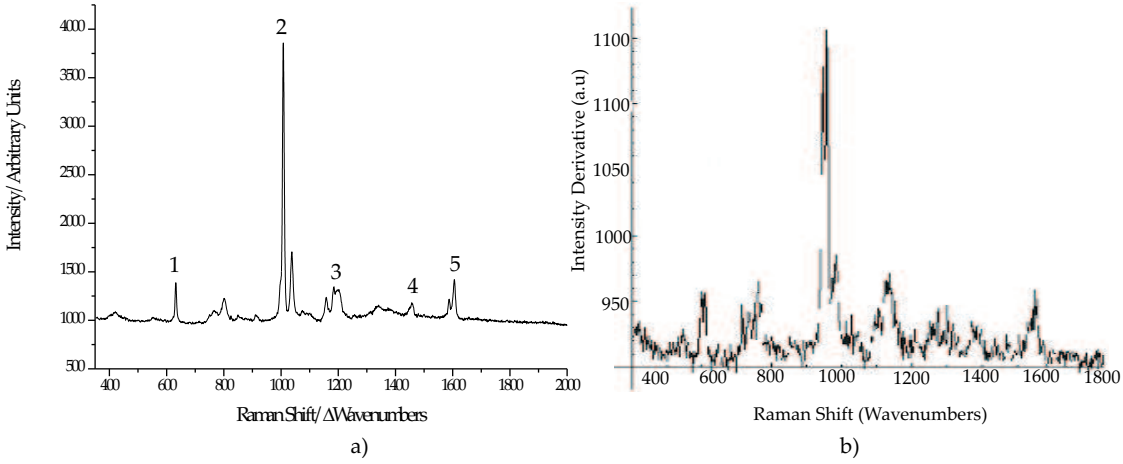

Figure 6.20: **Comparison between traditional and modulated Raman spectra on polymer spheres**
Raman spectra recorded using the traditional method in 2 minutes (a) and the modulation method in 100ms (b). Both traces show features identified as 1: a ring deformation mode; 2: ring breathing mode; 3: C-C stretch; CH scissoring; 4: ring-skeletal stretch; These bands have been assigned according to [34].

The modulated Raman spectra shows the resolution of features that are seen by the direct Raman methods, but the acquisition time for the modulated spectrum was much shorter than for the direct spectrum. All of the features from the polymer microspheres are types of double carbon and hydrogen bonds and those that can be determined have been labelled. An improvement in the signal to noise was obtained by averaging repeated spectra, shown in Figure 6.21. Again, this improved SNR was achieved in a shorter acquisition time than the direct spectrum.

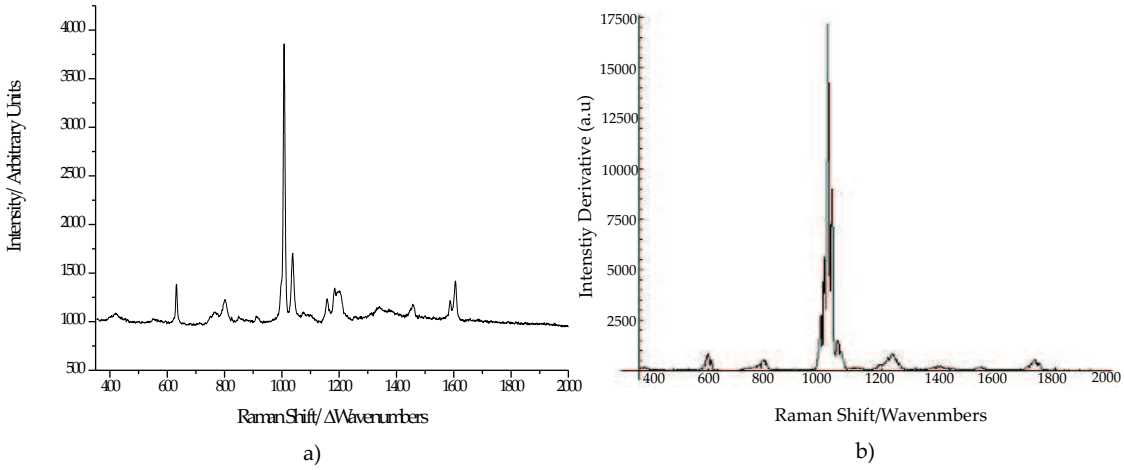

Figure 6.21: **Increased Signal to Noise with Modulation Spectroscopy**
A direct Raman spectrum (a) and a wavelength modulated Raman spectrum (b) of polymer spheres

The maximum signal obtained with the direct measurement was 4000 units with a background noise level of 900 with an acquisition time of 90 seconds whereas the wavelength modulated signal gave a maximum signal of 17500 with a background noise level of zero. This signal was taken in 400ms.

In addition Figure 6.22 shows a method of analysis of the modulated Raman data which yields significant improvements in the rejection of background fluorescence and signal to noise in short acquisition times. This method referred to as 'variance' can be explained by thinking of each of the 1024 pixels on the CCD detector as an individual single channel detector. Each detector detects the Raman signal at a different pixel and thus a different wavelength. This results in the shifting of the Raman features due to the wavelength shift, however the background fluorescence will occur in the same place each time regardless of the wavelength shift. This means that with the variance technique the background effect from each detector can be eliminated and only the Raman signal remains. With the wavelength modulated method the Raman signal is tracked across all the pixels - and only the background is removed. The modulated spectra show the Raman spectrum without any contributions from the background fluorescence, ensuring that the only features that are visible are those from the sample

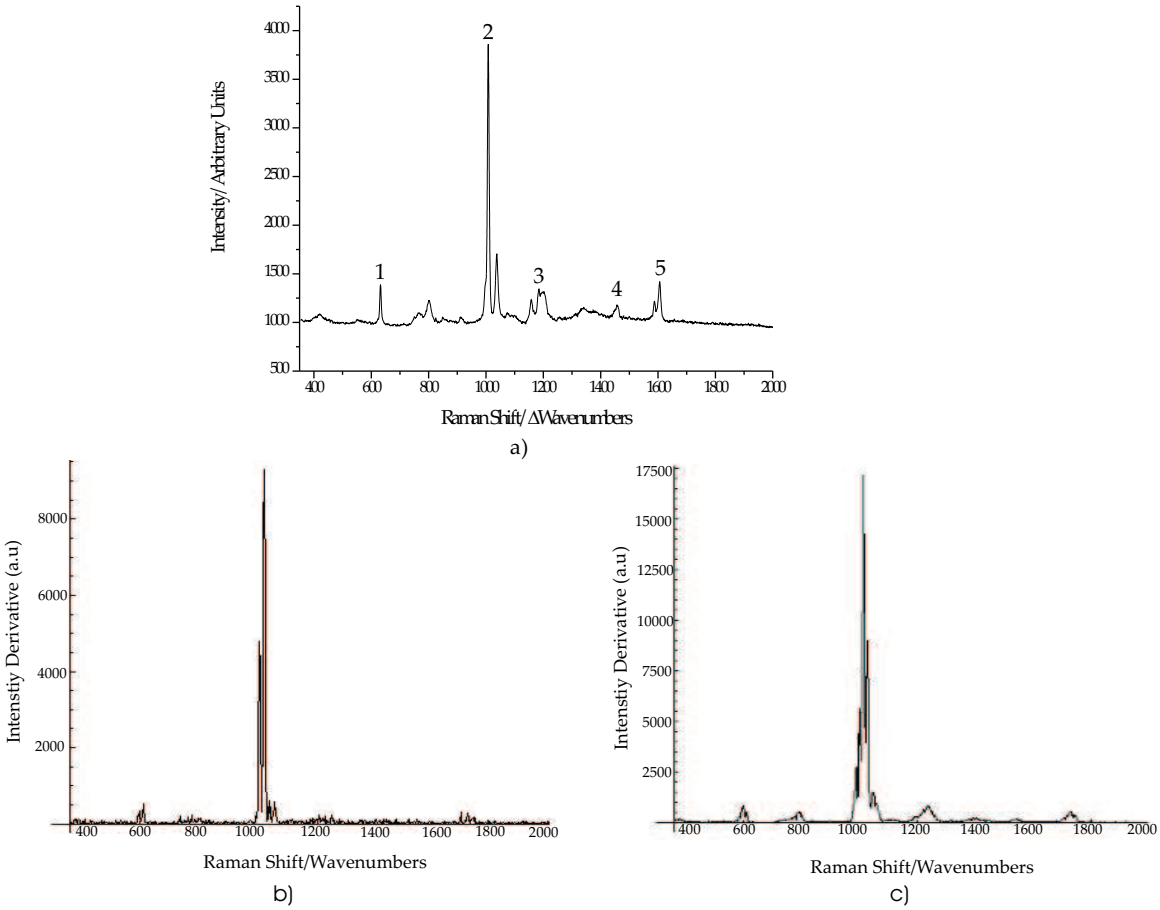

Figure 6.22: **Variance**
Raman spectra for polymer spheres for direct detection in 2 minutes (a) and modulation spectroscopy where the background fluorescence has been eliminated via a variance technique in 100ms (b) & in 400ms (c).

of interest. The intensity of these features could be improved by integrating over a longer time - however the acquisition time of 400ms is much shorter that the time taken to obtain the direct spectrum(2 minutes). This suggests that an acquisition time of a few seconds would yield spectra with no effect of background but with more visible features. In addition there are some features that are not completely resolved. Alterations in the modulation parameters could provide clearer spectra and reveal the nature of other features within the sample.

6.8.2 Cells

The modulation system was used to obtain spectra on cervical cancer cells. The modulation frequency applied here was 0.03Hz and the amplitude of this modulation was 1V. Spectra were recorded over short acquisition times and then over similar acquisition times to the traditional methods. The modulation results were integrated to allow a more simple direct comparison with the traditional spectrum. Figure 6.23 shows the Raman spectra for a cell line for a direct spectrum and wavelength modulated spectra.

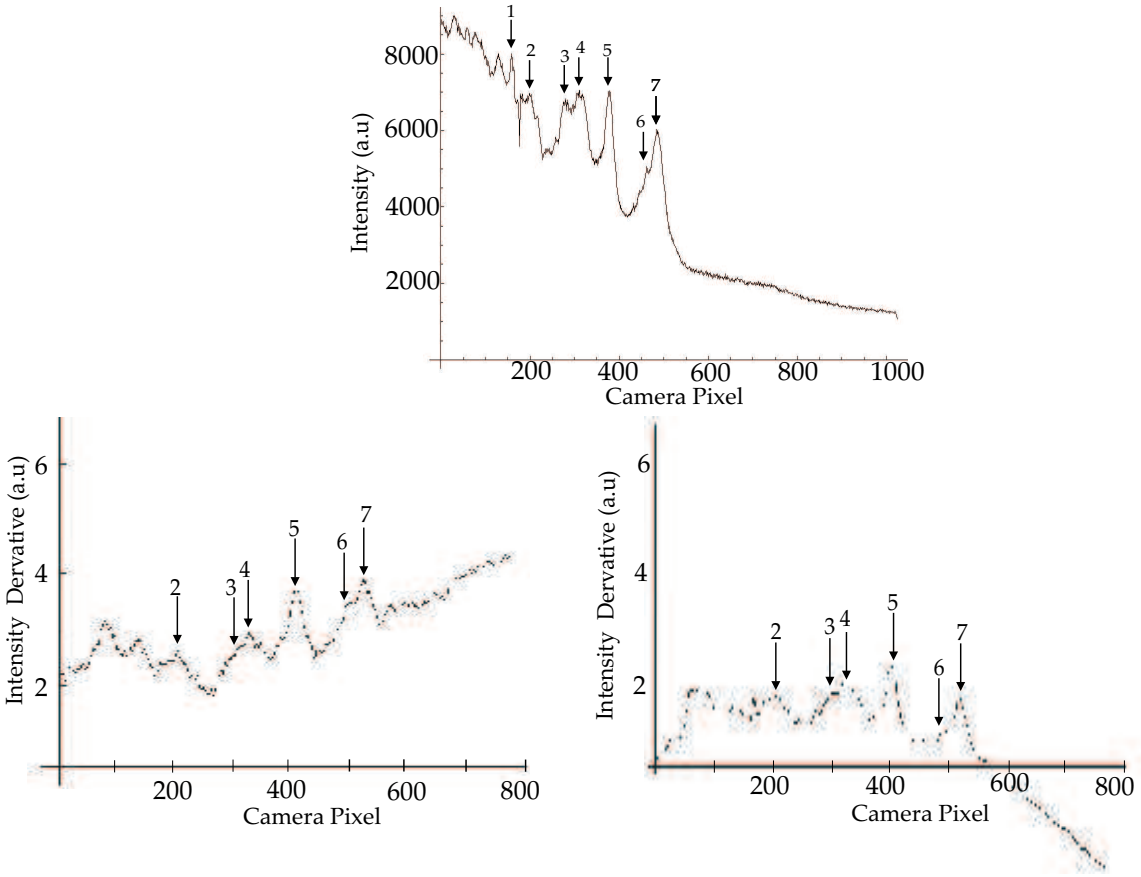

Figure 6.23: **Reduction in Acquisition Time for Raman Spectra**
Figure (a) shows the Raman spectra obtained from a cell in 90s. Figure (b) shows a modulated Raman spectra obtained in 10 seconds and Figure (c) shows the modulated spectra obtained in 90 seconds. The numbers 1-7 are the features of the cell that can be determined with certainty. Those that are assigned are : 1:DNA, 2:DNA Backbone 5: Membrane, 7: Protein. The remaining features are not assigned yet.

In Figure 6.23 the unmodulated trace clearly shows features but the effect of the background fluorescence is evident. In (b) a Raman WMS spectrum taken in 10 seconds the features are visible but the background is still making a significant contribution. In (c) the WMS spectrum is taken over 90seconds and the background contribution has been eliminated. The resolution of features with the modulation spectra is shown. The assignment of features is an ongoing process with further research on the samples required to be able to determine the properties of the sample with any certainty. These results show that there is great potential in refining the system parameters to yield detailed Raman spectra in short acquisition times (less than one minute) with minimal effect of background noise and increased signal to noise.

6.9 Summary

The spectroscopic investigations carried out in this chapter have attempted to both yield information about spectroscopic samples and develop methods that can be further refined and improved to be used in real applications.

This chapter detailed the assembly and successful generation of UV light at 254nm from an SFG system based upon the mixing of two microlensed diode lasers (MDLs) within a non-linear crystal. The assembly of the experiment was described in detail, along with the methods used to overlap the beams within the crystal for maximum non-linear conversion. The system described was successful in generating UV light and the output powers obtained were over an order of magnitude greater than that previously reported. This result and the greater conversion efficiency was as a direct result of the use of MDLs and the precise determination of optimum beam parameters.

Following on from the development of this system, it was applied to trace gas detection, to obtain detailed spectral information about mercury. Two different methods of absorption spectroscopy were used to measure the isotope separation within a natural mix of mercury vapour. The direct detection system was used to obtain the structure

of the mercury vapour within a single scan of the system. Previous work had relied upon combining adjacent scans to observe all of the features. A precise measurement of the scan allowed the determination of the frequency separation between all of the isotopes within the natural mix.

The system was then adapted to allow wavelength modulated detection to be used. The results from the WMS system were used firstly to obtain the optimum parameters for the system to yield the clearest spectra. Analysis showed that there was no benefit in shifting detection to higher harmonics as has been common in other applications. This was largely attributed to the use of a detector (photomultiplier tube) that had negligible effects from 1/f noise at the modulation frequencies used. The optimum parameters were a modulation frequency of 1KHz with amplitude of 12mV. Accurate frequency intervals between the isotopes were determined from the WMS spectra and matched those determined by the direct detection system.

The system was also used to observe the spectrum from a mercury cell containing a source of ^{198}Hg. Here the WMS system was shown to be more powerful over direct detection, allowing features to be observed because of the increased signal to noise. These were identified as mercury features, showing resolution of individual isotopes within a features, showing a level of detail previously unresolved. To the best of my knowledge this level of detailed investigation into the mercury line has not been carried out with a diode laser spectroscopy system. The work here provides a platform for more high sensitive diode laser based WMS experiments. These are described in further detail in Chapter 7.

Modulation with diode lasers was also applied with success to a Raman spectroscopy technique. To the best of my knowledge this was the first example of a WMS system applied to Raman tweezers spectroscopy using a diode laser. Spectra were obtained for polymer spheres and for biological cell samples. A comparison between the WMS spectra and the direct spectra showed clear and substantial benefits with the use of a WMS detection system. Improvements in the acquisition time, signal to noise and

the effect of background fluorescence interference were all seen with very elementary results, demonstrating real promise for this technique in developing systems to provide *in vivo* studies on biological tissue samples.

The work in this chapter unites all of the major themes in this thesis, diode lasers, enhancement of the properties of diode lasers through circularisation and extended cavity geometries, use of violet emitting diode lasers, non-linear frequency conversion and specialised applications in spectroscopy.

Bibliography

[1] Kyuseok Song and Euo Chang Jung. Recent developments in modulation spectroscopy for trace gas detection using tunable diode lasers. *Applied Spectroscopy Reviews*, 38(4):395–432, 2003.

[2] Liantuan Xiao, Changyong Li, Quian Li, Suotang Jia, and Guosheng Zhou. Low-frequency wavelength modulation spectroscopy with D_2 transition of atomic cesium by use of an external-cavity diode laser. *Applied Optics*, 39(6):1049–1052, 2000.

[3] Ulf Gustafsson, Gabriel Somesfalean, Janis Alnis, and Sune Svanberg. Frequency-modulation spectroscopy with blue diode lasers. *Applied Optics*, 39(21):3774–3780, 2000.

[4] New Focus. Fm spectroscopy with tunable diode lasers. Appliction Note 7, 5215 Hellyer Avenue, San Jose CA 95138-1001,USA.

[5] James P Jacobs and R. Bruce Warrington. Pressue shift and broadening of the 254-nm intercombination line of mercury by N_2. *Physical Review A*, 68, 2003.

[6] J. Alnis, U. Gustafsson, G. Somesfalean, and S. Svanberg. Sum frequency generation with a blue diode laser for mercury spectroscopy at 254nm. *Applied Physics Letters*, 76(10):1234–1236, 2000.

[7] Antonia E. Carruthers, Tanya K. Lake, Anjali Shah, John W. Allen, Wilson Sibbett, and Kishan Dholakia. Erratum to single-scan spectroscopy at 235.7nm by sum frequency mixing of violet and red microlensed diode lasers. *Optics Communications*, 261(3):381–382, 2006.

[8] Hermann Haken and Hans C. Wolf. *The Physics of Atoms and Quanta : Introduction to Experiments and Theory*. Springer, 6th edition, 1998.

[9] Hans Edner, Gregory W. Faris, Anders Sunesson, and Sune Svanberg. Atmospheric atomic mercury monitoring using differential absorption lidar techniques. *Applied Optics*, 28(5):921–930, 1989.

[10] Petter Weibring, Hans Edner, and Sune Svanberg. Versatile mobile lidar system for environmental monitoring. *Applied Optics*, 42(18):3583–3594, 2003.

[11] A.E. Carruthers, T.K. Lake, A. Shah, J.W. Allen, W. Sibbet, and K. Dholakia. Microlensed red and violet diode lasers in an extended cavity geometry. *Review of Scientific Instruments*, 75(10):3360–3362, 2004.

[12] G.D. Boyd and D.A. Kleinman. Parametric interaction of focussed gaussian light beams. *Journal of Applied Physics*, 39(8):3597, 1969.

[13] I.D. Lindsay. *High Spatial and Spectral Quality Diode-Laser-Based Pump Sources for Solid-State Lasers and Optical Parametric Oscillators*. PhD thesis, University of St Andrews, 1999.

[14] A.E. Carruthers. *Novel optical micromanipulation techniques and applications of violet diode lasers*. PhD thesis, School of Physics and Astronomy, University of St Andrews, 2005.

[15] B. Ruffing, A. Nebel, and R. Wallenstein. High-power picosecond LiB_3O_5 optical parametric oscillators tunable in the blue spectral range. *Applied Physics B : Lasers and Optics*, 72(2):137–149, 2000.

[16] David S. Bomse, Alan C. Stanton, and Joel A. Silver. Frequency modulation and wavelength modulation spectroscopies: comparison of experimental methods using a lead-salt diode laser. *Applied Optics*, 31(6):718–731, 1992.

[17] James M. Supplee, Edward. A. Whittaker, and Wilfried Lenth. Theoretical description of frequency modulation and wavelength modulation spectroscopy. *Applied Optics*, 33(27):6294–6302, 1994.

[18] Louis C. Philippe and Ronald K. Hanson. Laser diode wavelength-modulation spectroscopy for simultaneous measurement of temperature, pressure and velocity in shock-heated oxygen flows. *Applied Optics*, 32(30):6090, 1993.

[19] Stephane Schilt and Luc Thevenaz. Experimental method based on wavelength-modulation spectroscopy for the characterisation of semicondictor lasers under direct modulation. *Applied Optics*, 43(22):4446–4453, 2004.

[20] Y.T. Zhao, J.M. Zhao, T. Huang, L.T. Xiao, and S.T. Jia. Frequency stabilisation of an external-cavity diode laser with a thin cs vapour cell. *Journal of Physics D Applied Physics*, 37(–):1316–1318, 2004.

[21] Jr. Charles P. Poole. *Electron Spin Resonance: A comprehensive treatise on experimental techniques*. Dover Publications, 31 East 2nd Street, Mineola, New York, 11501, second edition, 1996.

[22] Antonia E. Carruthers, Tanya K. Lake, Anjali Shah, John W. Allen, Wilson Sibbett, and Kishan Dholakia. Single-scan spectroscopy of mercury at 253.7nm by sum frequency mixing of violet and red microlensed diode lasers. *Optics Communications*, 255(4–6):261–266, 2005.

[23] H. Wieczorek. 1/f noise in amorphous silicon nip and pin diodes. *Journal of Applied Physics*, 77(7):3300–3308, 1995.

[24] M.B. Weissman, R.A. Isaacson, and G. Feber. Experimental verification of a theory of 1/f noise in a model system. *Physical Review Letters*, 43(11):733–737, 1979.

[25] Kenneth K. Clarke and Donald T. Hess. *Communication Circuits: Analysis and Design*. Addison-Wesley Publishing Company, first edition, 1971.

[26] Joel A. Silver. Frequency-modulation spectroscopy for trace species detection: theory and comparison among experimental methods. *Applied Optics*, 31(6):707–717, 1992.

[27] J. Reid and D. Labrie. Second-harmonic detection with tunable diode lasers - comparison of experiment and theory. *Applied Physics B*, 26(–):203–210, 1981.

[28] C.V. Raman and K.S. Krishnan. The optical analog of the compton effect. *Nature*, 121(–):711, 1928.

[29] A. Ashkin, J.M. Dziedzic, J.E. Bjorkholm, and S. Chu. Observation of a single-beam gradient force optical trap for dielectric particles. *Optics Letters*, 11(–):1996, 1986.

[30] K. Ajito, M. Morita, and K. Torimitsu. Investigation of the molecular extraction process in single subpicoliter droplets using a near-infrared laser raman trapping syystem. *Analytical Chemistry*, 72(–):4721–4725, 2000.

[31] C. Xie, M.A. Dinno, and Y. Li. Near-ir raman spectroscopy of single optically trapped biological cells. *Optics Letters*, 27(–):249–251, 2002.

[32] K.H.Levin and C.L.Tang. Wavelength modulation raman spectroscopy. *Applied Physics Letters*, 33(9):817–819, 1978.

[33] M. van de Ven, J. Meijer, W. Verwer, Y.K. Levine, and J.P. Sheridan. Derivative raman spectroscopy applied to biomembrane systems. *Journal of Raman Spectroscopy*, 15(2):86–89, 1984.

[34] T.E. Bridges, M.P. Houlne, and J.M. Harris. Spatially resolved analysis of small particles by confocal raman microscopy: depth profiling and optical trapping. *Analytical Chemistry*, 76(–):576–584, 2004.